50272-101

REPORT DOCUMENTATION PAGE	1. REPORT NO. NSF/RA-790486	2.	3. Recipient's Accession No. PB80 209810

4. Title and Subtitle
NGI Direct Simple Shear Tests on Concord Blue Clay, Interim Report

5. Report Date

6.

7. Author(s)
D. J. Kopal, T. F. Zimmie

8. Performing Organization Rept. No.

9. Performing Organization Name and Address
Rensselaer Polytechnic Institute
Civil Engineering Department
Troy, NY 12181

10. Project/Task/Work Unit No.

11. Contract(C) or Grant(G) No.
(C)
(G) PFR7818743

12. Sponsoring Organization Name and Address
Engineering and Applied Science (EAS)
National Science Foundation
1800 G Street, N.W.
Washington, D.C. 20550

13. Type of Report & Period Covered
Interim

14.

15. Supplementary Notes
This is a progress report of "Simple Shear Behavior of Fine Grained Soils Subjected to Earthquake and Other Repeated Loading," (PB298123).

16. Abstract (Limit: 200 words)
A laboratory study investigated the dynamic behavior of clay soils on an effective stress basis. Emphasis was placed on high strain cyclic loading that occurs during earthquakes and storm wave loads. A direct simple shear device of the Norwegian Geotechnical Institute (NGI) was used to test the consolidated constant volume static and cyclic strength characteristics. Laboratory tests were conducted on Concord Blue Clay having two different consolidation histories (consolidation refers to the application of vertical normal stress to the soil sample). The first set of tests cyclically loaded normally consolidated clay and the second set cyclically loaded overconsolidated clay. Stress-controlled cyclic tests conducted to maintain constant cyclic shear levels measured lateral shear strains and effective vertical stresses as a function of the number of loading cycles. Static load tests provided a comparison with cyclic loading tests. It was demonstrated that clay strength degradation can be affected by cyclic shear stress levels, effective stresses, consolidation ratios, and number of loading cycles. Clay degradation was examined by employing the Ramberg-Osgood model. A correlation between experimental and mathematical modeling results was developed to determine the accuracy of the Ramberg-Osgood model. A literature review, equipment descriptions, testing procedures, and test results are included.

17. Document Analysis a. Descriptors
Mathematical models
Earthquakes
Stress analysis
Cyclic loads
Static loads
Shear tests

b. Identifiers/Open-Ended Terms
Concord Blue Clay
Soil consolidation
Ramberg-Osgood model
Cyclic strength
Shear devices
Earthquake Hazards Mitigation

c. COSATI Field/Group

18. Availability Statement	19. Security Class (This Report)	21. No. of Pages
	20. Security Class (This Page)	22. Price

(See ANSI-Z39.18) See Instructions on Reverse

OPTIONAL FORM 272 (4-77)
(Formerly NTIS-35)
Department of Commerce

NGI DIRECT SIMPLE SHEAR TESTS ON CONCORD BLUE CLAY

by

David J. Kopal
PRINCIPAL INVESTIGATOR
Thomas F. Zimmie

NSF Grant No. PFR-7818743

INTERIM REPORT

NGI DIRECT SIMPLE SHEAR TESTS

ON

CONCORD BLUE CLAY

To: William Hakala, Program Manager
National Science Foundation

FROM: Thomas F. Zimmie, Associate Professor
Civil Engineering Department
Rensselaer Polytechnic Institute
Troy, New York

The report attached is a progress report on NSF Grant No. PFR-7818743 titled "Simple Shear Behavior of Fine Grained Soils Subjected to Earthquake and Other Repeated Loading", under the direction of Thomas F. Zimmie.

The report was done by David J. Kopal under the supervision of Professor Thomas F. Zimmie. Mr. Kopal also used the report as his Master Project in partial fulfillment of the requirements for the degree of Master of Engineering at Rensselaer Polytechnic Institute.

NGI DIRECT SIMPLE SHEAR TESTS

ON

CONCORD BLUE CLAY

by

David J. Kopal

Sponsored by the National Science Foundation,

Directorate for Engineering and Applied Science,

Division of Problem-Focused Research (PFR),

Earthquake Hazards Mitigation Program

Grant No. PFR-7818743

Interim Report

Principal Investigator

Thomas F. Zimmie

Associate Professor of Civil Engineering

Rensselaer Polytechnic Institute
Troy, New York

December 1979

CONTENTS

LIST OF TABLES iv

LIST OF FIGURES v

ACKNOWLEDGEMENT vi

NOTATIONS vii

ABSTRACT viii

PART 1 INTRODUCTION 1

1.1 Background 1
1.2 Definitions 2
1.3 General Clay Behavior 3

PART 2 EQUIPMENT 5

2.1 Shear Apparatus 5

2.1.1 Background 5
2.1.2 Basic Principles 5
2.1.3 General Description and Operation 7
2.1.4 Trimming Apparatus 8

2.2 Data Acquisition 8

2.2.1 False Deformation 9

2.3 Assumptions and Limitations 9

2.4 Shear Modulus Values 11

PART 3 TESTING CRITERIA 12

3.1 Soil 12

3.2 Testing Procedure 12

PART 4 TEST RESULTS AND ANALYSIS 14

4.1 Initial (First Cycle) Backbone Curves 14

4.1.1 Curve Determination 14
4.1.2 Comparison with Static Loading Tests 14
4.1.3 $(G_0)_1$ Values 17

4.2 Other Cyclic Loading Curves 17

4.2.1 Curve Determination 17
4.2.2 Clay Behavior 17
4.2.3 Secant Shear Modulus Degradation 19
4.2.4 Degradation Index Variation 21
4.2.5 Synopsis 22

4.3 Effect of Cyclic Shear Stress Level 23

4.3.1 Total Stress Level 23
4.3.2 Effective Stress Level 25

4.4 Effect of Number of Loading Cycles 26

4.5 Effect of Pore Pressure Changes 27

PART 5 CYCLIC LOADING MODELS 29

5.1 Ramberg-Osgood Model 29

5.1.1 Derivation of R-O Parameters 30

5.1.1.1 γ_y and $(G_0)_1$ Determination 30
5.1.1.2 R Determination 30
5.1.1.3 α (Alpha) Determination 31

5.1.2 Other Cyclic Loading Curves 32

5.1.3 Comparison With Experimental Results 33

5.1.3.1 Backbone Curves 33
5.1.3.2 R-O Model Sensitivity 33
5.1.3.3 Secant Shear Moduli 34

PART 6 DISCUSSION AND CONCLUSIONS 35

6.1 Test Parameter Results 35

6.1.1 Number of Loading Cycles 35
6.1.2 Pore Pressure and Effective Stress Changes 35
6.1.3 Cyclic Shear Stress Level 36

6.2 Comparison Between NC and (OCR=2) Clays 36

6.2.1 Similarities 36
6.2.2 Differences 37

6.3 Ramberg-Osgood Modelling Results 37

6.3.1 Model Sensitivity 38
6.3.2 Secant Shear Moduli Comparison 38

PART 7 REFERENCES 39

PART 8 TABLES 41

PART 9 FIGURES 58

LIST OF TABLES

TABLE 1	Geotechnical Data for Concord Blue Clay	42
TABLE 2	Individual Test Data	43-48
TABLE 3	Ramberg-Osgood Model Parameters	49-55
TABLE 4	Degradation Index Values Experimental and R-O Calculated $(G_s)_N$ Values	56-57

LIST OF FIGURES

FIGURE 1	Cyclic and Static Loading Stress - Strain Curves...	59-60
FIGURE 2	Shear Stress vs. Shear Strain	61-62
FIGURE 3	Effective Stress Paths and Failure Lines	63-64
FIGURE 4	Typical Cyclic Loading Test Results	65
FIGURE 5	Secant Shear Modulus vs. N Cycles	66-67
FIGURE 6	Secant Shear Modulus vs. Normalized Shear Stress...	68-69
FIGURE 7	Secant Shear Modulus vs. Normalized Vertical Stress.....	70-71
FIGURES 8a, 8b	Degradation Index vs. Shear Stress	72-73
8c	Degradation of Initial Backbone Curve	74
FIGURE 9	Degradation Index vs. Normalized Pore Pressure.....	75-76
FIGURE 10	Shear Strain vs. Normalized Pore Pressure	77-78
FIGURE 11	Shear Strains and Pore Pressures vs. N Cycles For Test 5	79
FIGURE 12	Normalized Pore Pressure and Shear Strain vs. N Cycles	80-83
FIGURE 13	Total Shear Stress Level vs. N Cycles.....	84-85
FIGURE 14	Normalized Shear Stress vs. N Cycles Evaluated At Varying Shear Strains	86-87
FIGURE 15	Effective Shear Stress Levels vs. Strain For Various Cyclic Loading Tests and Clays.....	88
FIGURE 16	Determination of γ_y From Initial Backbone Curves...	89
FIGURE 17	Determination of R	90
FIGURE 18	Ramberg-Osgood Model Backbone Curves	91-92
FIGURE 19	Secant Shear Modulus vs. Shear Strain	93-94

ACKNOWLEDGEMENT

The author gratefully acknowledges the assistance and guidance given by Professor Thomas F. Zimmie, Department of Civil Engineering, Rensselaer Polytechnic Institute.

The author also wishes to express his thanks to Professor Ricardo Dobry, Department of Civil Engineering at R.P.I., whose notes and comments on soil dynamics helped considerably in the writing of this paper. Appreciation is also expressed to Carsten Floess, Doctoral Candidate in Civil Engineering at R.P.I., for his experimental testing and suggestions.

The author would also like to thank Brenda Grundy, Virginia Herrera, Audrey Jordan, Cynthia Quintanilla, Patricia Saavedra, and Robin Tingley for assisting in proofing and for typing this report.

NOTATIONS

A,B,C	-----	Points on the backbone curves in Figure 2
N	-----	Loading Cycle number
$(G_s)_N$	-----	Secant shear modulus at cycle N
G_O	-----	Maximum secant shear modulus
$(G_O)_N$	-----	Maximum secant shear modulus at cycle N
NC	-----	Normally consolidated
(OCR=2)	-----	Overconsolidation ratio of 2
R, α	-----	Constants in Ramberg-Osgood Model
γ	-----	Shear strain during static loading
γ_c	-----	Shear strain during cyclic loading
δ_N	-----	Degradation index at loading cycle N
$\overline{\sigma}_{vo}$	-----	Initial effective vertical stress
$\overline{\sigma}_v$	-----	Experimental effective vertical stress
τ	-----	Shear stress
τ_c	-----	Cyclic shear stress
τ_{hc}	-----	Horizontal cyclic shear stress
τ_{hf}	-----	Horizontal shear stress at failure for undrained static loading
$(SSL)_T$	-----	Shear stress level defined on a total stress basis
$(SSL)_E$	-----	Shear stress level defined on an effective stress basis
ϕ	-----	Mohr-Coulomb angle of internal friction
S_u	-----	Undrained soil strength for static loading
Δu, u	-----	Excess hydrostatic pore pressure (referred to as pore pressure)

ABSTRACT

This report contains the results of a laboratory investigation on the behavior of clay with two different consolidation histories. Emphasis was placed on high strain level cyclic loading such as that caused by earthquakes and storm waves.

The investigation consists of two parts:

In the first part, consolidated constant volume (CCV) static and cyclic tests were performed using a Norwegian Geotechnical Institute (NGI) direct simple shear device. In addition, only natural undisturbed clay samples were tested because the in situ structure of cohesive soils is an important parameter in determining their behavior.

Laboratory tests were conducted on Concord Blue Clay having two different consolidation histories. The first set of tests (Tests 5 through 10) cyclically loaded normally consolidated clay and the second set of tests (Tests 13 through 18, and 21) cyclically loaded overconsolidated clay. The normally consolidated clay (NC) was tested at a vertical confining stress of 3.369 kg/cm^2. The slightly overconsolidated clay, (OCR=2), was tested at a vertical confining stress of 1.685 kg/cm^2, a value that was one-half of its previous maximum stress of 3.369 kg/cm^2.

Stress-controlled cyclic tests were conducted so that constant cyclic shear stress levels were maintained during each test. The test data consisted of the measurement of lateral shear strains and effective vertical stresses as a function of the number of loading cycles.

Static loading tests were performed to achieve a comparison with cyclic loading tests. Static loading Tests 2, 9, and 10 loaded normally

consolidated clay while Tests 11, 12, and 21 statically loaded slightly overconsolidated clay.

The laboratory investigation demonstrated that clay strength degradation can be affected by cyclic shear stress levels, effective stresses, consolidation ratios, and the number of loading cycles.

The second part of the investigation interprets clay degradation by employing the Ramberg-Osgood model. A correlation between experimental and mathematical modelling results is developed to determine the accuracy of the Ramberg-Osgood model.

Included in the report is a literature review, a description of equipment and testing procedures, and the presentation of test results.

PART 1

INTRODUCTION

1.1 Background

In recent years, the geotechnical engineer has recognized the importance of soil strength characteristics under cyclic loading. Typical examples of cyclic loadings include traffic activity, blasting, machinery vibrations, and of course, wave loading and earthquakes. Designers have increasingly sought to account for soil strength deterioration during cyclic loading in their analyses.

Soil failure resulting from cyclic loading is a common destructive mechanism. Earthquake damage to every conceivable structure, including buildings, pipelines, and dams have at times been attributed to soil failure. Besides the relative frequent occurrence of soil failure when exposed to cyclic loading, many examples can be cited in which such failures were catastrophic (14,22).

Soil failures often occur because of rapid increases in stress from seismic accelerations by soil strength degradation and increased pore pressures. The term "liquefaction" is generally applied to the extreme form of this type of failure. Most of the research designed to study this mode of soil strength deterioration has been associated with cohesionless soils. There has been much less accomplished in determining soil strength degradation of clays during cyclic loading.

The major objective of the laboratory investigation reported herein is to study the dynamic behavior of clay soils on an effective stress basis. Emphasis was placed on the high strain level cyclic loading that occurs during earthquakes and storm wave loads.

Direct simple shear devices are increasingly being utilized to study fine grained soil characteristics, particularly under cyclic loading conditions. All laboratory testing was performed using the Norwegian Geotechnical Institute (NGI) direct simple shear device. The NGI device is an accepted and appropriately sophisticated apparatus for the measurement of cyclic strength characteristics of fine grained cohesive soils. This device, with modifications, allows for repetitive loadings in alternate directions in an attempt to more closely simulate in situ cyclic loading conditions, such as for earthquakes. Overall it is an excellent device, although it does have some limitations (20).

1.2 Definitions

There are levels of cyclic shear stress that can be tolerated indefinitely without causing ultimate soil failure. One cyclic shear stress category, the "threshold condition", is defined by Sangrey to be a specific soil strength wherein the shear strains and pore pressures remain constant for any number of loading cycles (16).

Pore pressures and shear strains can increase to a level after which a large number of loading cycles generates no significant change in pore pressure. The "critical stress level" defines the cyclic shear stress level in which a limiting value of shear strains and pore pressures occurs. The maximum level of cyclic stress that will not lead to soil failure (referred to as nonfailure equilibrium), is termed the "critical level of repeated stress" after Larew and Leondards (16). This phenomenon is discussed more thoroughly and illustrated with test results in Sections 4.2.2 and 4.3.

At shear stress levels above the critical level of repeated

stresses, substantial cumulative increases in shear strains and pore pressures develop, causing soil failure ultimately (16).

1.3 General Clay Behavior

When an undrained saturated clay is subjected to a stress reversal, a change in pore pressure can result. Sangrey concludes that the build-up of positive pore pressures in normally consolidated clays leads to a reduction in shear strength in which the critical level of repeated stresses is significantly lower than the peak undrained shear strength from static loading tests (14). In this study, overconsolidated clays, tested at an experimental vertical stress exactly 50 percent of that for normally consolidated clays, developed both positive and negative pore pressures. In both clay types, however, a nonfailure equilibrium condition was observed. Andersen has concluded that the amount of pore pressure accumulation is dependent on the consolidation ratio, and is more importantly affected by the maximum and current confining stresses (1).

According to Sangrey, when saturated clay is subjected to cyclic stresses, a net nonrecoverable deformation and substantial amount of pore pressure remains after the first loading cycle (14). In this study, this behavior was observed whether or not the clay experienced the failure condition of $\pm 3\%$ shear strain. Others have agreed that depending primarily on the cyclic shear stress level, subsequent loading cycles can continue to generate larger pore pressures in saturated clay (1, 14).

During cyclic loading, the stress-strain behavior of soils is nonlinear and hysteretic. Particularly for soft clays, their dynamic properties can change significantly during cyclic loading. As evidenced

by test data in this investigation, these changes in properties can neither be accounted for by assuming equivalent linear properties nor by assuming nonlinear properties with a constant backbone curve.

PART 2

EQUIPMENT

2.1 Shear Apparatus

The NGI direct simple shear apparatus, Model 4, is manufactured by Geonor and was used in this investigation. Additional details and procedures for the specific equipment used in this study are more thoroughly covered in a study by Zimmie and Floess (22).

2.1.1 Background

The NGI apparatus is built for testing undisturbed soil for conditions of simple shear and plane strain. These conditions are similar to the strain conditions that exist in the field, and they cannot be obtained in the laboratory using triaxial and shearbox devices. In addition, Ladd and Edgers have concluded that consolidated undrained direct simple shear tests are easier to perform than K_o - consolidated triaxial tests to obtain pore pressure measurements (11).

Consequently, simple shear tests of various forms have been conducted to simulate the cyclic stress-strain conditions of a soil element in the field during an earthquake. The NGI direct simple shear apparatus has increasingly been used for the determination of dynamic properties and cyclic strength of soils.

2.1.2 Basic Principles

The basic principle of the NGI direct simple shear apparatus is the application of a shearing force to a cylindrical soil sample, which is confined in the radial direction by a wire reinforced rubber membrane. The shearing action causes a shearing displacement of the top of the

sample relative to the bottom. The reinforcement in the rubber membrane allows for vertical deformations and horizontal displacements in the soil, but retains a constant cross-sectional area during consolidation and shearing.

Consolidation is conducted by applying a vertical normal stress to the sample, allowing for drainage. During shear, constant volume conditions are maintained by adjusting the applied vertical stress, thus simulating undrained shear conditions. In such tests, the change of vertical stress required to keep a constant volume is equal to the change in pore pressure.

Figure 4 presents traces of stress-time and strain-time histories that show two typical cyclic tests conducted on soft clay specimens (9). The upper two traces are results from a strain-controlled cyclic loading test in which a uniform sinusoidal strain-time history is applied and the corresponding cyclic stress measured. The stress decreases with time and indicates soil strength degradation, or soil structure weakening. The lower two curves are taken from a stress-controlled cyclic loading test in which a uniform sinusoidal stress-time history is applied and the corresponding shear strain measured. The shear strain increases with time and indicates soil strength degradation.

In this study, stress-controlled tests applied square wave loading to the soil specimen instead of sinusoidal wave loading. This change in wave loading geometry did not affect the sample's response because shear strains increased as a function of time, in a similar manner as illustrated by Figure 4.

2.1.3 General Description and Operation

The NGI direct simple shear apparatus is composed of a sample assembly, vertical loading unit, and horizontal loading unit.

The sample assembly consists of a pedestal, an upper and lower cap, a reinforced rubber membrane and O-rings. The sample assembly unit is available in either the standard 50 cm^2 sample cross-sectional area or the smaller 17.81 cm^2 area. In this study, the smaller cross-sectional area (17.81 cm^2) was utilized and the soil sample heights varied from 1.326 to 2.045 cm.

The upper and lower caps have recesses for porous stones and were connected to water tanks through drainage tubes. The O-rings provided a water tight seal between the reinforced rubber membranes and caps. Reinforced rubber membranes, manufactured by Geonor, were used for the measurement of lateral shear stresses and shear strains in the sample. These membranes provided adequate lateral strength to maintain a constant cross-sectional area during consolidation and shear loadings.

The vertical loading unit, used for consolidation, consists of a base, tower, 10:1 lever arm, load gauge, piston, dial gauge, and load adjusting mechanism.

The horizontal loading unit includes a gearbox with a variable speed motor, proving ring load gauge, connection fork, sliding shear box, locking clamp, and horizontal dial gauge. The gearbox and electric motor, which applied a constant rate of shear strain during static loading, has a speed adjustment range between 10 and 300 minutes per millimeter. From Table 2, the static loading speed utilized was about 75 minutes per millimeter.

With cyclic loading capabilities available, stress-controlled tests applying square wave loadings were conducted. The loading unit consists of a hydraulic piston connected to a set of pulleys, wires, weights on hangers, and connection forks. A pulse generator and timer controlled a four-way solenoid operated air valve that caused air pressure fluctuation and actuated piston motion. This piston motion, which created the square wave loading used in this investigation, was maintained at a frequency of 0.5 cps.

2.1.4 Trimming Apparatus

The trimming apparatus was developed so that soft and sensitive soil specimens could be trimmed and tested with a minimum of sample disturbance.

The trimming apparatus consists of a base, pedestal, and a set of yokes. The soil specimen was cut into a cylindrical test sample by a system of stainless steel cutting blades. With a minimal amount of handling, a reinforced rubber membrane was mounted on the sample. Proper use of the apparatus resulted in a vertical soil sample with both of its ends being horizontal and parallel.

2.2 Data Acquisition

A proving ring load cell and a DCDT-050 Hewlett Packard Linear Variable Differential Transformer (LVDT) were electrically connected to a stripchart recorder in order to give a graphical representation of the clay's dynamic characteristics. The vertical load proving ring measured vertical loads on the sample.

Pore pressures were determined from the change in vertical stresses used to maintain a constant sample height. The LVDT measured horizontal

displacements of the sample, which were later converted to shear strains. A horizontal dial gauge was also connected to the sample mounting block. As a result, horizontal displacements could be measured by either the LVDT or by the dial gauge, thus providing a crosscheck at all times.

The voltage outputs of the LVDT and load cell were recorded on a four channel recorder. The three output channels utilized in this study consisted of the cyclic shear stress level, the shear strain level, and the pore pressure level.

2.2.1 False Deformation

Some of the changes in vertical stress of the samples could be attributed to the seating and compression of the porous stones. It was important to distinguish the porous stone deformation from the soil sample deformation in order to perform constant volume tests.

The false deformations were measured by inserting a steel dummy sample between the caps. Vertical loads were applied incrementally until consolidation loads were reached, and then unloaded while vertical deformations were measured and recorded.

During soil testing, the deformation curves were entered at the appropriate consolidation (vertical stress), and the vertical loads were further compensated to maintain constant soil heights, and hence constant soil volumes.

2.3 Assumptions and Limitations

Evaluation of NGI direct simple shear test results is contingent on several assumptions. An undrained shear condition is simulated by sustaining a constant soil sample volume. Because a reinforced rubber membrane keeps the sample cross-sectional area essentially constant, a

constant volume test is performed by adjusting the normal vertical load to maintain a constant soil sample height. Measured changes in the vertical normal stress is assumed to equal the changes in excess hydrostatic pressure (pore pressure) in an undrained test.

In addition, shear stresses acting at the center of the soil sample are assumed to be uniform and complementary. As previously, discussed, the NGI direct simple shear apparatus subjects a cylindrical soil sample to a shearing displacement of the top of the sample relative to the bottom. Horizontal and vertical normal compressive stresses are applied and a reinforced rubber membrane constrains the lateral expansion of the soil. This type of loading involves stress distributions that are not exactly symmetrical about the axis of the cylinder. In small test specimens, soil elements are not far from a boundary where shearing is imposed. Therefore, a coupling of shear and normal strains exists in a specimen.

Woods has concluded that because of this complex behavior, an applied shearing strain cannot, in general, produce a uniform distribution of stresses in a soil specimen. In addition, the generation of nonuniform stress conditions causes samples to experience failure at lower applied stresses than those required in the field (20). These differences, however, can be minimized by careful sample preparation and cap seating (20).

It has been concluded by others, however, that the distribution of stresses in an NGI apparatus tested specimen is better than in other conventional direct shear devices (13, 18). Lucks, et al. observed that approximately 70 percent of the stresses can be considered uniform in the

central region of a NGI apparatus tested soil specimen, while stress conditions at the edges are localized (12). Others have supporting evidence indicating that the central region of a NGI apparatus tested specimen experiences quite uniform stresses (18).

2.4 Shear Modulus Values

Shen, Hermann, and Sadigh initially stated that the boundary effects during cyclic loading from a NGI apparatus produce incorrect shear modulus values. Tests that were later conducted by these authors, however, concluded that the shear modulus values obtained from a NGI apparatus agree well with the shear modulus values developed for a corresponding input strain level (18).

The reduction in error is apparently due to boundary effects that are compensated for and minimized by the strain softening nonlinear behavior of soil. Furthermore, test errors introduced by the nonuniform stress conditions stiffen a soil while the edge effects soften it. The stiffening effect is due to higher shear modulus values, for a strain softening material, in those samples experiencing low shear strains attributed to edge effects. A strain softening material indicates that the shear modulus decreased with increasing shear strain.

Consequently, Shen, Hermann, and Sadigh concluded that for strain softening soils such as clay, a NGI direct simple shear apparatus can be used to accurately determine the dynamic shear modulus values during cyclic shear conditions (18).

PART 3

TESTING CRITERIA

3.1 Soil

The undisturbed clay specimens used in this investigation were obtained from a trail cut southeast of Buffalo, New York. Concord Blue clay geotechnical data is listed in Table 1.

Block samples of the clay were cut in the field, encased in wax, and stored in a cool damp container. Core samples for testing were cut from block samples using a fine wire saw. From the sample trimming apparatus, the final trimmed size of the test specimens was 4.763 cm in diameter and varied in height from 1.326 to 2.045 cm after initial consolidation.

Table 2 lists the specimen's geotechnical characteristics and dimensions for each test. As shown in Table 2, there was an insignificant variation in the post consolidation void ratio for each test specimen. Hence, it was assumed that a constant void ratio existed for each soil sample. Consequently, this investigation did not study void ratio effects on the clay's dynamic behavior.

3.2 Testing Procedure

After the clay specimen was removed from its wax encasement, sample trimming was completed. The sample was supported in a reinforced rubber membrane and transferred to the NGI apparatus for consolidation and shearing. The upper and lower caps of the sample were connected to drainage hoses leading to small tanks of water. The water was circulated through the caps and porous stones to insure saturated soil conditions during testing.

The sample was then clamped in the NGI apparatus. The sliding shear box was brought into contact with the top of the sample by a small mass to the normal (vertical) loading lever arm. After the vertical loading lever was leveled and the initial vertical dial reading recorded, consolidation began. Consolidation loads were applied in increments similar to standard laboratory consolidation tests, and the final load was applied for a minimum of 24 hours.

After consolidation, the clay sample was ready for shear loading. In the static and cyclic tests, changes in the vertical stress necessary to maintain constant sample volume were equated to the excess hydrostatic pressure, and noted as pore pressures.

Static loading tests, loaded at small loading rates to minimize strain rate effects, were typically completed in approximately six hours. Stress-
controlled cyclic tests were conducted at a frequency of 0.5 cps with square wave loading applications. Lateral displacements, changes in vertical stress, and the cyclic shear stress level were monitored and recorded on a stripchart recorder during cyclic loading.

PART 4

TEST RESULTS AND ANALYSIS

4.1 Initial Backbone Curves

4.1.1 Curve Determination

Initial backbone curves were obtained by plotting the shear strain as a function of shear stress during the first loading cycle for each of the stress-controlled NGI direct simple shear tests.

4.1.2 Comparison with Static Loading Tests

Figure 1 compares the initial backbone curves with the static loading stress-strain curves tested at various loading rates. The initial backbone curve, derived as the best fit to data, was reproduced in Figure 1 for NC and (OCR=2) clay in addition to static loading tests.

In Figure 1a, a stress-strain curve was obtained from Test 1, a very rapid static loading monotonic undrained test (11.8%/hour) performed at a lower vertical confining stress (1.123 kg/cm^2) than the cyclic loading tests for NC clay (3.369 kg/cm^2). Test 2 was performed at a much lower static loading rate (2.1%/hour) than Test 1 (11.8%/hour), but had the same vertical stress as during cyclic loading. The other set of curves include static loading Tests 9 and 10, performed after cyclic loading on normally consolidated clay. Tests 9 and 10 utilized loading rates of 4.5%/hour and 4.3%/hour, respectively.

From Figure 1, Tests 2 and 9 most accurately represented the initial backbone curve. The prior cyclic loading in Test 9 and Test 10 probably lowered the ultimate shear strength of the NC clay by rearranging and loosening its structure. Therefore, the curves for Tests 9 and 10

resembled the curve for Test 2 at loading strain rates approximately twice that for Test 2. Test 1, which utilized the lowest vertical confining stress (1.123 kg/cm^2) and highest loading rate (11.8%/hour), produced a less stiff and weaker soil structure. Consequently, in spite of the high loading rate, the ultimate shear strength of NC clay in Test 1 was less than that indicated by the initial backbone curve.

The stress path diagram in Figure 3a illustrates the changes in effective stress in a clay specimen subjected to cyclic loading. The effective stress path for a typical undrained static loading test started at point "a" and reached the Mohr-Coulomb failure line at point "g". The static loading effective stress path for a specimen that had experienced previous cyclic loading is represented by the curve between points "h" and "i". Point "i" has a lower shear stress value than at point "g" indicating that the failure shear stress, or clay shear strength, has been reduced by cyclic loading.

The same results are shown in Figure 1b for static loading Test 12, performed on (OCR=2) clay using the same vertical stress as in the cyclic loading tests (1.685 kg/cm^2). Test 12 was performed at a relatively high loading rate (5.0%/hour), and closely simulated the initial backbone curve. The (OCR=2) clay in static loading Test 21, loaded at a slightly higher loading rate (5.6%/hour) than Test 12, had a lower ultimate shear strength attributed to previous cyclic loading. Static loading Test 11, performed at the lowest loading rate (4.2%/hour), yielded the largest shear strength. This was attributed to Test 11 utilizing a vertical confining stress (6.738 kg/cm^2) four times as large as the vertical confining stress in the cyclic loading tests. The higher confining

stress stiffened and strengthened the clay structure to a larger degree.

As previously mentioned, static loading tests initially subjected to cyclic loading developed a reduction in clay stiffness and ultimate shear strength. Figure 2a indicates that for NC clay, the reduction in undrained shear strength from Tests 2 and 9 was approximately 50 percent of the NC clay initial backbone curve. In Figure 2b, (OCR=2) clay in Test 21 also gave an approximate 50 percent reduction of the initial backbone curve. Dobry has determined that this reduction is independent of the cyclic shear stress level and consolidation ratio (4).

Consequently, the stress-strain data acquired from cyclic loading tests was significantly larger than the curve obtained from slow static loading undrained tests. Test results concluded that the stress-strain curves obtained from rapid static loading tests, which were about 50 percent greater than those from slow static loading tests with no prior cyclic loading, agreed with the initial backbone curves in Figures 1 and 2. This 50 percent difference between rapid and slow static loading tests is of the order reported by others (5). Dobry has ascertained that initial backbone curves can be approximated by undrained rapid static loading tests (4).

In summary, Figures 1 and 2 illustrate that for both NC and (OCR=2) clays, the cyclic loading shear strengths were about 50 percent larger than those from static loading tests with previous cyclic loading. In Figure 2b, however, the overconsolidated clay's stress-strain curves for the initial backbone curve and Test 2 intersected at a shear strain of 0.6 percent, indicating possible experimental errors, measurement deviations, or a sudden weakening of the clay structure.

4.1.3 $(G_0)_1$ Values

The initial backbone curve's maximum slope at the origin of Figure 2 signified that the clay structure was the stiffest, since no degradation had occurred. The maximum slope at very small cyclic shear stresses and shear strains defines $(G_0)_1$, the maximum shear modulus during the first loading cycle. Figures 2a and 2b show that $(G_0)_1$ for NC and (OCR=2) clay was 516.7 kg/cm^2 and 437.5 kg/cm^2, respectively. The higher shear modulus value indicated that the normally consolidated clay structure was initially stiffer than (OCR=2) clay. This could be attributed to (OCR=2) clay having a smaller vertical confining stress than that for NC clay.

4.2 Other Cyclic Loading Curves

4.2.1 Curve Determination

Figure 2 indicates that the strength degradation behavior of Concord Blue clay specimens was analyzed from the first through the 400th loading cycle. These curves were obtained by plotting the shear stress and its corresponding shear strain as a function of the number of loading cycles for each test. Subsequent cyclic loading curves plotted below previous loading cycles (i.e., the second loading cycle plotted lower than the first loading cycle, etc.), exhibiting typical soil strength degradation due to cyclic loading.

4.2.2 Clay Behavior

Figures 2a and 2b show the backbone curves for normally consolidated clay and overconsolidated clay, respectively. In Figure 2a, at very low cyclic stresses, a threshold condition existed because there was no variation between the shear strains for the first and subsequent loading

cycles. However, as the critical cyclic stress level line $\overline{PP'}$ was approached in Figure 2a, the shear strains became progressively larger than during the first loading cycle. At line $\overline{PP'}$, soil structure equilibrium was no longer possible in that cumulative cyclic shear strains increased without bound. Figure 2a and Table 2 for NC clay indicate that line $\overline{PP'}$ corresponded to a critical cyclic stress level of 0.184 kg/cm^2. Figure 2b and Table 2 indicate that (OCR=2) clay did not have a threshold condition, but possessed a critical cyclic stress level of 0.067 kg/cm^2.

Andersen ascertained that the critical cyclic stress level is the lowest level that brings the clay's failure strength to the Mohr-Coulomb failure line (1). Figure 3a illustrates that the shear strength at low cyclic stress levels moved from points "a" to "b" during loading and from "b" to "e" during unloading. Points "a" and "e" did not coincide because the clay was not purely elastic, and after one loading cycle, a permanent pore pressure, Δu_p, remained. During a series of loading cycles, permanent pore pressures accumulated, the effective stress reduced, and the effective stress path moved from points "a" to "b" in Figure 3a. At low cyclic stress levels and a large number of loading cycles, Table 2 and Figure 3a indicate that for Tests 9 and 10, the effective stress path moved an insignificant amount toward the failure line.

Concord Blue clay subjected to higher levels of cyclic stress had its effective stress path move from points "a" to "d" during the first cycle due to larger pore pressures being generated. During a certain number of loading cycles, the effective stress path moved quickly to the left and intersected the failure line at point "c". Consequently, the

specimen experienced large shear strains and failed during cyclic loading.

From Figure 3a, the most noticeable difference between Tests 5 and 10 was that the large amount of pore pressure generation in Test 5 caused the effective stress path to intersect the Mohr-Coulomb failure line. That is, nonrecoverable specimen deformations increased with the number of loading cycles in Test 5.

However, the lower cyclic stress level during Test 10 developed a minimal amount of pore pressure accumulation in the clay. This resulted in a nonfailure equilibrium condition because the small amount of pore pressure generation was insufficient to bring the effective stress path to the Mohr-Coulomb failure line. An increase in pore pressure, or a reduction in effective stress, would not exceed point "k" in Figure 3a unless the cyclic shear stress level increased.

From Table 2, undrained cyclic loading for NC and (OCR=2) Concord Blue clay resulted in a reduction in shear strength due to pore pressure accumulation. Clay failure occurred (defined as a soil condition of ±3% shear strain) when the cyclic stress during a test exceeded the critical level of cyclic stress. Sangrey determined that the critical stress level, which separates the failure and nonfailure conditions, is related to the effective stress state of the clay prior to cyclic loading and to the cyclic stress level (14). The results of this study were based on this conclusion.

4.2.3 Secant Shear Modulus Degradation

During stress-controlled cyclic loading tests, a uniform cyclic stress-time history was applied and the shear strain measured. The

secant shear modulus at cycle N, $(G_s)_N$, is equal to the ratio of the shear stress at loading cycle N divided by the shear strain at loading cycle N. Idriss has termed the decrease in the secant shear modulus with the number of loading cycles as "modulus degradation" and attributes it to cyclic loading (9).

Modulus degradation is illustrated in Figure 5, which shows the values of the secant shear modulus calculated from the graphical method mentioned in a study by Idriss (9). The secant shear modulus values in Figure 5 were calculated by dividing the shear stress by the shear strain at specified loading cycles for each test, and are listed in Table 4. Figures 5a and 5b, for NC and (OCR=2) clay respectively, show that tests at lower cyclic stresses yielded higher secant shear modulus values than tests at higher cyclic stresses. This agrees with Figure 3 in that tests at higher cyclic stresses generated larger pore pressures and soil strength degradation than tests at lower cyclic stresses. Consequently, the amount of soil strength degradation was influenced by the amount of pore pressure generation. This concept is thoroughly discussed in Section 4.5.

Figure 6 illustrates the effect of the cyclic stress level on secant shear moduli. In Figure 6, the secant shear moduli decreased as a function of increased normalized cyclic stress levels and number of loading cycles. Figures 6a and 6b both indicate that the secant shear modulus at the first loading cycle was higher than the secant shear modulus from a static loading test, and can be attributed to the strain loading rate. Static loading tests were performed at a strain rate of 2.1%/hour for NC during Test 2 and 5.0%/ hour for (OCR=2) clay during

Test 12, whereas cyclic loading was applied at a frequency of 0.5 cps. In Figure 6a, the secant shear modulus values converged at low cyclic stress levels indicating normally consolidated clay's threshold characteristic. The curves in Figure 6b did not converge at low cyclic stress levels for (OCR=2) clay.

In Figure 7, the secant shear modulus decreased as a function of decreasing normalized effective stresses. Figure 7a illustrates that tests performed at lower levels of cyclic stress developed larger secant shear modulus values for a given effective stress and decreased proportionately less than tests at higher cyclic stresses. This was attributed to NC clay in Tests 9 and 10 developing less pore pressures than Tests 5 and 6. For overconsolidated clay, Figure 7b did not indicate the same trend as in Figure 7a. A single curve could be fitted to the data in Figure 7b to approximate the results of all the tests.

4.2.4 Degradation Index Variation

The degradation index is a measure of the irreversible degradation process and is denoted as " δ " in this study. Idriss defines the degradation index as the ratio of the cyclic stress level of the degraded backbone curve divided by the cyclic stress level of the initial backbone curve at a specified cyclic shear strain (9). The degradation index values for the N^{th} loading cycle is:

$$\delta_N = \overline{B_N C_N} \; / \; \overline{A_N C_N} \qquad (1)$$

in which the equation parameters A_N, B_N, and C_N are defined in Figure 2.

Figure 8 illustrates that cyclic loading developed lower strengths

because the δ_N values decreased, or strength degradation increased, as the number of loading cycles increased. The degradation index curves, evaluated at different cyclic stress levels and numbers of loading cycles, converged at a low cyclic stress of 0.119 kg/cm^2, indicating that a threshold condition existed for normally consolidated clay. In Figure 8b, (OCR=2) clay did not exhibit a threshold condition because the degradation index curves remained parallel at very low cyclic stress levels.

However, Figures 8a and 8b both reveal a noticeable increase in the degradation indexes, or a reduction in soil strength deterioration, at higher cyclic stress levels. Dobry's explanation for the increase in degradation indexes is illustrated by the degradation of the initial backbone curve at high levels of cyclic stress in Figure 8c (4). From Figure 8c, lines "1" and "2", at higher cyclic stresses, experienced less degradation than at lower cyclic stresses depicted by lines "3" and "4". Consequently, degradation of the initial backbone curve at high cyclic stress levels produced larger degradation index values than those at low stress levels.

4.2.5 Synopsis

Sangrey and Andersen have concluded that the critical level of cyclic stress depends primarily on the consolidation history of a clay. In addition, they have determined that an ultimate failure condition or nonfailure equilibrium condition resulting from cyclic loading is also dependent on the cyclic shear stress level (1, 14). This study will discuss the influence of the cyclic stress level on the amount of pore pressure generation, the number of loading cycles to achieve a failure

condition, and the effective stress state of the Concord Blue clay.

4.3 Effect of Cyclic Shear Stress Level

4.3.1 Total Stress Level

The magnitude of change in pore pressure and shear strain generation during cyclic loading depended on the cyclic shear stress level. This level can be defined as the degree of strength mobilization on a total stress basis from the equation,

$$(SSL)_T = \frac{\tau_{hc}}{S_u} \qquad (2)$$

in which τ_{hc}, the horizontal cyclic shear stress, is normalized with respect to S_u, the undrained ultimate shear strength for static loading. The static loading tests, used for normalizing Equation 2, most accurately simulated the initial backbone curves for NC and (OCR=2) clay in Figure 1. The clay used in Tests 2 and 12 developed ultimate shear strengths of 0.734 kg/cm^2 and 0.700 kg/cm^2, respectively.

The behavior of the NC and (OCR=2) clays during undrained cyclic loading is summarized in Figures 13a and 13b. The total cyclic stress level, $(SSL)_T$, was plotted as a function of the number of loading cycles necessary to develop a failure condition of ±3.0% shear strain. Sangrey ascertained that the highest level of nonfailure equilibrium corresponds to the limit of failure, or the critical level of cyclic stress (14). Figure 13 indicates that NC and (OCR=2) Concord Blue clay developed critical stress levels of approximately 26.0 percent and 14.0 percent of the static undrained shear strength. These critical stress levels approximated the cyclic stresses in Tests 10 and 21.

Figures 2 through 13 illustrate the strength degradation process of

Concord Blue clay. This process, manifested by shear strain accumulation, progressively decreased the secant shear modulus and degradation index values as a function of increasing cyclic stress levels. An example of strength degradation is illustrated during Tests 5 and 13 in Figures 10, 11, and 12. Substantial strength degradation did not occur for Tests 9 and 21, as shown in Figures 10 and 12.

Figure 10 indicates that the cyclic shear stress level was an important parameter in determining Concord Blue clay failure or nonfailure conditions. In each part, tests with higher cyclic stress levels (Tests 5, 6, 13, and 17) produced larger shear strains at a specified normalized pore pressure. Figures 9, 12, and 13 illustrate that higher cyclic stress levels caused the clay to reach a failure condition at a lower number of loading cycles because the shear stains increased more quickly at lower normalized pore pressures. Extremely low cyclic stress levels produced a nonfailure equilibrium condition in the clay, as evidenced by a stabilization of shear strains and pore pressures in Tests 9, 10, and 21.

Examples of the development of shear strains and pore pressures as a function of the cyclic stress level are presented in Figures 10 and 12. The number of loading cycles to produce a failure condition increased rapidly for decreasing cyclic stress levels. As shown in Figure 14a, a total stress level less than 0.25 for the NC clay, caused cyclic loading to have a negligible effect on development of the specified shear strain levels of 0.5, 1.0, 1.5, and 3.0 percent. The total stress level of 0.184 kg/cm^2, approximately 0.25 of the static undrained shear strength in Test 2 (0.734 kg/cm^2), corresponded to the critical stress level of

0.180 kg/cm^2 in Figures 2a and 13a. Figure 14b shows that the (OCR=2) clay possessed a critical stress level of approximately 0.14 of the static undrained shear strength from Test 12 (0.700 kg/cm^2). This critical stress level, calculated to be 0.100 kg/cm^2, corresponded to the critical stress level in Figures 2b and 13b.

4.3.2 Effective Stress Level

Andersen has concluded that the cyclic shear stress level can also be defined on an effective stress basis,

$$(SSL)_E = \frac{\tan \phi_{MOBILIZED}}{\tan \phi} \qquad (3)$$

in which ϕ is the angle of internal friction (1). Figure 3a illustrates the procedure for obtaining the ϕ parameter in Equation 3. For the effective stress principle to be utilized, a reliable prediction of pore pressures had to be made for different cyclic stress levels.

In Figure 15, cyclic strains were plotted as a function of the effective stress level for tests with different types of cyclic loading performed on Drammen clay (1). Figure 15 contains data from triaxial and simple shear tests using one-way and two-way cyclic loadings at a frequency of 0.1 cps. In addition, the Drammen clay had consolidation ratios of 1, 2, 4, and 10. Andersen determined that the relationship between the cyclic stress level and its associated shear strains is independent of the number of loading cycles (1).

The results of Tests 5 through 10 using NC Concord Blue clay and Tests 13 through 18, and 21 using (OCR=2) Concord Blue clay were included in Figure 15 for comparison. In this investigation, Concord Blue clay

was tested at a frequency of 0.5 cps.

The good agreement in Figure 15 revealed that one characteristic curve, based on effective stresses, could reasonably describe the dynamic behavior of both clays. Consequently, the good correlation between the normally consolidated and overconsolidated Drammen clay and Concord Blue clay indicated that the dynamic behavior of clays could be explained by considering effective stresses.

Figure 7 relates the secant shear modulus to the normalized effective confining stress ($\bar{\sigma}_v/\bar{\sigma}_{vo}$), in which $\bar{\sigma}_{vo}$ is the initial effective confining stress. Figure 7 discloses that the clay was stiffest when the effective confining stress was at its maximum value. As cyclic loading progressed, permanent pore pressures accumulated and normalized effective stresses decreased. At high cyclic stress levels, an increase in the pore pressures caused the effective stress path to intersect the Mohr-Coulumb failure line, as indicated in Figure 3 for Tests 5 and 17. For Tests 9 and 21 (performed at low cyclic stresses), the shear strains and pore pressures increased to a limiting level after which a large number of loading cycles did not produce a change in the effective stresses. Consequently, the effective stress paths for Tests 9 and 21 remained far to the right of the failure line.

4.4 Effect of Number of Loading Cycles

Table 2 shows the cyclic stress-strain behavior of NC and (OCR=2) clays during undrained stress-controlled cyclic loading conditions. As presented in Figure 11, the cyclic stress level during Test 5, maintained at ± 0.353 kg/cm^2, caused the shear strain to increase from ± 0.19 percent during the first loading cycle to ± 1.02 percent for the 400th loading

cycle.

In addition, the development of symmetrically assumed shear strains and pore pressures with an increasing number of loading cycles is depicted in Figures 11 and 12. The increase in pore pressure was relatively small at first, but after 300 loading cycles, the pore pressures increased rapidly. After 520 loading cycles, the pore pressure was 2.9 kg/cm^2. Figure 11 also illustrates that there was extremely good correlation between the rate of increase in shear strains with respect to the rate of pore pressure accumulation.

Figures 5, 11, and 12 illustrate that the clay became increasingly less stiff for an increasing number of loading cycles. Figures 2 and 12 indicate that for all cyclic stress levels above the critical stress level, shear strains increased and secant shear moduli decreased with the number of loading cycles. In addition, Figure 8 shows that as the number of loading cycles increased, the degradation index decreased.

4.5 Effect of Pore Pressure Changes

Andersen and Sangrey concluded that pore pressure accumulation resulting from cyclic loading controls the effective stress conditions in clay, and consequently its ultimate dynamic behavior (1, 14). In Figure 7, the secant shear moduli decreased as pore pressure generation increased in the clay. Figure 9 shows that the degradation indexes decreased, or the amount of strength degradation increased, for increasing values of pore pressure. This indicated that the amount of pore pressure accumulation determined the degree of soil strength degradation. Figure 9 also illustrates that the normally consolidated Concord Blue clay produced only positive pore pressures while the

overconsolidated clay generated both negative and positive pore pressures.

As shown in Figure 10, the increase in shear strains was a function of the increase in pore pressures. In addition, Figure 10 indicates that as the normalized pore pressure values approached approximately 0.85, the Concord Blue clay experienced extremely high shear strains. Figure 10 also shows that the shear strain curves at a specified normalized pore pressure value were different for each test. This indicated that pore pressure accumulation did not completely describe the Concord Blue clay's dynamic behavior. As previously mentioned, other factors considered were the number of loading cycles and more importantly, the cyclic shear stress level.

PART 5

CYCLIC LOADING MODELS

5.1 Ramberg-Osgood Model

Degradation in soils due to cyclic loading has been recognized for many years, but it has not been explicitly incorporated into current methods of analysis until the last few years (9). The initial backbone and other backbone curves can be expressed in various forms, either in terms of discrete experimental cyclic stress-strain coordinates, or as a function of mathematical modelling equations. For the purpose of application to clays, several simple mathematical models have been developed. These include the bilinear (9), multi-linear (9,10), hyperbolic, and Ramberg-Osgood models (3,9,10). In this study, the Ramberg-Osgood (R-O) formulation was adopted and analyzed (9).

The equation of the R-O initial backbone curve is (9):

$$(\gamma_c)_1 = \gamma_y \left[\frac{\tau_c}{(G_0)_1 \gamma_y}\right]\left[1 + \alpha\left|\frac{\tau_c}{(G_0)_1 \gamma_y}\right|^{R-1}\right] \qquad (4)$$

Values of the secant shear modulus for the first cycle, $(G_s)_1$, can be explicitly derived as a function of the same equation parameters:

$$(G_s)_1 = \frac{(G_0)_1}{1 + \alpha\left[\tau_c \,/\, (G_0)_1 \gamma_y\right]^{R-1}} \qquad (5)$$

Equations 4 and 5 consist of the same terms and are derived in Section 5.1.1. γ_y is the reference strain, α and R are dimensionless constants, $(G_o)_1$ is the maximum shear modulus during the first cycle at very low

shear strains as shown in Figure 2, and $(\gamma_c)_1$ and τ_c are points on the initial backbone curve describing the coordinates of hysteresis loops (9). Idriss concluded that writing the R-O formulation in this manner allows the use of non-integer values of R, thus providing more flexibility in simulating experimental data (9).

Consequently, the Ramberg-Osgood model was utilized to describe the nonlinear and degraded cyclic stress-strain behavior of Concord Blue clay. Potential applications of the proposed model to experimental results are discussed in Section 5.1.3.

5.1.1 Derivation of R-O Parameters

A backbone curve for a given loading cycle describes the coordinates defining the tips of hysteresis loops measured during that particular loading cycle. R-O backbone curves can be fitted from the appropriate selection of R-O parameters.

5.1.1.1 γ_y and $(G_o)_1$ Determination

Idriss has defined γ_y, the reference strain, as the shear strain at which the backbone curve initially becomes nonlinear (9). Figure 16 indicates that the NC and (OCR=2) clays had reference strains of 0.016 percent and 0.013 percent, respectively.

$(G_o)_1$ is the maximum slope of the initial backbone curve. The $(G_o)_1$ values, calculated in Figures 2a and 2b for the NC and (OCR=2) clay, were 516.7 kg/cm^2 and 437.5 kg/cm^2, respectively.

5.1.1.2 R Determination

A procedure utilized by Idriss (9) for the direct determination of R was used as an initial estimate of R. At large shear strains, Equation 4 can be simplified to:

$$\gamma_c \text{ proportional to } \tau_c^R$$

or (6)

$$\log \gamma_c \text{ proportional to } R \log \tau_c$$

Therefore, a graph of log γ_c versus log τ_c yields a straight line whose slope equals R. The coordinates describing the tips of hysteresis loops during the first cycle are presented in Figure 17. The line that provided the best fit to the data points had a slope of R=2.9 for both the normally consolidated and overconsolidated Concord Blue clay.

5.1.1.3 α (Alpha) Determination

Once γ_y, $(G_o)_1$, and R were selected, Equation 4 was used directly to calculate alpha at a given shear stress and shear strain for each test. Table 3 shows that the scatter in alpha values ranged from 0.01 to 0.30 for NC clay and from 0.10 to 1.0 for (OCR=2) clay. The average alpha values were 0.155 for NC clay and 0.215 for (OCR=2) clay. These values, which correlated well with the alpha values obtained by Idriss (9), were incorporated into Equations 4 and 5.

Substituting the previously calculated values of γ_y, $(G_o)_1$, R_1 and α into Equation 4 yielded the following relationships for the initial backbone curve for NC clay,

$$\gamma_c = 0.016 \left[\frac{\tau_c}{0.083}\right]\left[1 + 0.155\left(\frac{\tau_c}{0.083}\right)^{1.9}\right] \quad (7)$$

and for (OCR=2) clay,

$$\gamma_c = 0.013 \left[\frac{\tau_c}{0.070}\right]\left[1 + 0.215\left(\frac{\tau_c}{0.070}\right)^{1.9}\right] \quad (8)$$

in which γ_c was expressed in percentage and τ_c in kg/cm^2.

5.1.2 Other Cyclic Loading Curves

Test results could also be used to predict the behavior of Concord Blue clay after the first loading cycle. As previously defined, the degradation index during the N^{th} cycle, δ_N, is equal to the ratio of the shear stress during the N^{th} cycle divided by the shear stress for the first cycle at a specified shear strain. Consequently, the shear stress during the N^{th} cycle is equal to the product of the shear stress during the first cycle and the degradation index during the N^{th} cycle, or

$$(\tau_c)_N = [\delta_N (\tau_c)_1]_{\text{AT A SPECIFIED } (\gamma_c)_N} \tag{9}$$

Incorporating Equation 9 into Equation 4 yields (9):

$$(\gamma_c)_N = \gamma_y \left[\frac{\tau_c}{\delta_N (G_0)_N \gamma_y}\right]\left[1 + \alpha\left|\frac{\tau_c}{\delta_N (G_0)_N \gamma_y}\right|^{R-1}\right] \tag{10}$$

For the first cycle, δ_1 equalled one and Equation 10 reduced to Equation 4. As cyclic loading progressed, δ_N became less than one, and the backbone curves in Equation 10 reduced accordingly. The results of Equation 10 are plotted in Figure 18 and compared to the initial backbone curves from experimental data in Section 5.1.3.1.

Secant shear modulus values during the N^{th} loading cycle, $(G_s)_N$, can be explicitly derived as a function of the R-O parameters in Equation 5. For the Nth loading cycle, Equation 5 becomes (9),

$$(G_s)_N = \frac{\delta_N (G_0)_1}{1 + \alpha[\tau_c / \delta_N (G_0)_1 \gamma_y]^{R-1}} \qquad (11)$$

and is plotted in Figures 5 and 19.

5.1.3 Comparison with Experimental Results

5.1.3.1 Backbone Curves

Having derived an expression representing the backbone curves for NC and (OCR=2) clay, it was possible to examine the accuracy of the R-O model for fitting experimental data.

Backbone curves in Figure 18, obtained by using Equations 7, 8, and 10, were compared with experimental results. From Figure 18, a comparison between the initial backbone curves disclosed that the predicted backbone curves accurately simulated the experimental curves at lower and moderate cyclic stress levels, but did not simulate the test data as well at larger levels. However, the overconsolidated clay yielded a better correlation than did the normally consolidated clay, for the entire range of cyclic stress levels.

Dobry's explanation for this discrepancy at higher cyclic stresses and shear strains is that the Ramberg-Osgood model does not account for initial degradation of the initial backbone curve, and therefore will plot above the experimental curve (4).

5.1.3.2 R-O Model Sensitivity

Table 3 presents shear stresses and shear strains calculated from Equation 4 during the first cycle for a large range of R and γ_y values. The R values ranged from 2.5 to 3.0 for both clay types, while the range of γ_y values was from 0.0125 to 0.0190 percent shear strain. The

variation of R and γ_y values in Data Table 3 indicates that the R-O model was more sensitive to changes in the R parameter than to the reference strain, γ_y. Consequently, a lower correlation between the R-O model and experimental data existed as the R value varied, particularly at higher cyclic stresses.

The R and γ_y values determined in this study yielded the best correlation between the R-O model and experimental initial backbone curves. Figures 18a and 18b illustrate that the R-O parameters R and γ_y, initially derived in Sections 5.1.1.1 and 5.1.1.2, accurately predicted the dynamic behavior of the Concord Blue clay.

5.1.3.3 Secant Shear Moduli

Figure 5 illustrates a relatively good correlation between the graphically derived secant shear modulus values and the predicted values from R-O Equations 5 and 11. The agreement, however, was better at larger cyclic stresses and larger number of loading cycles for both the NC and (OCR=2) clay.

Figure 19 indicates a closer correlation between the $(G_s)_N$ values at lower shear strains than at higher shear strains, when the secant shear moduli was normalized with respect to the maximum secant shear modulus for each test.

PART 6

DISCUSSION AND CONCLUSIONS

The results obtained in this investigation indicated the following characteristics of Concord Blue clay:

6.1 Test Parameter Results

6.1.1 Number of Loading Cycles

Soil strength degradation developed with an increasing number of loading cycles for tests performed at cyclic stress levels greater than the critical level of cyclic stress. In these tests, the secant shear modulus and degradation index values decreased while the shear strains and pore pressures accumulated as a function of the number of loading cycles. However, as evidenced by test data, a large number of loading cycles generated a limiting value of shear strains and pore pressures in some tests, compared to large increases in shear strains and pore pressures in other tests. Consequently, to describe the dynamic behavior of the clay, other test parameters must also be considered.

6.1.2 Pore Pressure and Effective Stress Changes

Experimental results indicated that the degree of soil degradation was associated with the amount of pore pressure accumulation. A decrease in the effective stress (or an increase in pore pressure) degraded the clay structure, as manifested by the effective stress path moving toward the Mohr-Coulomb failure line. Some tests did not develop large pore pressures and shear strains. Instead, limiting values were reached after a certain number of loading cycles. In addition, as indicated by Figure 10, normalized pore pressures did not reach comparable values at the clay

failure condition (± 3.0% strain) for each test. Therefore, the clay failure condition was also a function of other test parameters.

6.1.3 Cyclic Shear Stress Level

Experimental results indicated that Concord Blue clay tests that experienced higher cyclic stress levels required a smaller number of loading cycles to generate a specified shear strain and pore pressure level than at lower cyclic stresses. In addition, a critical level of cyclic stress existed in which cyclic stresses smaller than the critical stress level created a state of nonfailure equilibrium. Cyclic stresses greater than the critical stress level eventually produced a failure condition. Consequently, the dynamic behavior of Concord Blue clay was considerably affected by the cyclic stress level.

6.2 Comparison Between NC and (OCR=2) Clays

6.2.1 Similarities

The elastic state in clays is indicated by the condition in which no residual shear strains remained after an applied shear stress is removed. Applied cyclic stresses less than the critical stress level develop an insignificant amount of pore pressure accumulation. This critical stress level can be considered as an approximation to the upper limit of elastic properties. In this study, cyclic stresses larger than the critical stress level carried the clay beyond its elastic range. Cumulative pore pressure increases, associated with a reduction in effective stress caused the effective stress path to move toward and eventually intersect the Mohr-Coulomb failure line.

It was concluded from cyclic test results that:

- Cyclic shear strains and pore pressures increased gradually until

failure was imminent, after which they increased very rapidly.

- Cyclic loading failure did not occur if the cyclic shear stress was below the critical level of repeated stress.
- The shear modulus was found to decrease gradually until failure was imminent; thereafter the shear modulus rapidly decreased.

6.2.2 Differences

Experimental results yielded the following comparisons between the two clay types:

- The normally consolidated clay exhibited both a threshold condition and a critical level of cyclic stress. The overconsolidated clay did not develop a threshold condition, but exhibited a critical cyclic stress level.
- The critical cyclic stress level was found to be 25% of the static shear strength for the NC clay and 14% of the static shear strength for the (OCR=2) clay.
- The backbone curves for the NC clay generated lower shear strains than the (OCR=2) clay at specified cyclic shear stresses.
- At comparable cyclic shear stresses and shear strains, the shear moduli and degradation index values were larger for the NC clay than the (OCR=2) clay.
- For the normally consolidated clay, a larger pore pressure accumulation and a larger number of loading cycles were required to develop a specified shear strain.

6.3 Ramberg-Osgood Modelling Results

A good correlation between the experimentally and mathematically derived backbone curves were obtained for lower to moderate cyclic stress

levels. The agreement was somewhat less at higher cyclic stress levels. This could be attributed to the degradation of the experimentally derived initial backbone curves. The overconsolidated clay yielded better agreement than normally consolidated clay for the entire range of cyclic stress levels.

6.3.1 Model Sensitivity

The R-O model was found to be more sensitive to the variation of R values than γ_y values. However, the R and γ_y values calculated in this investigation yielded the best correlation between the experimentally and R-O mathematically derived backbone curves.

6.3.2 Secant Shear Moduli Comparison

A good correlation was obtained between secant shear modulus values derived from experimental data and the Ramberg-Osgood model.

PART 7

REFERENCES

1. Andersen, K. H. (1976), "Behavior of Clay Subjected to Undrained Cyclic Loading", Proc., International Conf. on the Behavior of Offshore Structures, Norwegian Institute of Technology, Trondheim, Vol. 1, pp. 392-403.

2. Castro, G. and Christian, J. T. (1976), "Shear Strength of Soils and Cyclic Loading", Journal of the Geotechnical Engineering Division, ASCE, Vol. 102, No. 6T9, pp. 887-894.

3. Dobry, R. (1970), "Damping in Soils: Its Hysteretic Nature and the Linear Approximation", Soils Publication No. 253, Department of Civil Engineering, Massachusetts Institute of Technology, Cambridge, Mass.

4. Dobry, R. (1977), "Stress-Strain Behavior of Soils During Cyclic-Dynamic Loading", Proc., 14th Annual Meeting Society of Engineering Science, Lehigh University, Bethlehem, Pa., pp. 1181-1189.

5. Duncan, J. M. and Dunlop, P. (1969), "Behavior of Soils in Simple Shear Tests", Proc., 7th ICSMFE, Mexico City, Vol. 1, pp. 101-109.

6. Geonor (1968), "Description and Instruction for Use of Direct Simple Shear Apparatus h-12", Geonor A/S, Oslo.

7. Hardin, B. O. and Drnevich, V. P. (1972), "Shear Modulus and Damping in Soils: Design Equations and Curves", Journal of Soil Mechanics and Foundations Division, ASCE, Vol. 98, No. SM7, pp. 667-692.

8. Hardin, B. O. and Drnevich, V. P. (1972), "Shear Modulus and Damping in Soils: Measurement and Parameter Effects", Journal of Soil Mechanics and Foundations Division, ASCE, Vol. 98, No. SM6, pp. 603-624.

9. Idriss, I. M., Dobry, R., and Singh, R. D. (1978), "Non-Linear Behavior of Soft Clays During Cyclic Loading", Journal of Geotechnical Engineering Division, ASCE, Vol. 104, No. GT12, pp. 1427-1447.

10. Idriss, I. M. Dobry R., Singh, R. D., and Doyle, E. H. (1976), "Behavior of Soft Clays Under Earthquake Loading Conditions", Proc., Offshore Technology Conference, OTC 2671, Dallas, Texas.

11. Ladd, C. C. and Edgers, L. (1972), "Consolidated Undrained Direct-Simple Shear Tests on Saturated Clays", Soils

Publication No. 284, Dept. of Civil Engineering, Massachusetts Institute of Technology, Cambridge, Mass.

12. Lucks, A. S., Christian, J. T., Brandow, G. E., and Hoeg, K. (1972), "Stress Conditions in NGI Simple Shear Test", Journal of Soil Mechanics and Foundations Division, ASCE, Vol. 98, No. SM1, pp. 155-160.

13. Prevost, J. H. and Hoeg, K. (1976), "Reanalysis of Simple Shear Soil Testing", Canadian Geotechnical Journal, Vol. 13, pp. 418-429.

14. Sangrey, D. A. (1971), "Changes in Strength of Soils Under Earthquake and Other Repeated Loading", Proc., First Canadian Conf. on Earthquake Engineering, Vancouver, pp. 82-96.

15. Sangrey, D. A., Castro, G., Poulos, S. J., and France, J. W. (1978), "Cyclic Loadings on Sand, Silts, and Clays", Proc., Earthquake Engineering and Soil Dynamics, ASCE Specialty Conf., Pasadena, pp. 836-851.

16. Sangrey, D. A., Henkel, D. J., and Esrig, M. I. (1969), "The Effective Stress Response of a Saturated Clay to Repeated Loading", Canadian Geotechnical Journal, Vol. 6, pp. 241-252.

17. Sangrey, D. A., Pollard, W. S., and Egan, J. A. (1976), "Effects of Rate of Testing on the Undrained Cyclic Behavior of Clay Soils", Final Report, School of Civil and Environmental Engineering, Cornell University, Ithaca, New York.

18. Shen, C. K., Hermann, L. R., and Sadigh K. (1978), "Analysis of Cyclic Simple Shear Test Data", Proc., Earthquake Engineering and Soil Dynamics, ASCE Specialty Conf., Pasadena, pp. 864-874.

19. Wilson, N. E. and Greenwood, J. R. (1974), "Pore Pressures and Strains After Repeated Loading of Saturated Clay", Canadian Geotechnical Journal, Vol. 11, pp. 269-277.

20. Woods, R. D. (1978), "Measurement of Dynamic Soil Properties", Proc., Earthquake Engineering and Soil Dynamics, ASCE Specialty Conf., Pasadena, pp. 99-178.

21. Yoshimi, Y., Richart, F. E. Jr., Prakash, S., Barkan, D. D., and Ilyichev, V. A. (1977), "Soil Dynamics and Its Application to Foundation Engineering", Proc., 9th ICSMFE, Tokyo, Vol. 2, pp. 605-647.

22. Zimmie, T. F. and Floess, C. H. L. (1979), "Simple Shear Behavior of Fine Grained Soils Subjected to Earthquake and Other Repeated Loading", National Science Foundation Directorate for Applied Science and Research Applications (ASRA), Final Report, March 1979, Rensselaer Polytechnic Institute, Department of Civil Engineering.

PART 8

TABLES

TABLE 1. GEOTECHNICAL DATA FOR CONCORD BLUE CLAY

CONCORD BLUE CLAY

SITE: SE OF BUFFALO, N. Y.

TYPE: UNDISTURBED 1 ft^3 BLOCKS

GEOTECHNICAL DATA	
WATER CONTENT	27 - 28%
LIQUID LIMIT	34%
PLASTIC LIMIT	21%
SPECIFIC GRAVITY	2.76
Ø	25^o
SENSITIVITY (FALL CONE)	1.4
CONSOLIDATION HISTORY	NORMALLY CONSOLIDATED

1	2	3	4	5	6	7	8	9	10	11	12	13	14	15
		BEFORE TEST							CONSOLIDATION					
Test No.	D	w %	e	H_i cm	S_u kg/cm^2	S_u kg/cm^2	S_u kg/cm^2	S_t	σ_{vo} kg/cm^2	τ_{ho} kg/cm^2	σ_{vm} kg/cm^2	OCR	H_f cm	ϵ_v %
01S	S	28.4	.785	1.75	-	-	-	-	1.12	0.0	1.12	1.0	1.69	3.4
02S	S	27.8	.767	1.54	1.00	.60	.58	-	3.37	0.0	3.37	1.0	1.44	6.6
03														
04														
05C	S	28.2	.781	1.49	.80	.40	.46	-	3.37	0.0	3.37	1.0	1.44	3.0
06C	S	28.1	.776	1.97	.75	-	-	-	3.37	0.0	3.37	1.0	1.84	6.6
07C	S	27.4	.759	2.05	-	-	-	-	3.37	0.0	3.37	1.0	1.90	6.9
08C	S	27.6	.762	1.58	-	-	-	-	3.37	0.0	3.37	1.0	1.47	6.9
09C/S	S	27.0	.759	1.42	.80	-	-	-	3.37	0.0	3.37	1.0	1.33	6.8
10C/S	S	27.9	.770	1.49	-	-	-	-	3.37	0.0	3.37	1.0	1.39	6.4
11S	S	28.5	.787	2.03	-	-	.31	-	3.37	0.0	6.74	2.0	1.91	5.5

TABLE 2. SUMMARY OF TESTS - CONCORD BLUE CLAY

1	2	3	4	5	6	7	8	9	10	11	12	13	14	15
		BEFORE TEST							CONSOLIDATION					
Test No.	D	w %	e	H_i cm	S_u kg/cm^2	S_u kg/cm^2	S_u kg/cm^2	S_t	σ_{vo} kg/cm^2	τ_{ho} kg/cm^2	σ_{vm} kg/cm^2	OCR	H_f cm	ϵ_v %
12S	S	29.2	.806	1.74	.60	-	.31	-	1.68	0.0	3.37	2.0	1.61	7.7
13C	S	29.1	.803	1.52	.75	.35	.31	-	1.68	0.0	3.37	2.0	1.41	7.4
14C	S	28.6	.789	1.77	.70	-	.31	-	1.68	0.0	3.37	2.0	1.63	7.7
15C	S	28.5	.787	1.78	.75	.40	.37	-	1.68	0.0	3.37	2.0	1.65	7.3
16C	S	29.2	.806	1.98	.80	.40	.37	-	1.68	0.0	3.37	2.0	1.84	7.2
17C	S	29.8	.822	1.89	.75	.40	.37	-	1.68	0.0	3.37	2.0	1.74	8.3
18C	S	29.5	.817	1.54	.75	.45	.37	-	1.68	0.0	3.37	2.0	1.39	9.4
19C														
20C														
21C/S	S	29.2	.806	1.78	.75	.35	-	-	1.68	0.0	3.37	2.0	1.63	8.2

TABLE 2. (CONTINUED)

	16	17	18	19	20	21	22	23	24	25	26	27	28
	CYCLIC LOADING						STATIC LOADING				AFTER TEST		
Test No.	τ_c kg/cm^2	τ_c/S_u %	N	γ_N %	u_N kg/cm^2	f Hz	S_u kg/cm^2	γ_f %	u_f kg/cm^2	RATE min/mm	w %	e	Remarks
01S	-	-	-	-	-	-	.347	12.2	.302	30	28.7	.792	No corrections
02S	-	-	-	-	-	-	.744	10.3	1.260	200	-	-	
03													Large Stone in Sample
04													Large Stone in Sample
05C	.352	48	570	28.1	3.044	.5	-	-	-	-	26.0	.718	
06	.437	59	27	9.2	2.621	.5	-	-	-	-	25.1	.693	
07C	.296	40	1360	10.7	2.923	.5	-	-	-	-	25.5	.704	
08C	.212	29	5960	14.4	3.024	.5	-	-	-	-	26.5	.731	
09C/S	.156	21	3000	.04	.292	.5	.772	8.63	1.310	100	25.8	.712	
10C/S	.184	25	5000	.13	.726	.5	.675	14.1	1.613	100	-	-	
11S	-	-	-	-	-	-	1.106	10.4	.171	75	25.1	.693	

TABLE 2. (CONTINUED)

	16	17	18	19	20	21	22	23	24	25	26	27	28
	CYCLIC LOADING						STATIC LOADING				AFTER TEST		
Test No.	τ_c kg/cm^2	τ_c/S_u %	N	γ_N %	u_N kg/cm^2	f Hz	S_u kg/cm^2	γ_f %	u_f kg/cm^2	RATE min/mm	w %	e	Remarks
12S	-	-	-	-	-	-	.692	12.5	-.020	75	27.4	.756	
13C	.219	32	625	12.0	1.411	.5	-	-	-	-	26.5	.731	
14C	.191	28	789	11.7	1.512	.5	-	-	-	-	26.5	.731	
15C	.163	24	3630	11.3	1.512	.5	-	-	-	-	26.6	.734	
16C	.185	27	1286	9.2	1.411	.5	-	-	-	-	26.4	.729	
17C	.350	51	30	15.6	1.210	.5	-	-	-	-	26.8	.740	
18C	.124	18	4280	8.5	1.462	.5	-	-	-	-	26.9	.742	
19C						.1							Freq. of .1 cps
20C						.1							Freq. of .1 cps
21C/S	.067	10	6000	.05	-.010	.5	.568	11.0	.161	75	26.0	.718	

TABLE 2. (CONTINUED)

TABLE 2 APPENDIX. EXPLANATIONS FOR TABLE 2

COLUMN	EXPLANATION
1.	S = Static Loading Test, C = Cyclic Loading Test, C/S = Test with both loadings
2.	Sample Size : L = Large, S = Small
3.	Water Content of Trimmings
4.	Void Ratio of Trimmings
5.	Sample Height
6.	Undrained Shear Strength (Pocket Penetrometer)
7.	Undrained Shear Strength (Torvane)
8.	Undrained Shear Strength (Swedish Fall Cone)
9.	Sensitivity (Swedish Fall Cone)
10.	Vertical Consolidation Stress
11.	Static Shear Stress
12.	Maximum Consolidation Stress
13.	Overconsolidation Ratio
14.	Sample Height Following Consolidation
15.	Vertical Strain
16.	Cyclic Shear Stress
17.	Cyclic Shear Stress as a Percentage of Static Strength
18.	Number of Cycles Tested (N_T)
19.	Shear Strain at N_T Cycles
20.	Pore Pressure at N_T Cycles
21.	Frequency of Loading
22.	Static Undrained Shear Strength (Peak of Stress-Strain Curve)
23.	Shear Strain at Peak of Stress-Strain Curve

24. Pore Pressure at Peak of Stress-Strain Curve

25. Strain Rate

26. Water Content of Sample (After Test)

27. Void Ratio of Sample (After Test)

TABLE 3

FIRST CYCLE BEHAVIOR OF (OCR=1) CLAY

TEST	G(GRAPH) (KG/CM 2)	G RATIO	DAMPING RATIO R= 2.5	2.6	2.7	2.8	2.9	3.0	ALPHA R= 2.5	2.6	2.7	2.8	2.9	3.0	GAMMA Y
5	176.50	0.3416	0.180	0.186	0.193	0.199	0.204	0.210	0.128	0.108	0.091	0.077	0.065	0.055	0.000125
5	176.50	0.3416	0.180	0.186	0.193	0.199	0.204	0.210	0.152	0.129	0.110	0.094	0.080	0.069	0.000140
5	176.50	0.3416	0.180	0.186	0.193	0.199	0.204	0.210	0.168	0.145	0.124	0.107	0.092	0.079	0.000150
5	176.50	0.3416	0.180	0.186	0.193	0.199	0.204	0.210	0.185	0.160	0.139	0.120	0.104	0.090	0.000160
5	176.50	0.3416	0.180	0.186	0.193	0.199	0.204	0.210	0.203	0.177	0.154	0.134	0.116	0.101	0.000170
5	176.50	0.3416	0.180	0.186	0.193	0.199	0.204	0.210	0.212	0.185	0.161	0.141	0.123	0.107	0.000175
5	176.50	0.3416	0.180	0.186	0.193	0.199	0.204	0.210	0.221	0.193	0.169	0.148	0.130	0.113	0.000180
5	176.50	0.3416	0.180	0.186	0.193	0.199	0.204	0.210	0.240	0.211	0.186	0.163	0.144	0.126	0.000190
6	97.10	0.1879	0.222	0.230	0.238	0.245	0.252	0.258	0.286	0.236	0.195	0.161	0.133	0.110	0.000125
6	97.10	0.1879	0.222	0.230	0.238	0.245	0.252	0.258	0.339	0.283	0.236	0.198	0.165	0.138	0.000140
6	97.10	0.1879	0.222	0.230	0.238	0.245	0.252	0.258	0.376	0.316	0.266	0.224	0.188	0.158	0.000150
6	97.10	0.1879	0.222	0.230	0.238	0.245	0.252	0.258	0.414	0.350	0.297	0.251	0.213	0.180	0.000160
6	97.10	0.1879	0.222	0.230	0.238	0.245	0.252	0.258	0.453	0.386	0.329	0.280	0.239	0.203	0.000170
6	97.10	0.1879	0.222	0.230	0.238	0.245	0.252	0.258	0.473	0.404	0.345	0.295	0.252	0.215	0.000175
6	97.10	0.1879	0.222	0.230	0.238	0.245	0.252	0.258	0.494	0.423	0.362	0.310	0.266	0.228	0.000180
6	97.10	0.1879	0.222	0.230	0.238	0.245	0.252	0.258	0.536	0.461	0.397	0.342	0.295	0.254	0.000190
7	227.70	0.4407	0.153	0.158	0.164	0.169	0.173	0.178	0.147	0.126	0.109	0.093	0.080	0.069	0.000125
7	227.70	0.4407	0.153	0.158	0.164	0.169	0.173	0.178	0.174	0.152	0.132	0.114	0.099	0.086	0.000140
7	227.70	0.4407	0.153	0.158	0.164	0.169	0.173	0.178	0.193	0.169	0.148	0.129	0.113	0.099	0.000150
7	227.70	0.4407	0.153	0.158	0.164	0.169	0.173	0.178	0.213	0.188	0.165	0.145	0.128	0.113	0.000160
7	227.70	0.4407	0.153	0.158	0.164	0.169	0.173	0.178	0.233	0.207	0.183	0.162	0.144	0.127	0.000170
7	227.70	0.4407	0.153	0.158	0.164	0.169	0.173	0.178	0.244	0.217	0.192	0.171	0.152	0.135	0.000175
7	227.70	0.4407	0.153	0.158	0.164	0.169	0.173	0.178	0.254	0.227	0.202	0.180	0.160	0.143	0.000180
7	227.70	0.4407	0.153	0.158	0.164	0.169	0.173	0.178	0.276	0.247	0.221	0.198	0.177	0.159	0.000190
8	311.80	0.6034	0.108	0.112	0.116	0.120	0.123	0.126	0.176	0.156	0.139	0.123	0.109	0.097	0.000125
8	311.80	0.6034	0.108	0.112	0.116	0.120	0.123	0.126	0.209	0.187	0.168	0.151	0.136	0.122	0.000140
8	311.80	0.6034	0.108	0.112	0.116	0.120	0.123	0.126	0.232	0.209	0.189	0.171	0.155	0.140	0.000150
8	311.80	0.6034	0.108	0.112	0.116	0.120	0.123	0.126	0.255	0.232	0.211	0.192	0.175	0.159	0.000160
8	311.80	0.6034	0.108	0.112	0.116	0.120	0.123	0.126	0.279	0.256	0.234	0.214	0.196	0.180	0.000170
8	311.80	0.6034	0.108	0.112	0.116	0.120	0.123	0.126	0.292	0.268	0.246	0.226	0.207	0.191	0.000175
8	311.80	0.6034	0.108	0.112	0.116	0.120	0.123	0.126	0.304	0.280	0.258	0.238	0.219	0.202	0.000180
8	311.80	0.6034	0.108	0.112	0.116	0.120	0.123	0.126	0.330	0.306	0.283	0.262	0.243	0.225	0.000190
9	390.00	0.7548	0.067	0.069	0.072	0.074	0.076	0.078	0.007	0.007	0.006	0.005	0.005	0.005	0.000125
9	390.00	0.7548	0.067	0.069	0.072	0.074	0.076	0.078	0.008	0.008	0.007	0.007	0.006	0.006	0.000140
9	390.00	0.7548	0.067	0.069	0.072	0.074	0.076	0.078	0.009	0.009	0.008	0.008	0.007	0.007	0.000150
9	390.00	0.7548	0.067	0.069	0.072	0.074	0.076	0.078	0.010	0.010	0.009	0.009	0.008	0.008	0.000160
9	390.00	0.7548	0.067	0.069	0.072	0.074	0.076	0.078	0.011	0.011	0.010	0.010	0.009	0.008	0.000170
9	390.00	0.7548	0.067	0.069	0.072	0.074	0.076	0.078	0.012	0.011	0.011	0.010	0.010	0.009	0.000175
9	390.00	0.7548	0.067	0.069	0.072	0.074	0.076	0.078	0.012	0.012	0.011	0.011	0.010	0.010	0.000180
9	390.00	0.7548	0.067	0.069	0.072	0.074	0.076	0.078	0.013	0.013	0.012	0.012	0.011	0.011	0.000190
10	353.80	0.6847	0.086	0.089	0.092	0.095	0.098	0.100	0.288	0.260	0.234	0.211	0.190	0.171	0.000125
10	353.80	0.6847	0.086	0.089	0.092	0.095	0.098	0.100	0.342	0.311	0.284	0.258	0.235	0.214	0.000140
10	353.80	0.6847	0.086	0.089	0.092	0.095	0.098	0.100	0.379	0.348	0.319	0.293	0.268	0.246	0.000150
10	353.80	0.6847	0.086	0.089	0.092	0.095	0.098	0.100	0.418	0.386	0.356	0.329	0.303	0.280	0.000160
10	353.80	0.6847	0.086	0.089	0.092	0.095	0.098	0.100	0.457	0.425	0.395	0.366	0.340	0.316	0.000170
10	353.80	0.6847	0.086	0.089	0.092	0.095	0.098	0.100	0.478	0.445	0.415	0.386	0.360	0.335	0.000175

10	353.80	0.6847	0.086	0.089	0.092	0.095	0.098	0.100	0.498	0.466	0.435	0.406	0.379	0.354	0.000180
10	353.80	0.6847	0.086	0.089	0.092	0.095	0.098	0.100	0.541	0.508	0.477	0.448	0.420	0.395	0.000190

TESTS	TAU C (KG/CM 2)	GAMMA C R= 2.5	2.6	2.7	2.8	2.9	3.0	GAMMA Y
5 10	0.100	0.00026	0.00025	0.00025	0.00024	0.00024	0.00023	0.000125
5 10	0.200	0.00075	0.00074	0.00073	0.00072	0.00071	0.00070	0.000125
5 10	0.300	0.00158	0.00159	0.00160	0.00161	0.00162	0.00165	0.000125
5 10	0.350	0.00215	0.00218	0.00222	0.00227	0.00231	0.00237	0.000125
5 10	0.400	0.00283	0.00291	0.00299	0.00308	0.00317	0.00330	0.000125
5 10	0.450	0.00363	0.00377	0.00392	0.00408	0.00425	0.00446	0.000125
5 10	0.100	0.00026	0.00025	0.00025	0.00024	0.00024	0.00023	0.000140
5 10	0.200	0.00075	0.00074	0.00073	0.00072	0.00071	0.00070	0.000140
5 10	0.300	0.00158	0.00159	0.00160	0.00161	0.00162	0.00164	0.000140
5 10	0.350	0.00215	0.00218	0.00222	0.00226	0.00230	0.00236	0.000140
5 10	0.400	0.00283	0.00290	0.00298	0.00308	0.00317	0.00328	0.000140
5 10	0.450	0.00363	0.00376	0.00391	0.00407	0.00424	0.00444	0.000140
5 10	0.100	0.00026	0.00025	0.00025	0.00024	0.00024	0.00023	0.000150
5 10	0.200	0.00075	0.00074	0.00073	0.00072	0.00071	0.00070	0.000150
5 10	0.300	0.00158	0.00159	0.00160	0.00161	0.00162	0.00164	0.000150
5 10	0.350	0.00215	0.00219	0.00222	0.00226	0.00230	0.00236	0.000150
5 10	0.400	0.00283	0.00291	0.00299	0.00308	0.00317	0.00329	0.000150
5 10	0.450	0.00362	0.00378	0.00392	0.00407	0.00424	0.00445	0.000150
5 10	0.100	0.00026	0.00025	0.00025	0.00024	0.00024	0.00023	0.000160
5 10	0.200	0.00075	0.00074	0.00073	0.00072	0.00071	0.00070	0.000160
5 10	0.300	0.00158	0.00159	0.00160	0.00161	0.00162	0.00164	0.000160
5 10	0.350	0.00215	0.00218	0.00222	0.00226	0.00231	0.00235	0.000160
5 10	0.400	0.00283	0.00291	0.00299	0.00307	0.00317	0.00328	0.000160
5 10	0.450	0.00364	0.00377	0.00391	0.00407	0.00425	0.00443	0.000160
5 10	0.100	0.00026	0.00025	0.00025	0.00024	0.00024	0.00023	0.000170
5 10	0.200	0.00075	0.00074	0.00073	0.00072	0.00071	0.00070	0.000170
5 10	0.300	0.00158	0.00159	0.00160	0.00161	0.00162	0.00164	0.000170
5 10	0.350	0.00215	0.00219	0.00223	0.00226	0.00231	0.00236	0.000170
5 10	0.400	0.00283	0.00291	0.00299	0.00307	0.00317	0.00328	0.000170
5 10	0.450	0.00363	0.00377	0.00392	0.00407	0.00425	0.00444	0.000170
5 10	0.100	0.00026	0.00025	0.00025	0.00024	0.00024	0.00023	0.000175
5 10	0.200	0.00075	0.00074	0.00073	0.00072	0.00071	0.00070	0.000175
5 10	0.300	0.00158	0.00159	0.00160	0.00161	0.00162	0.00164	0.000175
5 10	0.350	0.00215	0.00218	0.00222	0.00226	0.00231	0.00236	0.000175
5 10	0.400	0.00283	0.00291	0.00299	0.00308	0.00318	0.00329	0.000175
5 10	0.450	0.00363	0.00377	0.00391	0.00408	0.00425	0.00445	0.000175
5 10	0.100	0.00026	0.00025	0.00025	0.00024	0.00024	0.00023	0.000180
5 10	0.200	0.00075	0.00074	0.00073	0.00072	0.00071	0.00070	0.000180
5 10	0.300	0.00158	0.00159	0.00160	0.00161	0.00162	0.00164	0.000180
5 10	0.350	0.00215	0.00218	0.00222	0.00227	0.00231	0.00236	0.000180
5 10	0.400	0.00282	0.00291	0.00299	0.00308	0.00317	0.00328	0.000180
5 10	0.450	0.00362	0.00377	0.00392	0.00408	0.00425	0.00444	0.000180
5 10	0.100	0.00026	0.00025	0.00025	0.00024	0.00024	0.00023	0.000190
5 10	0.200	0.00075	0.00074	0.00073	0.00072	0.00071	0.00070	0.000190
5 10	0.300	0.00158	0.00159	0.00160	0.00161	0.00162	0.00164	0.000190
5 10	0.350	0.00215	0.00218	0.00222	0.00227	0.00231	0.00236	0.000190
5 10	0.400	0.00283	0.00291	0.00299	0.00308	0.00318	0.00328	0.000190
5 10	0.450	0.00363	0.00377	0.00392	0.00408	0.00425	0.00444	0.000190

FIRST CYCLE BEHAVIOR OF (OCR=2) CLAY

TEST	G(GRAPH) (KG/CM 2)	G RATIO	DAMPING RATIO R= 2.5	2.6	2.7	2.8	2.9	3.0	ALPHA R= 2.5	2.6	2.7	2.8	2.9	3.0	GAMMA Y
13	156.40	0.3575	0.175	0.182	0.188	0.194	0.199	0.205	0.224	0.195	0.170	0.148	0.129	0.112	0.000125
13	156.40	0.3575	0.175	0.182	0.188	0.194	0.199	0.205	0.266	0.234	0.206	0.181	0.160	0.141	0.000140
13	156.40	0.3575	0.175	0.182	0.188	0.194	0.199	0.205	0.295	0.261	0.232	0.205	0.182	0.161	0.000150
13	156.40	0.3575	0.175	0.182	0.188	0.194	0.199	0.205	0.325	0.290	0.258	0.231	0.206	0.184	0.000160
13	156.40	0.3575	0.175	0.182	0.188	0.194	0.199	0.205	0.356	0.319	0.287	0.257	0.231	0.207	0.000170
13	156.40	0.3575	0.175	0.182	0.188	0.194	0.199	0.205	0.371	0.334	0.301	0.271	0.244	0.220	0.000175
13	156.40	0.3575	0.175	0.182	0.188	0.194	0.199	0.205	0.387	0.350	0.316	0.285	0.257	0.232	0.000180
13	156.40	0.3575	0.175	0.182	0.188	0.194	0.199	0.205	0.420	0.381	0.346	0.314	0.285	0.259	0.000190
14	191.00	0.4366	0.154	0.159	0.165	0.170	0.175	0.179	0.198	0.174	0.154	0.136	0.120	0.106	0.000125
14	191.00	0.4366	0.154	0.159	0.165	0.170	0.175	0.179	0.234	0.209	0.187	0.167	0.149	0.133	0.000140
14	191.00	0.4366	0.154	0.159	0.165	0.170	0.175	0.179	0.260	0.234	0.210	0.189	0.170	0.152	0.000150
14	191.00	0.4366	0.154	0.159	0.165	0.170	0.175	0.179	0.286	0.259	0.234	0.212	0.192	0.173	0.000160
14	191.00	0.4366	0.154	0.159	0.165	0.170	0.175	0.179	0.314	0.285	0.260	0.236	0.215	0.196	0.000170
14	191.00	0.4366	0.154	0.159	0.165	0.170	0.175	0.179	0.328	0.299	0.273	0.249	0.227	0.207	0.000175
14	191.00	0.4366	0.154	0.159	0.165	0.170	0.175	0.179	0.342	0.313	0.286	0.262	0.240	0.219	0.000180
14	191.00	0.4366	0.154	0.159	0.165	0.170	0.175	0.179	0.371	0.341	0.314	0.289	0.266	0.244	0.000190
15	232.80	0.5321	0.128	0.132	0.137	0.141	0.145	0.149	0.171	0.153	0.137	0.123	0.110	0.099	0.000125
15	232.80	0.5321	0.128	0.132	0.137	0.141	0.145	0.149	0.202	0.184	0.166	0.151	0.137	0.124	0.000140
15	232.80	0.5321	0.128	0.132	0.137	0.141	0.145	0.149	0.225	0.205	0.187	0.171	0.156	0.142	0.000150
15	232.80	0.5321	0.128	0.132	0.137	0.141	0.145	0.149	0.247	0.227	0.209	0.192	0.176	0.162	0.000160
15	232.80	0.5321	0.128	0.132	0.137	0.141	0.145	0.149	0.271	0.250	0.232	0.214	0.198	0.183	0.000170
15	232.80	0.5321	0.128	0.132	0.137	0.141	0.145	0.149	0.283	0.262	0.243	0.226	0.209	0.194	0.000175
15	232.80	0.5321	0.128	0.132	0.137	0.141	0.145	0.149	0.295	0.274	0.255	0.237	0.221	0.205	0.000180
15	232.80	0.5321	0.128	0.132	0.137	0.141	0.145	0.149	0.320	0.299	0.280	0.262	0.244	0.229	0.000190
16	201.00	0.4594	0.147	0.153	0.158	0.163	0.168	0.172	0.189	0.167	0.148	0.131	0.116	0.103	0.000125
16	201.00	0.4594	0.147	0.153	0.158	0.163	0.168	0.172	0.224	0.201	0.180	0.161	0.144	0.129	0.000140
16	201.00	0.4594	0.147	0.153	0.158	0.163	0.168	0.172	0.248	0.224	0.202	0.182	0.164	0.148	0.000150
16	201.00	0.4594	0.147	0.153	0.158	0.163	0.168	0.172	0.274	0.248	0.225	0.204	0.186	0.168	0.000160
16	201.00	0.4594	0.147	0.153	0.158	0.163	0.168	0.172	0.300	0.274	0.250	0.228	0.208	0.190	0.000170
16	201.00	0.4594	0.147	0.153	0.158	0.163	0.168	0.172	0.313	0.287	0.262	0.240	0.220	0.201	0.000175
16	201.00	0.4594	0.147	0.153	0.158	0.163	0.168	0.172	0.327	0.300	0.275	0.253	0.232	0.213	0.000180
16	201.00	0.4594	0.147	0.153	0.158	0.163	0.168	0.172	0.354	0.327	0.302	0.279	0.257	0.237	0.000190
17	44.30	0.1013	0.245	0.254	0.263	0.271	0.279	0.286	0.479	0.398	0.330	0.274	0.228	0.189	0.000125
17	44.30	0.1013	0.245	0.254	0.263	0.271	0.279	0.286	0.567	0.477	0.400	0.336	0.283	0.237	0.000140
17	44.30	0.1013	0.245	0.254	0.263	0.271	0.279	0.286	0.629	0.532	0.450	0.381	0.322	0.272	0.000150
17	44.30	0.1013	0.245	0.254	0.263	0.271	0.279	0.286	0.693	0.590	0.502	0.428	0.364	0.310	0.000160
17	44.30	0.1013	0.245	0.254	0.263	0.271	0.279	0.286	0.759	0.650	0.557	0.477	0.409	0.350	0.000170
17	44.30	0.1013	0.245	0.254	0.263	0.271	0.279	0.286	0.793	0.681	0.585	0.503	0.432	0.371	0.000175
17	44.30	0.1013	0.245	0.254	0.263	0.271	0.279	0.286	0.827	0.713	0.614	0.529	0.455	0.392	0.000180
17	44.30	0.1013	0.245	0.254	0.263	0.271	0.279	0.286	0.897	0.777	0.673	0.583	0.505	0.437	0.000190
18	310.00	0.7086	0.080	0.082	0.085	0.088	0.090	0.093	0.120	0.111	0.102	0.094	0.087	0.080	0.000125
18	310.00	0.7086	0.080	0.082	0.085	0.088	0.090	0.093	0.143	0.133	0.124	0.116	0.108	0.100	0.000140
18	310.00	0.7086	0.080	0.082	0.085	0.088	0.090	0.093	0.158	0.149	0.139	0.131	0.123	0.115	0.000150
18	310.00	0.7086	0.080	0.082	0.085	0.088	0.090	0.093	0.174	0.165	0.156	0.147	0.139	0.131	0.000160
18	310.00	0.7086	0.080	0.082	0.085	0.088	0.090	0.093	0.191	0.182	0.172	0.164	0.156	0.148	0.000170
18	310.00	0.7086	0.080	0.082	0.085	0.088	0.090	0.093	0.200	0.190	0.181	0.173	0.165	0.157	0.000175

18	310.00	0.7086	0.080	0.082	0.085	0.088	0.090	0.093	0.208	0.199	0.190	0.182	0.174	0.166	0.000180
18	310.00	0.7086	0.080	0.082	0.085	0.088	0.090	0.093	0.226	0.217	0.208	0.200	0.192	0.185	0.000190
21	372.20	0.8507	0.041	0.042	0.044	0.045	0.046	0.048	0.081	0.080	0.078	0.076	0.075	0.073	0.000125
21	372.20	0.8507	0.041	0.042	0.044	0.045	0.046	0.048	0.096	0.095	0.095	0.094	0.093	0.092	0.000140
21	372.20	0.8507	0.041	0.042	0.044	0.045	0.046	0.048	0.107	0.106	0.106	0.106	0.106	0.106	0.000150
21	372.20	0.8507	0.041	0.042	0.044	0.045	0.046	0.048	0.118	0.118	0.119	0.119	0.120	0.120	0.000160
21	372.20	0.8507	0.041	0.042	0.044	0.045	0.046	0.048	0.129	0.130	0.131	0.133	0.134	0.136	0.000170
21	372.20	0.8507	0.041	0.042	0.044	0.045	0.046	0.048	0.134	0.136	0.138	0.140	0.142	0.144	0.000175
21	372.20	0.8507	0.041	0.042	0.044	0.045	0.046	0.048	0.140	0.143	0.145	0.147	0.150	0.152	0.000180
21	372.20	0.8507	0.041	0.042	0.044	0.045	0.046	0.048	0.152	0.155	0.159	0.162	0.166	0.169	0.000190

TESTS	TAU C (KG/CM 2)	GAMMA C R= 2.5	2.6	2.7	2.8	2.9	3.0	GAMMA Y
13 21	0.100	0.00035	0.00034	0.00033	0.00032	0.00032	0.00031	0.000125
13 21	0.150	0.00067	0.00066	0.00065	0.00064	0.00063	0.00062	0.000125
13 21	0.200	0.00113	0.00112	0.00112	0.00112	0.00112	0.00112	0.000125
13 21	0.250	0.00174	0.00176	0.00178	0.00181	0.00184	0.00187	0.000125
13 21	0.300	0.00253	0.00260	0.00267	0.00276	0.00284	0.00293	0.000125
13 21	0.325	0.00299	0.00310	0.00320	0.00333	0.00347	0.00360	0.000125
13 21	0.100	0.00035	0.00034	0.00033	0.00032	0.00032	0.00031	0.000140
13 21	0.150	0.00067	0.00066	0.00065	0.00064	0.00063	0.00062	0.000140
13 21	0.200	0.00113	0.00112	0.00112	0.00112	0.00112	0.00112	0.000140
13 21	0.250	0.00174	0.00176	0.00178	0.00181	0.00185	0.00188	0.000140
13 21	0.300	0.00253	0.00259	0.00267	0.00276	0.00285	0.00294	0.000140
13 21	0.325	0.00299	0.00309	0.00320	0.00333	0.00347	0.00361	0.000140
13 21	0.100	0.00035	0.00034	0.00033	0.00032	0.00032	0.00031	0.000150
13 21	0.150	0.00067	0.00066	0.00065	0.00064	0.00063	0.00062	0.000150
13 21	0.200	0.00113	0.00112	0.00112	0.00112	0.00112	0.00112	0.000150
13 21	0.250	0.00174	0.00176	0.00178	0.00181	0.00184	0.00187	0.000150
13 21	0.300	0.00253	0.00260	0.00267	0.00275	0.00284	0.00294	0.000150
13 21	0.325	0.00299	0.00310	0.00320	0.00332	0.00346	0.00360	0.000150
13 21	0.100	0.00035	0.00034	0.00033	0.00032	0.00032	0.00031	0.000160
13 21	0.150	0.00067	0.00066	0.00065	0.00064	0.00063	0.00062	0.000160
13 21	0.200	0.00113	0.00112	0.00112	0.00112	0.00112	0.00113	0.000160
13 21	0.250	0.00174	0.00176	0.00178	0.00181	0.00184	0.00188	0.000160
13 21	0.300	0.00253	0.00259	0.00266	0.00275	0.00284	0.00294	0.000160
13 21	0.325	0.00299	0.00309	0.00320	0.00332	0.00346	0.00361	0.000160
13 21	0.100	0.00035	0.00034	0.00033	0.00032	0.00032	0.00031	0.000170
13 21	0.150	0.00067	0.00066	0.00065	0.00064	0.00063	0.00062	0.000170
13 21	0.200	0.00113	0.00112	0.00112	0.00112	0.00112	0.00112	0.000170
13 21	0.250	0.00174	0.00176	0.00178	0.00181	0.00184	0.00188	0.000170
13 21	0.300	0.00253	0.00260	0.00267	0.00275	0.00284	0.00294	0.000170
13 21	0.325	0.00300	0.00309	0.00320	0.00332	0.00346	0.00361	0.000170
13 21	0.100	0.00035	0.00034	0.00033	0.00032	0.00032	0.00031	0.000175
13 21	0.150	0.00067	0.00066	0.00065	0.00064	0.00063	0.00062	0.000175
13 21	0.200	0.00112	0.00112	0.00112	0.00112	0.00112	0.00112	0.000175
13 21	0.250	0.00174	0.00176	0.00178	0.00181	0.00184	0.00188	0.000175
13 21	0.300	0.00253	0.00259	0.00267	0.00275	0.00283	0.00294	0.000175
13 21	0.325	0.00299	0.00309	0.00321	0.00333	0.00345	0.00361	0.000175
13 21	0.100	0.00035	0.00034	0.00033	0.00032	0.00032	0.00031	0.000180
13 21	0.150	0.00067	0.00066	0.00065	0.00064	0.00063	0.00062	0.000180
13 21	0.200	0.00113	0.00112	0.00112	0.00112	0.00112	0.00112	0.000180
13 21	0.250	0.00174	0.00176	0.00178	0.00181	0.00184	0.00187	0.000180
13 21	0.300	0.00253	0.00260	0.00267	0.00275	0.00284	0.00293	0.000180
13 21	0.325	0.00299	0.00310	0.00321	0.00333	0.00345	0.00360	0.000180
13 21	0.100	0.00035	0.00034	0.00033	0.00032	0.00032	0.00031	0.000190
13 21	0.150	0.00067	0.00066	0.00065	0.00064	0.00063	0.00062	0.000190
13 21	0.200	0.00113	0.00112	0.00112	0.00112	0.00112	0.00112	0.000190
13 21	0.250	0.00174	0.00176	0.00178	0.00181	0.00184	0.00187	0.000190
13 21	0.300	0.00253	0.00259	0.00267	0.00275	0.00284	0.00294	0.000190
13 21	0.325	0.00299	0.00309	0.00320	0.00333	0.00346	0.00360	0.000190

TABLE 4

CLAY BEHAVIOR AT DIFFERENT CYCLES

TEST	CYCLE 1	2	3	16	50	100	200	300	400	
5	1.000	0.905	0.887	0.872	0.847	0.819	0.797	0.767	1.000	DEGRADATION INDEX
	176.5	130.8	119.7	112.4	98.6	85.1	72.8	55.2	0.0	G(GRAPH) KG/CM 2
	150.0	127.6	121.4	106.2	94.5	85.7	77.8	70.5	66.4	G(EQUATION) KG/CM 2
6	1.000	0.950	0.930	1.000	1.000	1.000	1.000	1.000	1.000	DEGRADATION INDEX
	97.1	70.0	60.0	0.0	0.0	0.0	0.0	0.0	0.0	G(GRAPH) KG/CM 2
	110.7	98.7	92.8	110.7	110.7	110.7	110.7	110.7	110.7	G(EQUATION) KG/CM 2
7	1.000	0.878	0.853	0.834	0.789	0.759	0.736	0.718	0.703	DEGRADATION INDEX
	227.7	164.4	151.8	142.3	123.3	108.0	97.1	87.1	80.0	G(GRAPH) KG/CM 2
	188.0	156.7	148.3	129.2	112.6	102.7	93.6	88.1	83.7	G(EQUATION) KG/CM 2
8	1.000	0.865	0.841	0.815	0.765	0.729	0.700	0.684	0.673	DEGRADATION INDEX
	311.8	255.4	233.0	216.3	192.7	169.6	153.6	146.2	141.3	G(GRAPH) KG/CM 2
	268.0	218.0	208.3	189.4	166.5	151.1	138.3	132.0	127.9	G(EQUATION) KG/CM 2
9	1.000	0.975	0.963	0.945	0.934	0.907	0.902	0.891	0.872	DEGRADATION INDEX
	390.0	380.4	362.8	354.5	332.0	325.0	318.0	312.0	300.0	G(GRAPH) KG/CM 2
	340.4	324.2	315.8	290.3	274.9	261.3	252.7	246.8	236.1	G(EQUATION) KG/CM 2
10	1.000	0.920	0.906	0.868	0.807	0.760	0.736	0.722	0.710	DEGRADATION INDEX
	353.8	306.7	291.1	270.6	245.3	221.7	204.4	193.7	187.3	G(GRAPH) KG/CM 2
	302.4	270.3	262.3	232.7	204.4	185.3	174.2	166.2	161.1	G(EQUATION) KG/CM 2
13	1.000	0.849	0.811	0.788	0.768	0.742	0.718	0.676	1.000	DEGRADATION INDEX
	156.4	95.2	81.1	74.0	66.8	58.4	50.9	38.7	0.0	G(GRAPH) KG/CM 2
	115.6	89.4	81.0	66.6	57.2	51.0	44.6	37.3	24.9	G(EQUATION) KG/CM 2
14	1.000	0.813	0.770	0.743	0.718	0.702	0.675	0.647	0.637	DEGRADATION INDEX
	191.0	110.4	93.2	84.9	74.9	69.5	59.7	49.6	46.8	G(GRAPH) KG/CM 2
	139.0	103.0	93.7	76.8	65.8	59.6	53.9	47.9	44.7	G(EQUATION) KG/CM 2
15	1.000	0.776	0.721	0.694	0.663	0.644	0.622	0.606	0.597	DEGRADATION INDEX
	232.8	127.3	108.0	93.1	83.5	76.8	68.0	60.8	57.0	G(GRAPH) KG/CM 2
	169.0	121.7	109.1	89.0	75.7	68.3	61.3	57.1	52.7	G(EQUATION) KG/CM 2
16	1.000	0.804	0.755	0.731	0.706	0.690	0.663	0.638	0.621	DEGRADATION INDEX
	201.0	115.6	96.4	86.0	77.1	70.9	61.7	52.9	49.3	G(GRAPH) KG/CM 2
	144.8	106.7	96.3	78.9	67.8	61.5	54.2	49.3	45.9	G(EQUATION) KG/CM 2
18	1.000	0.713	0.656	0.611	0.585	0.566	0.551	0.532	0.521	DEGRADATION INDEX
	310.0	157.0	130.5	112.7	95.4	85.5	77.5	73.4	70.4	G(GRAPH) KG/CM 2
	224.9	155.5	139.4	112.2	96.6	87.3	79.6	73.6	69.9	G(EQUATION) KG/CM 2
21	1.000	0.609	0.540	0.496	0.486	0.469	0.447	0.441	0.438	DEGRADATION INDEX
	372.2	203.0	167.5	145.7	136.7	126.4	113.6	111.8	110.0	G(GRAPH) KG/CM 2
	338.2	232.0	209.2	176.4	157.9	145.7	133.2	127.5	124.0	G(EQUATION) KG/CM 2

EXECUTION TERMINATED 17:52:37 T=.065 RC=0 $.10

$SIGNOFF

PART 9

FIGURES

FIGURE 1a. CYCLIC AND STATIC LOADING STRESS-STRAIN CURVES FOR NORMALLY CONSOLIDATED CLAYS

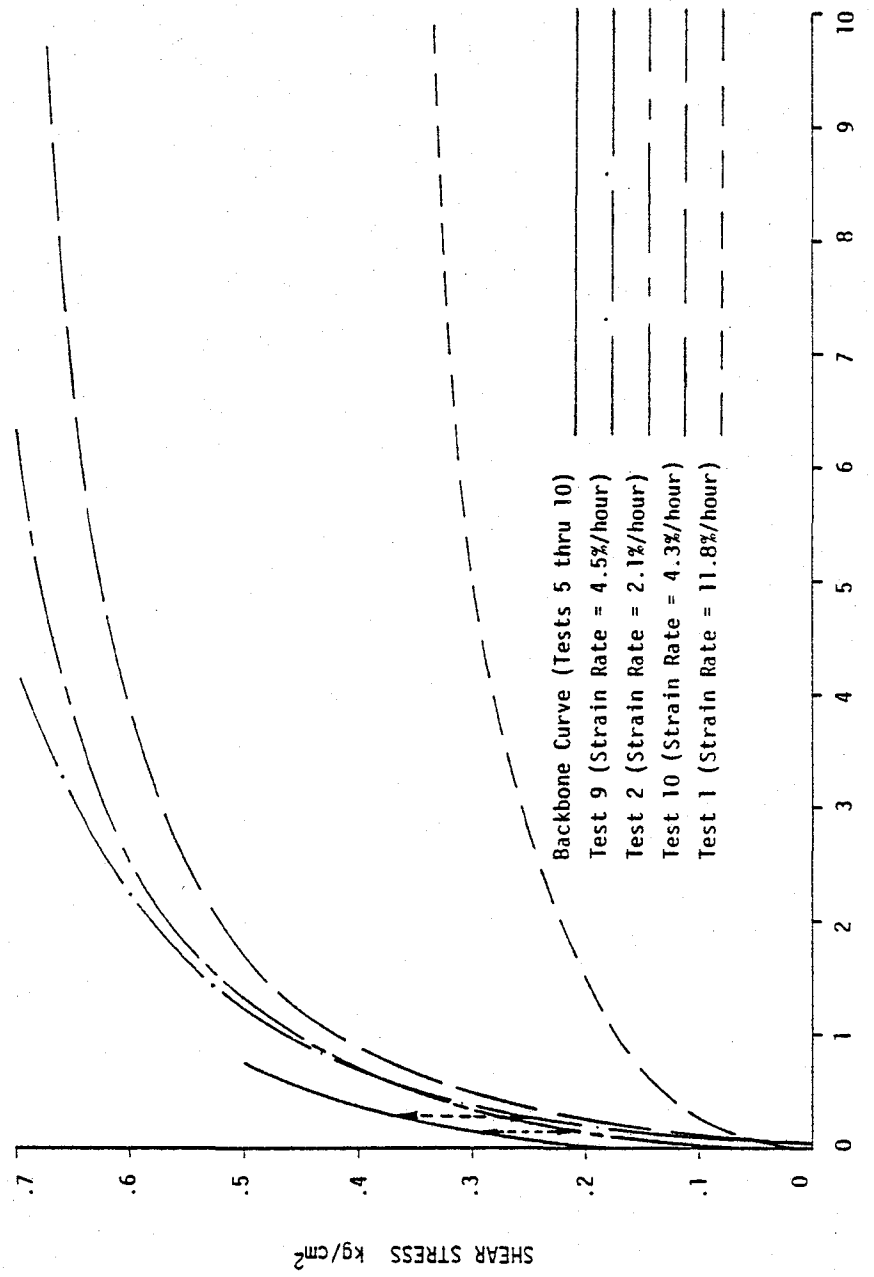

FIGURE 1b. CYCLIC AND STATIC LOADING STRESS-STRAIN CURVES FOR OVERCONSOLIDATED CLAYS

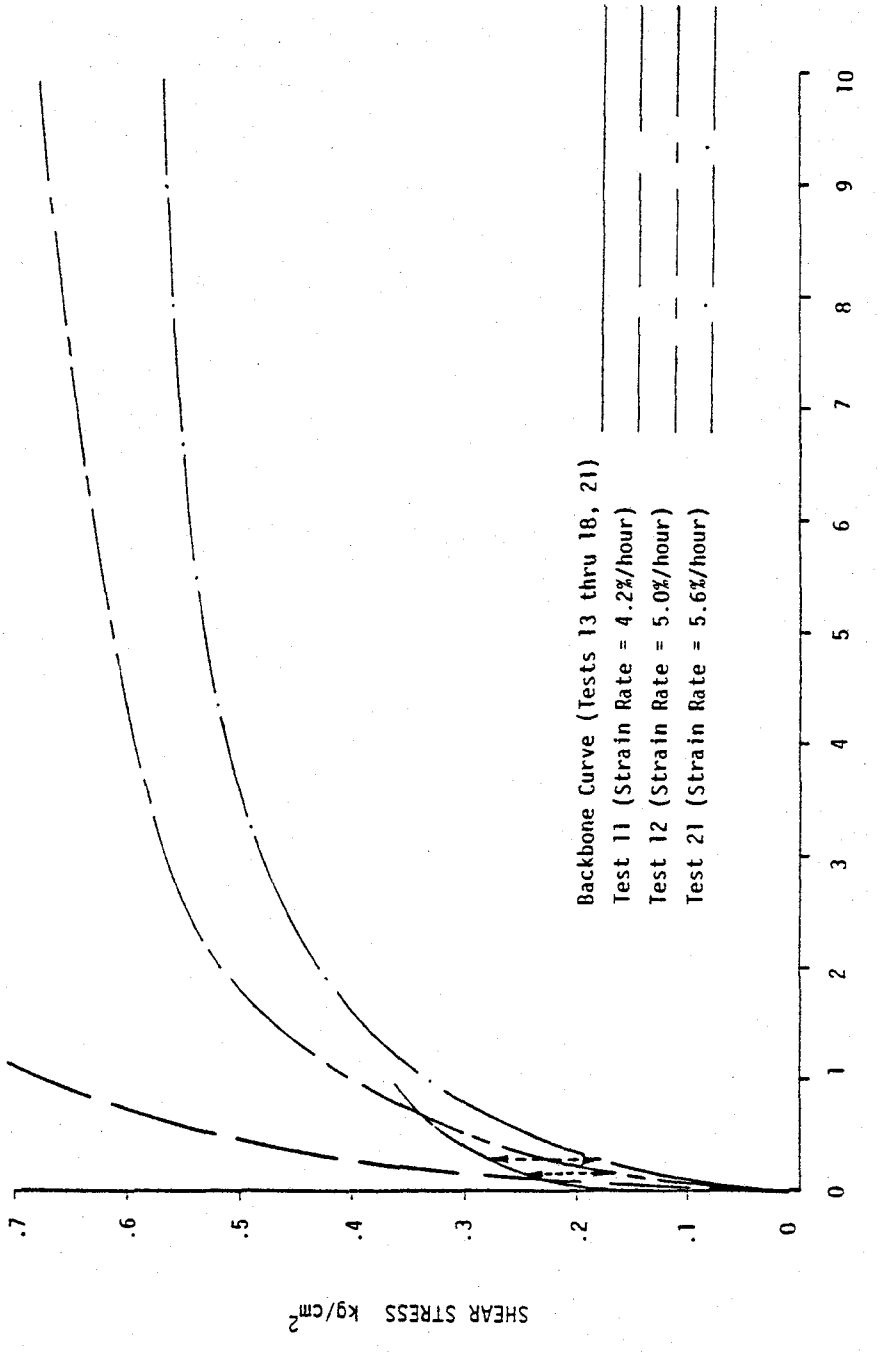

FIGURE 2a. SHEAR STRESS VS. SHEAR STRAIN FOR NORMALLY CONSOLIDATED CLAYS

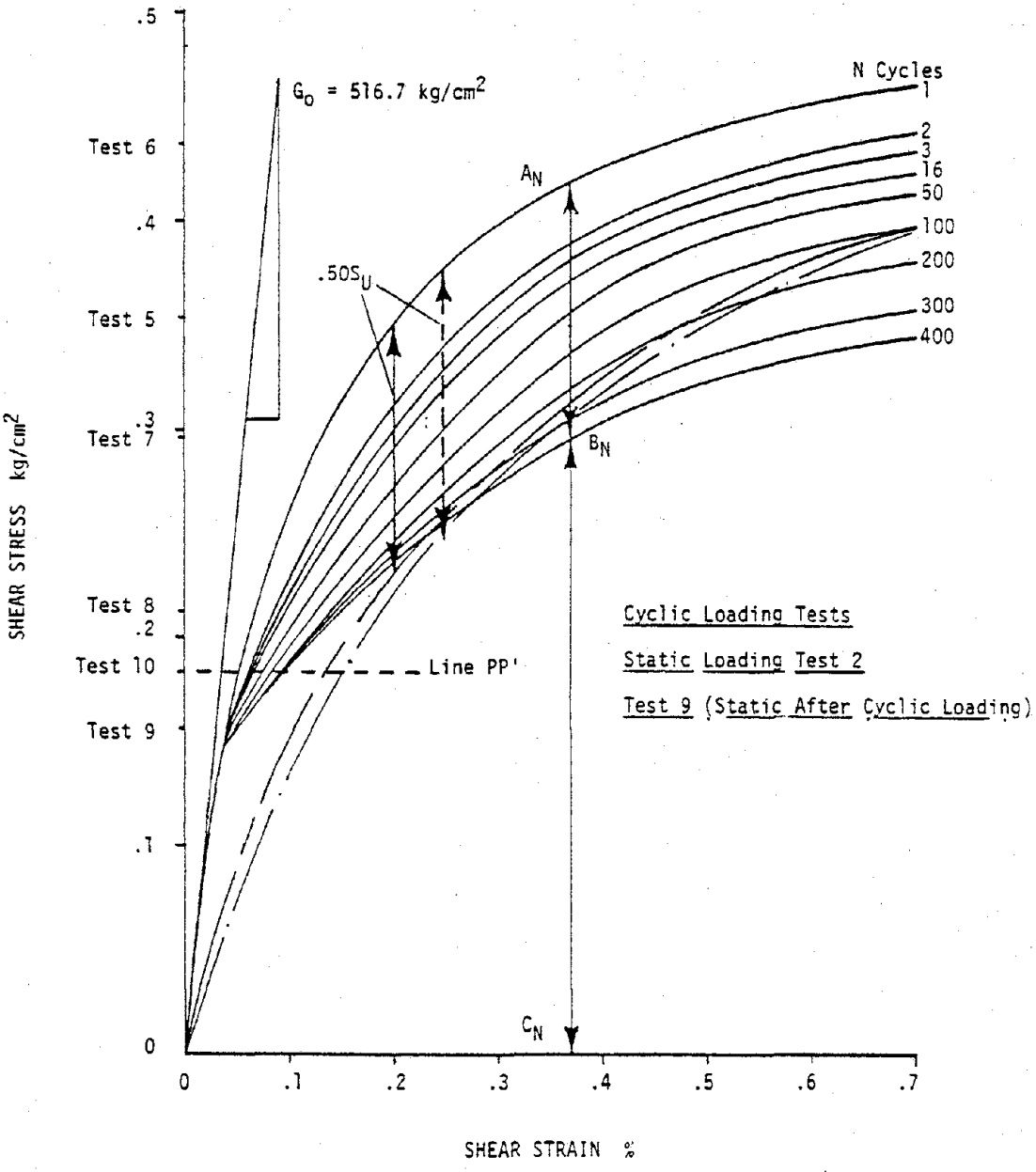

FIGURE 2b. SHEAR STRESS VS. SHEAR STRAIN FOR OVERCONSOLIDATED CLAYS

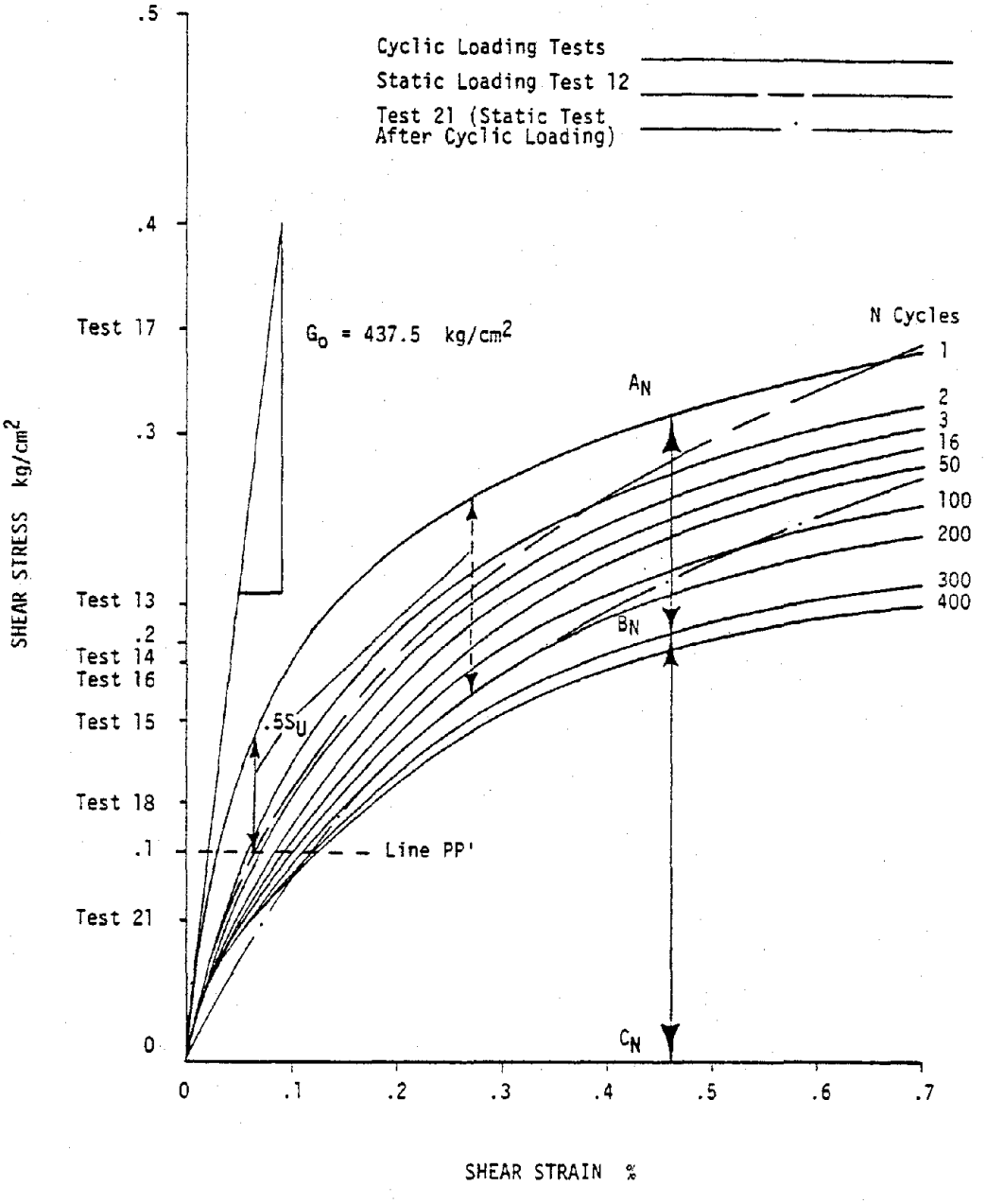

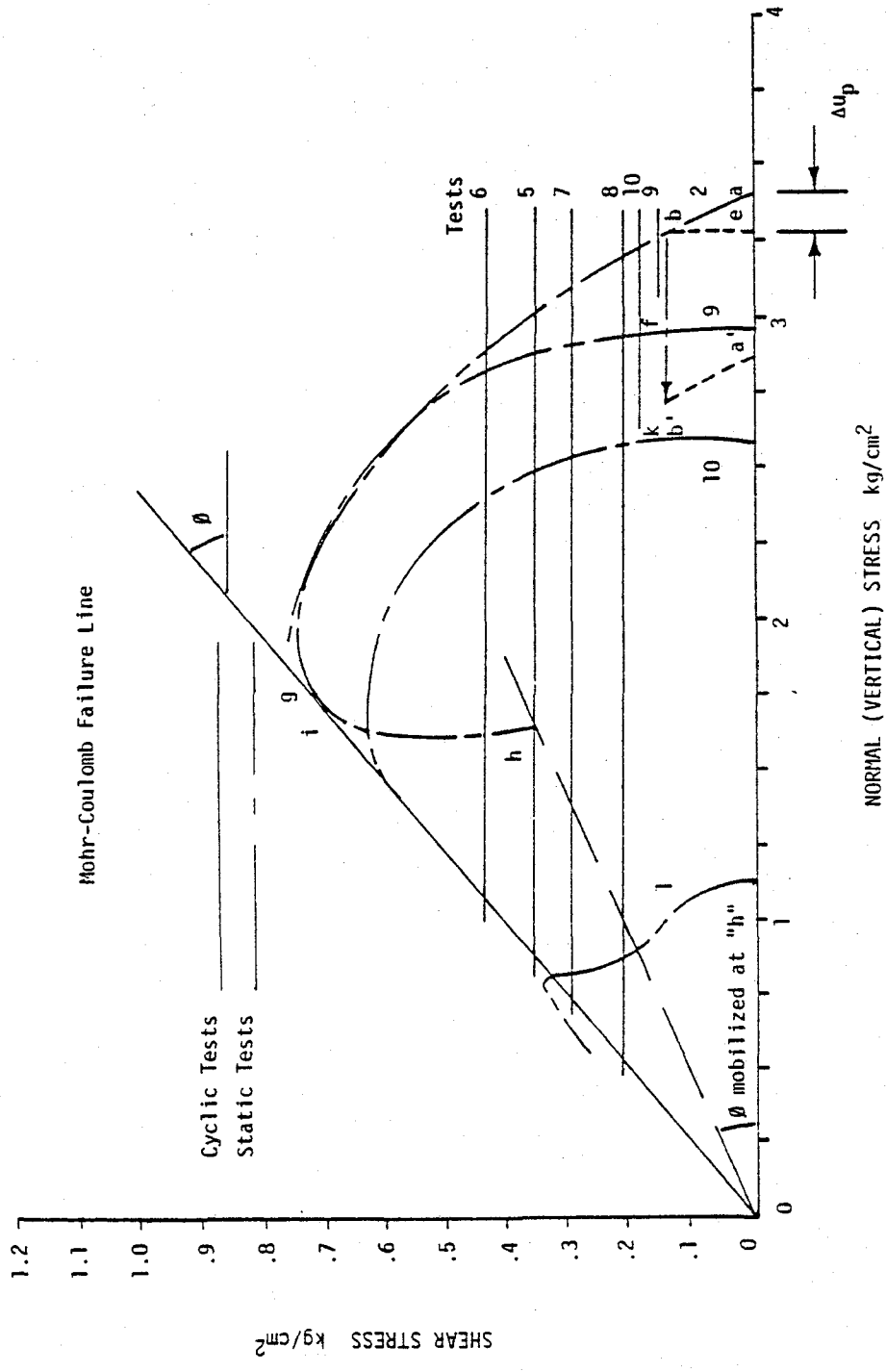

FIGURE 3a. EFFECTIVE STRESS PATHS FOR STATIC AND CYCLIC TESTS ON NORMALLY CONSOLIDATED CLAYS

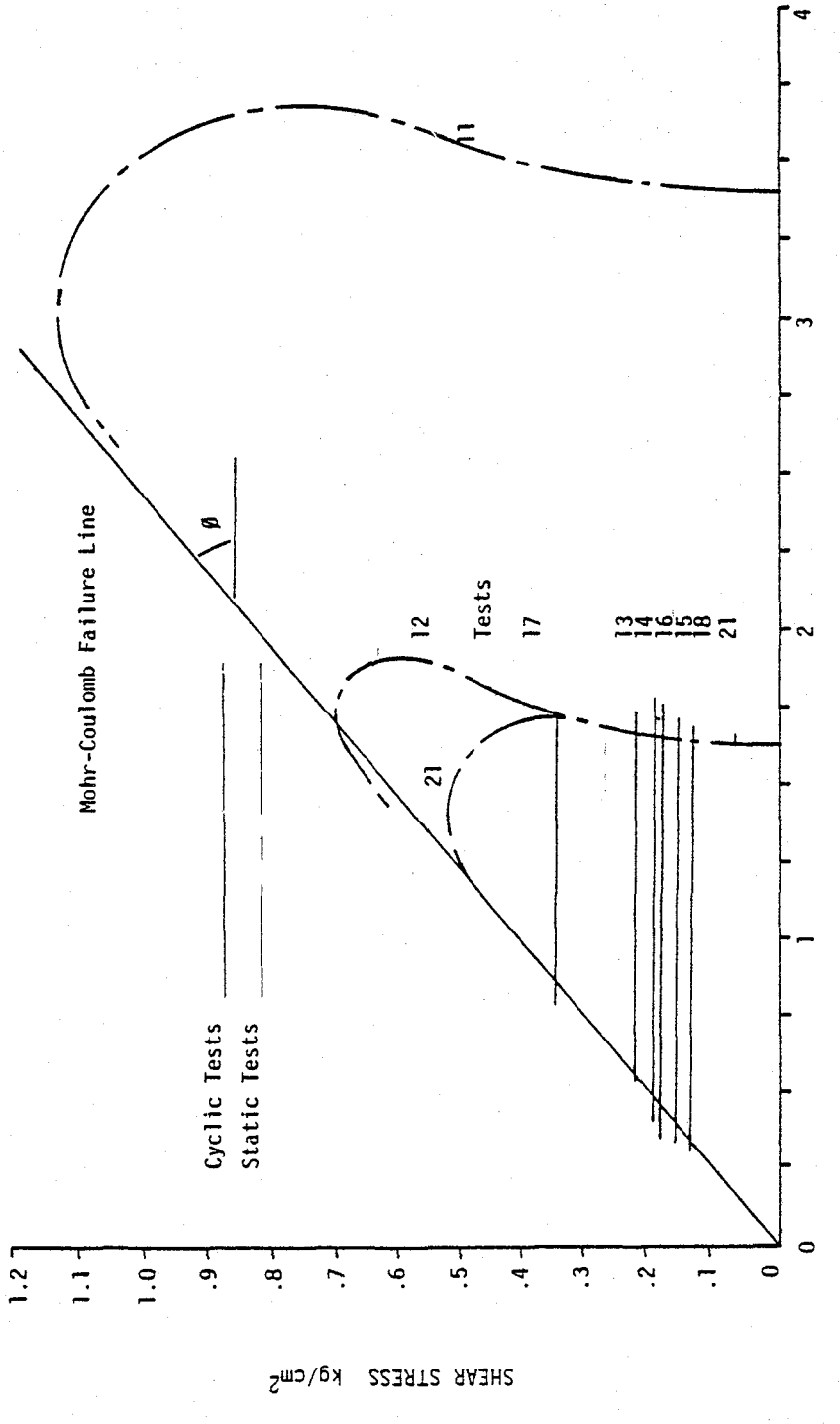

FIGURE 3b. EFFECTIVE STRESS PATHS FOR STATIC AND CYCLIC TESTS ON OVERCONSOLIDATED CLAYS

FIGURE 4. TYPICAL CYCLIC TEST RESULTS

(a) Typical Controlled-Strain Tests for Clays

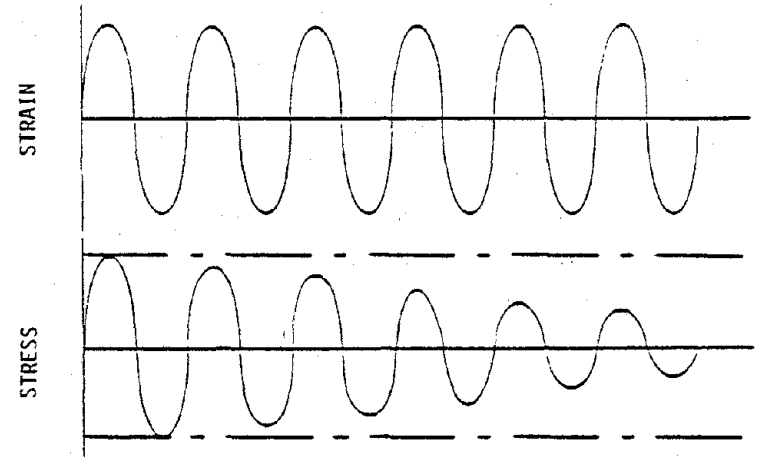

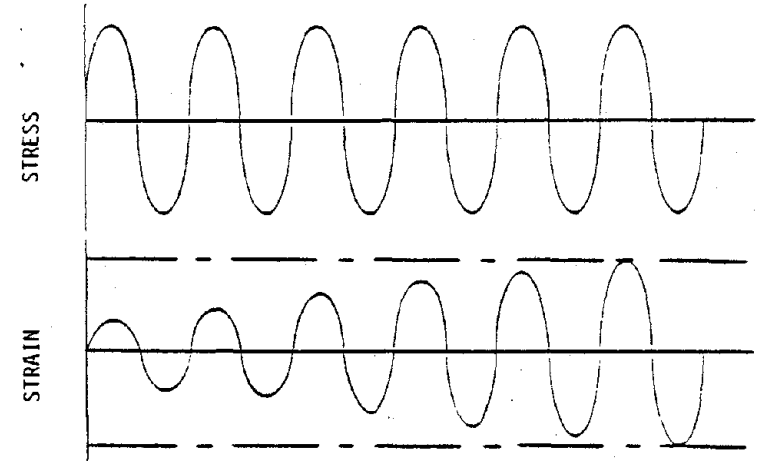

(b) Typical Controlled-Stress Tests for Clays

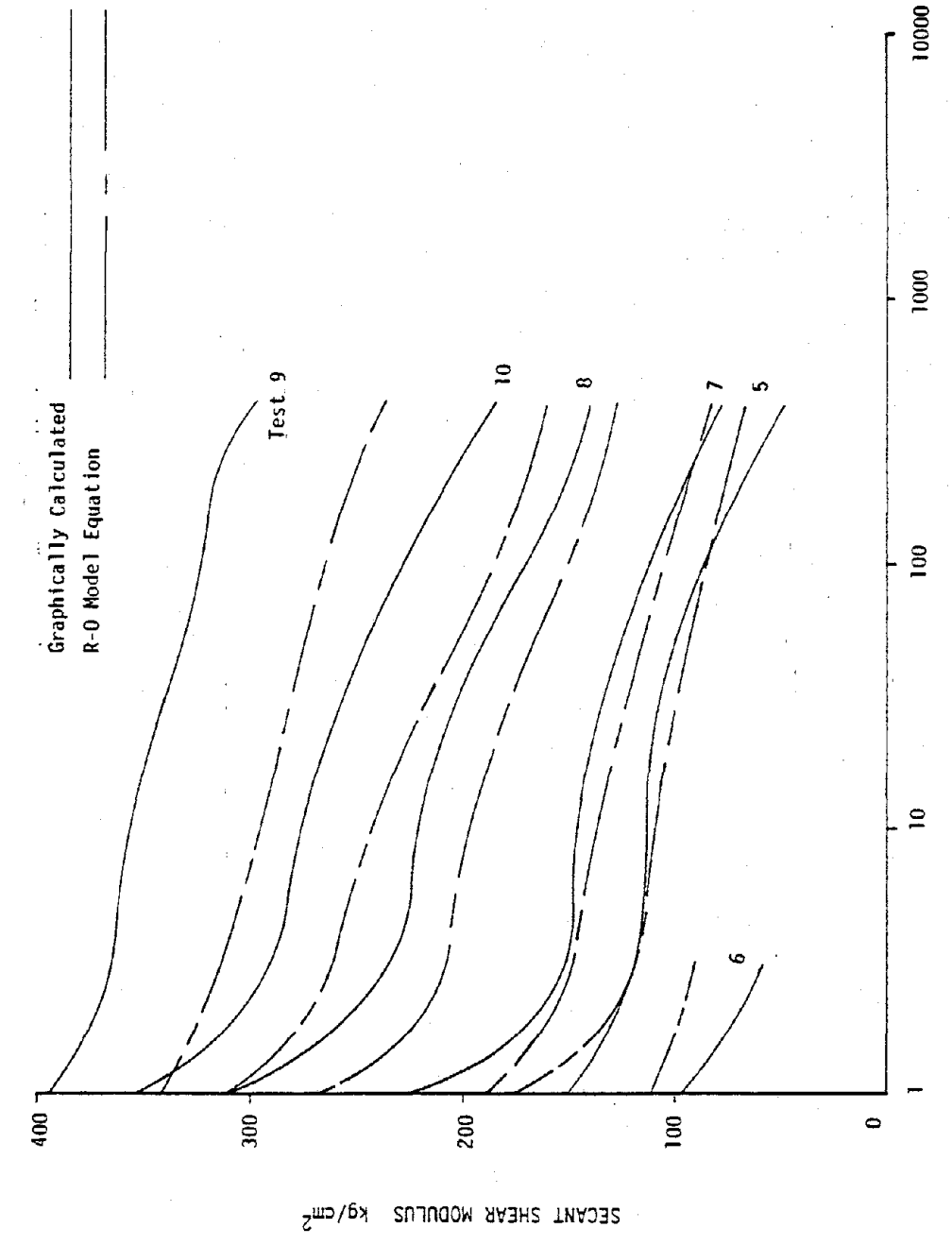

FIGURE 5a. SECANT SHEAR MODULUS VS. N CYCLES FOR NORMALLY CONSOLIDATED CLAYS

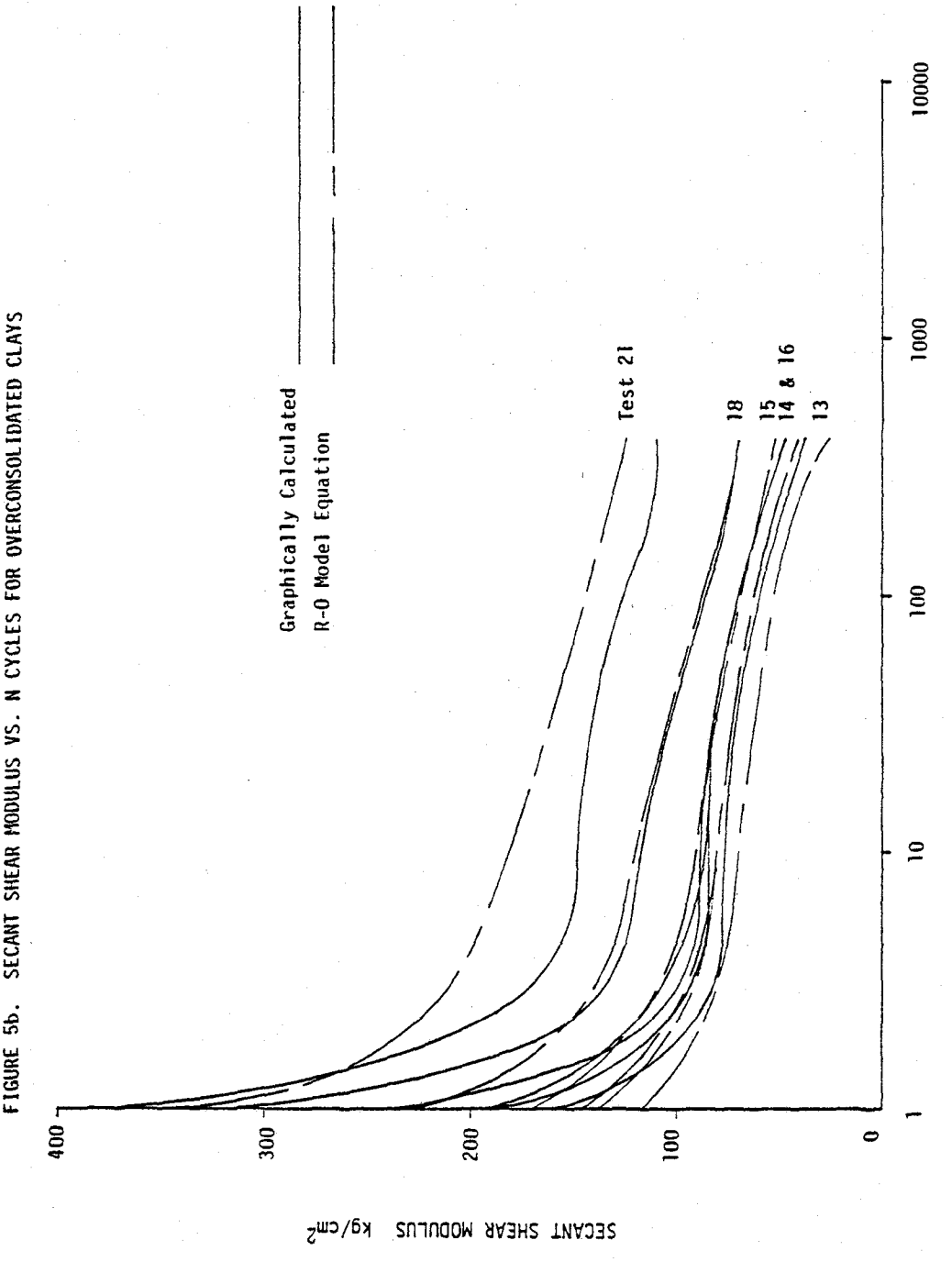

FIGURE 5b. SECANT SHEAR MODULUS VS. N CYCLES FOR OVERCONSOLIDATED CLAYS

FIGURE 6a. SHEAR MODULUS VS. NORMALIZED SHEAR STRESS FOR NORMALLY CONSOLIDATED CLAYS

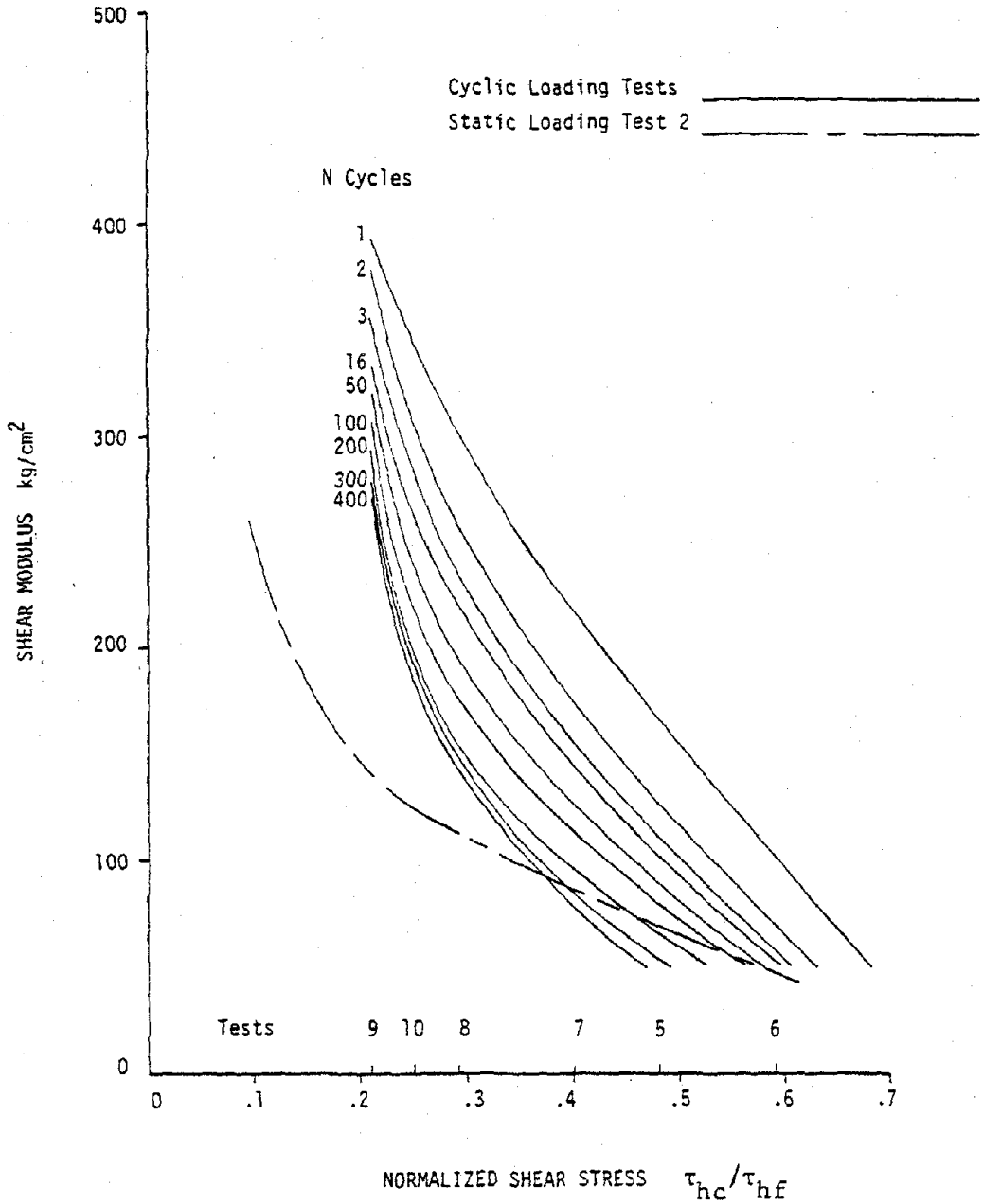

FIGURE 6b. SHEAR MODULUS VS. NORMALIZED SHEAR STRESS FOR OVERCONSOLIDATED CLAYS

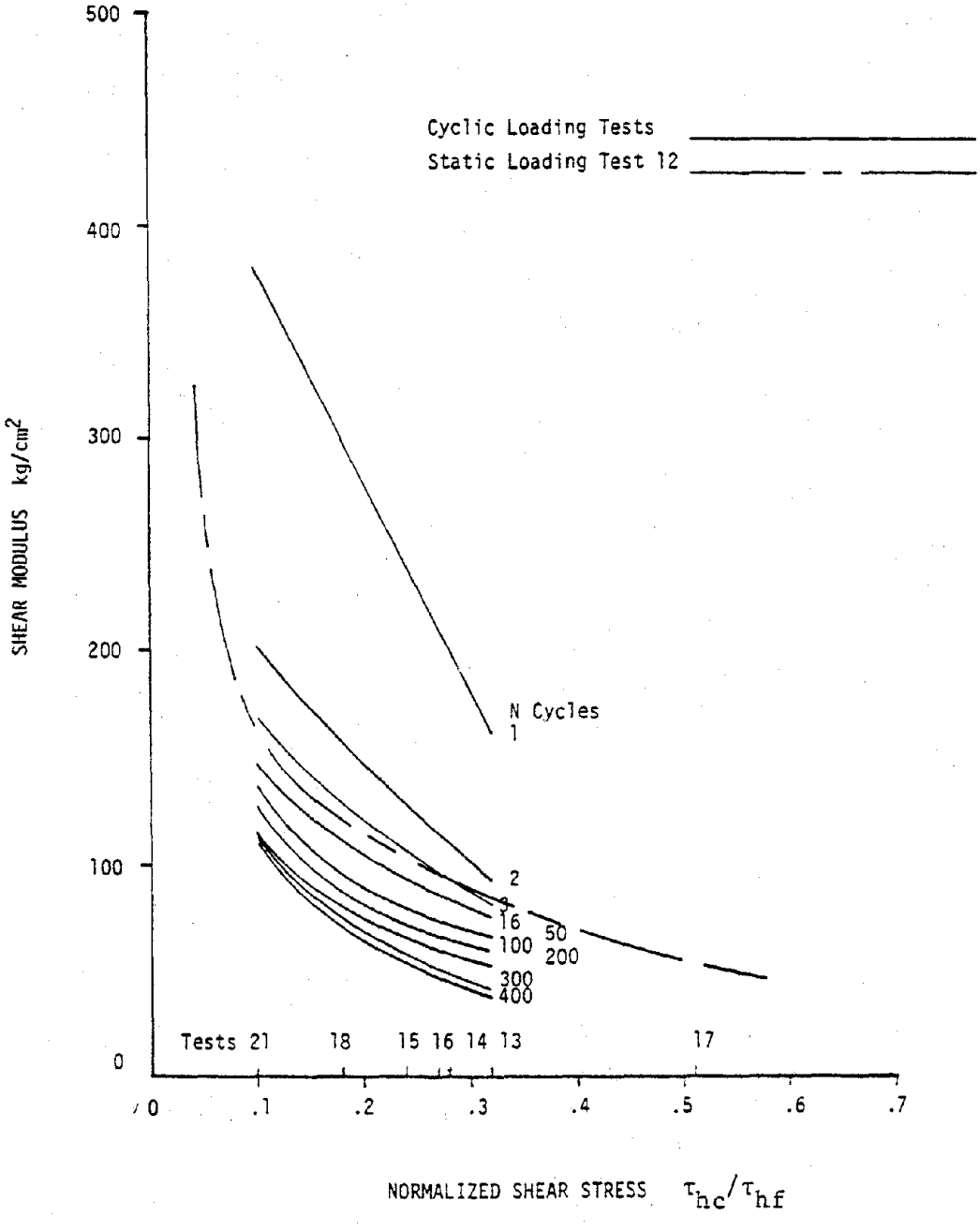

FIGURE 7a. SHEAR MODULUS VS. NORMALIZED VERTICAL STRESS FOR NORMALLY CONSOLIDATED CLAYS

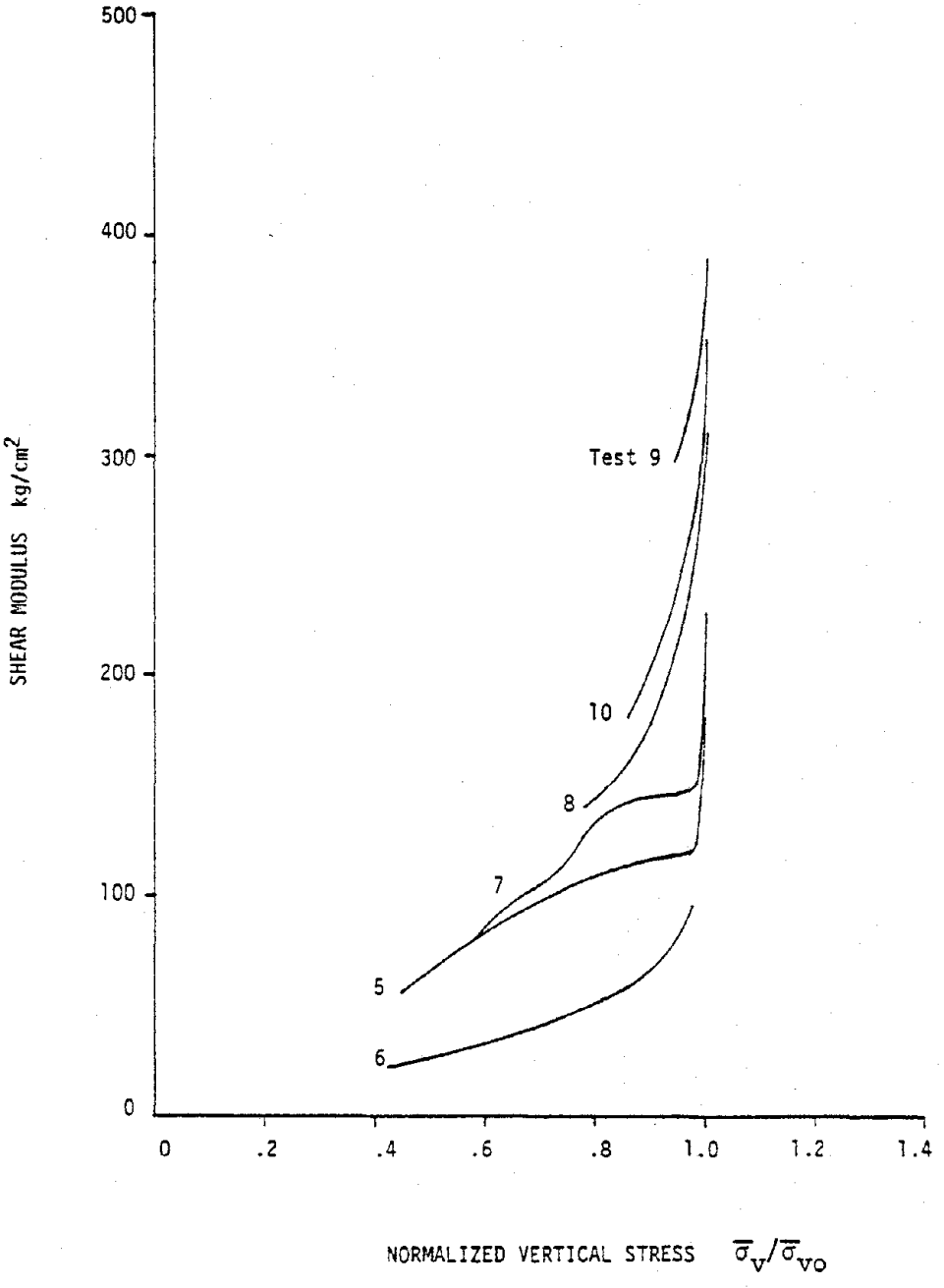

FIGURE 7b. SHEAR MODULUS VS. NORMALIZED VERTICAL STRESS FOR OVERCONSOLIDATED CLAYS

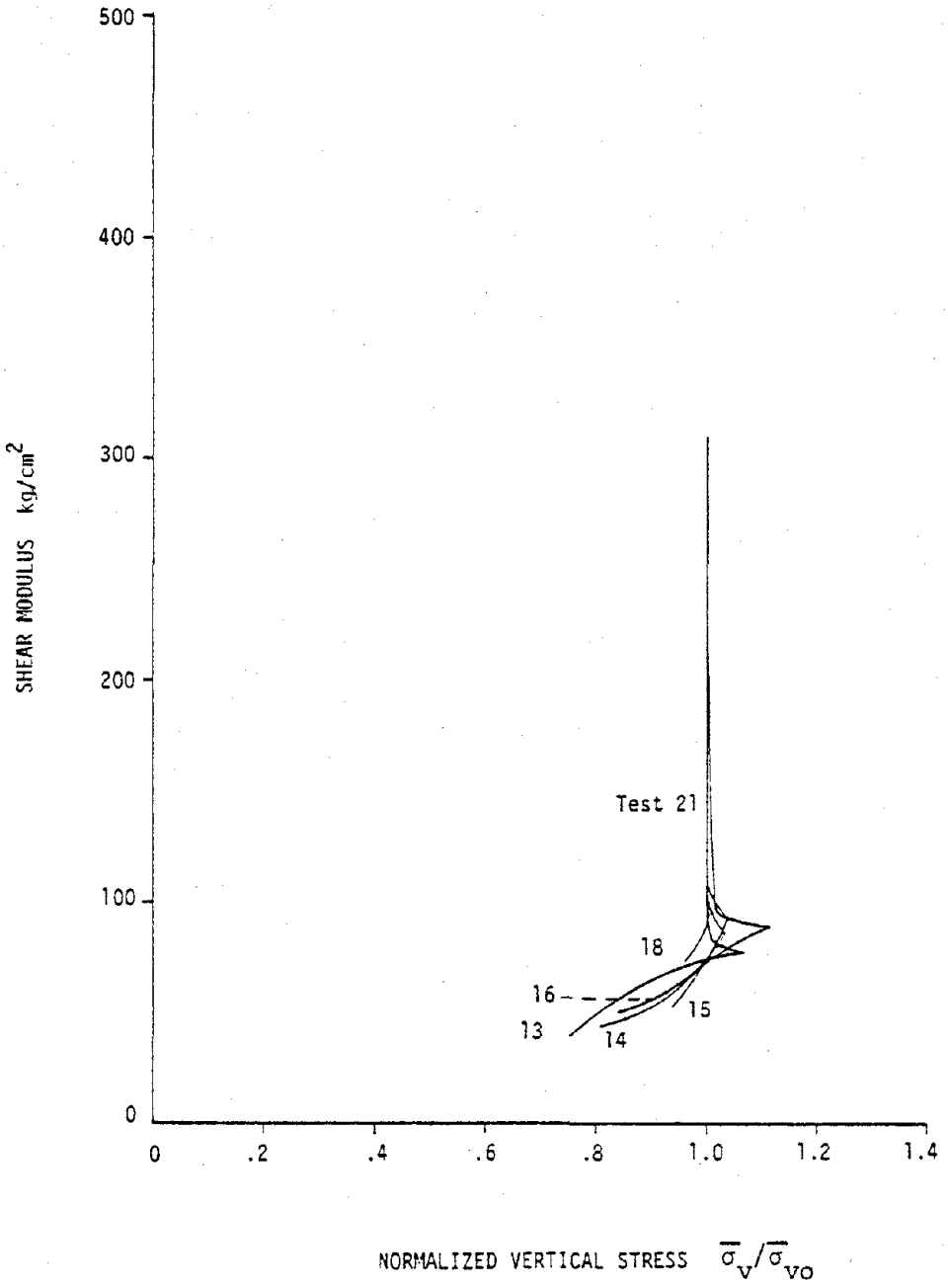

FIGURE 8a. DEGRADATION INDEX VS. SHEAR STRESS FOR NORMALLY CONSOLIDATED CLAYS

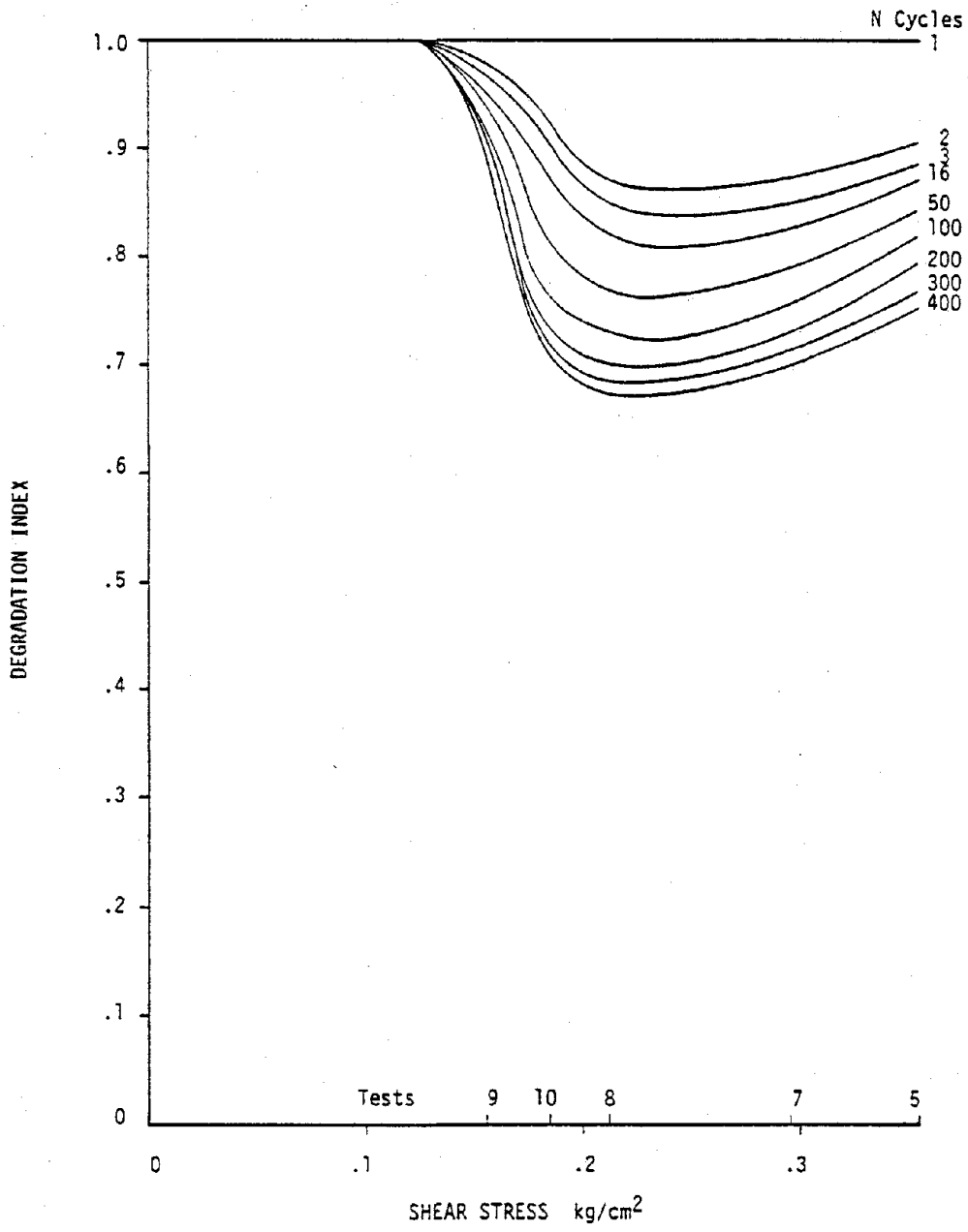

FIGURE 8b. DEGRADATION INDEX VS. SHEAR STRESS FOR OVERCONSOLIDATED CLAYS

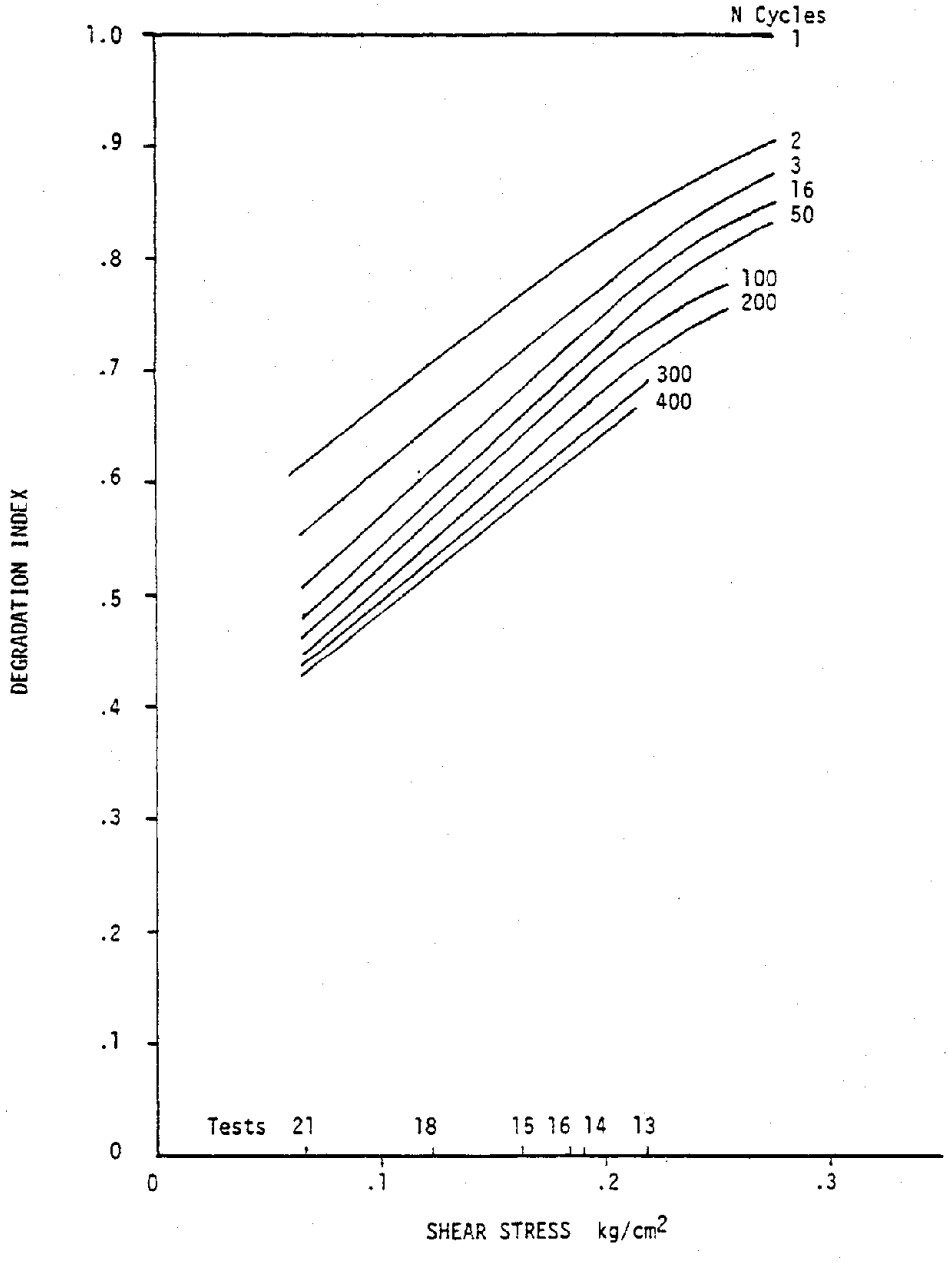

FIGURE 8c. DEGRADATION OF INITIAL BACKBONE CURVE FOR BOTH CLAY TYPES

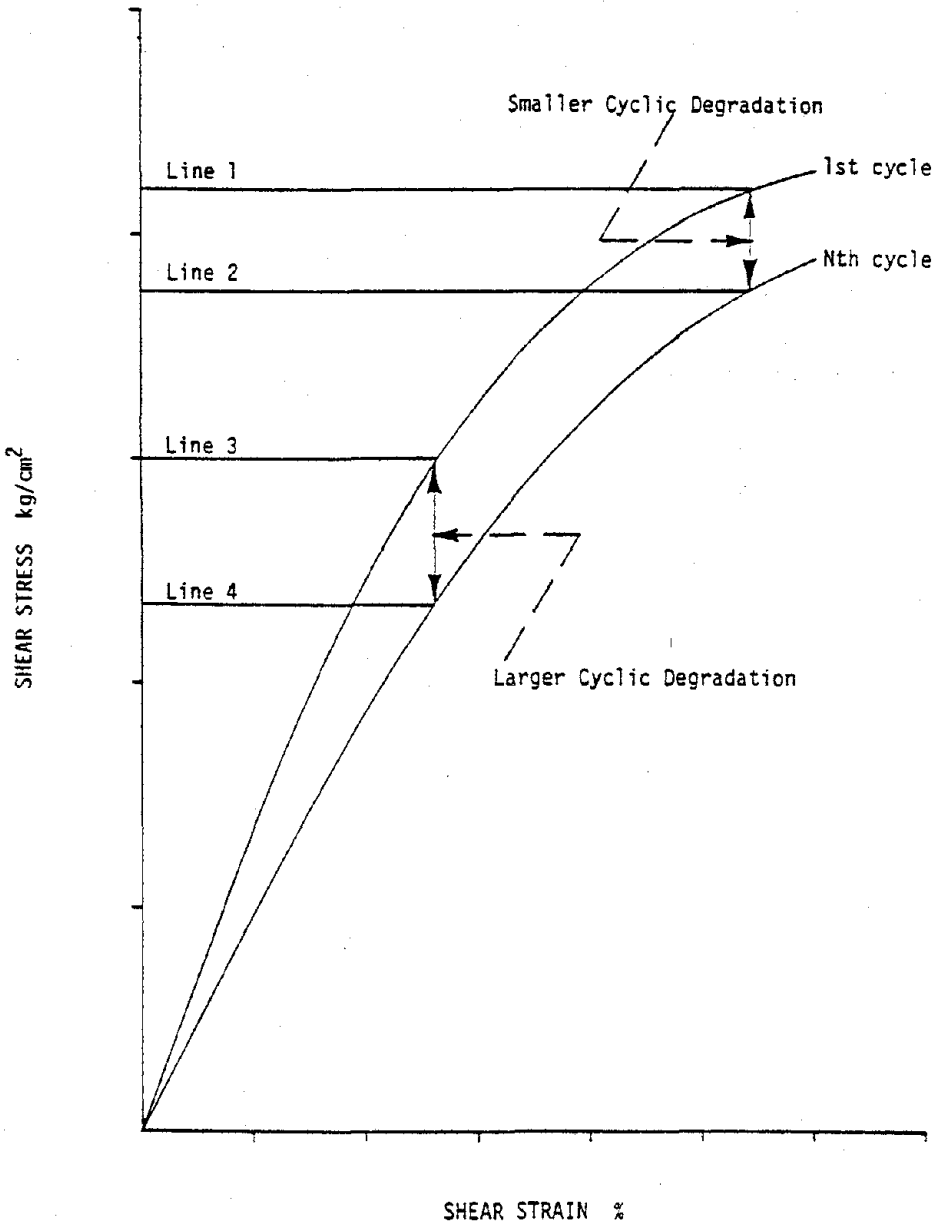

FIGURE 9a. DEGRADATION INDEX VS. NORMALIZED PORE PRESSURE FOR NORMALLY CONSOLIDATED CLAYS

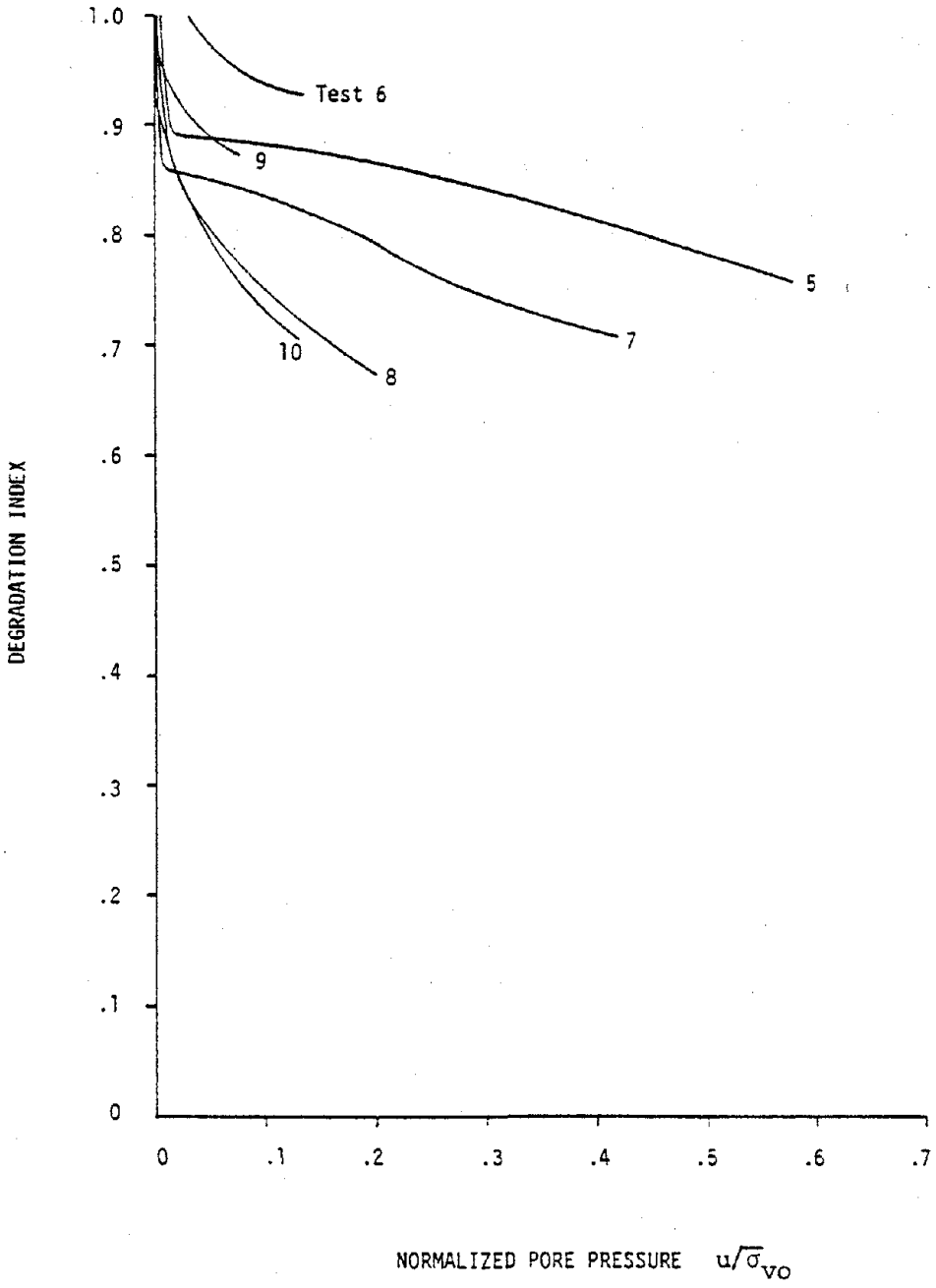

FIGURE 9b. DEGRADATION INDEX VS. NORMALIZED PORE PRESSURE FOR OVERCONSOLIDATED CLAYS

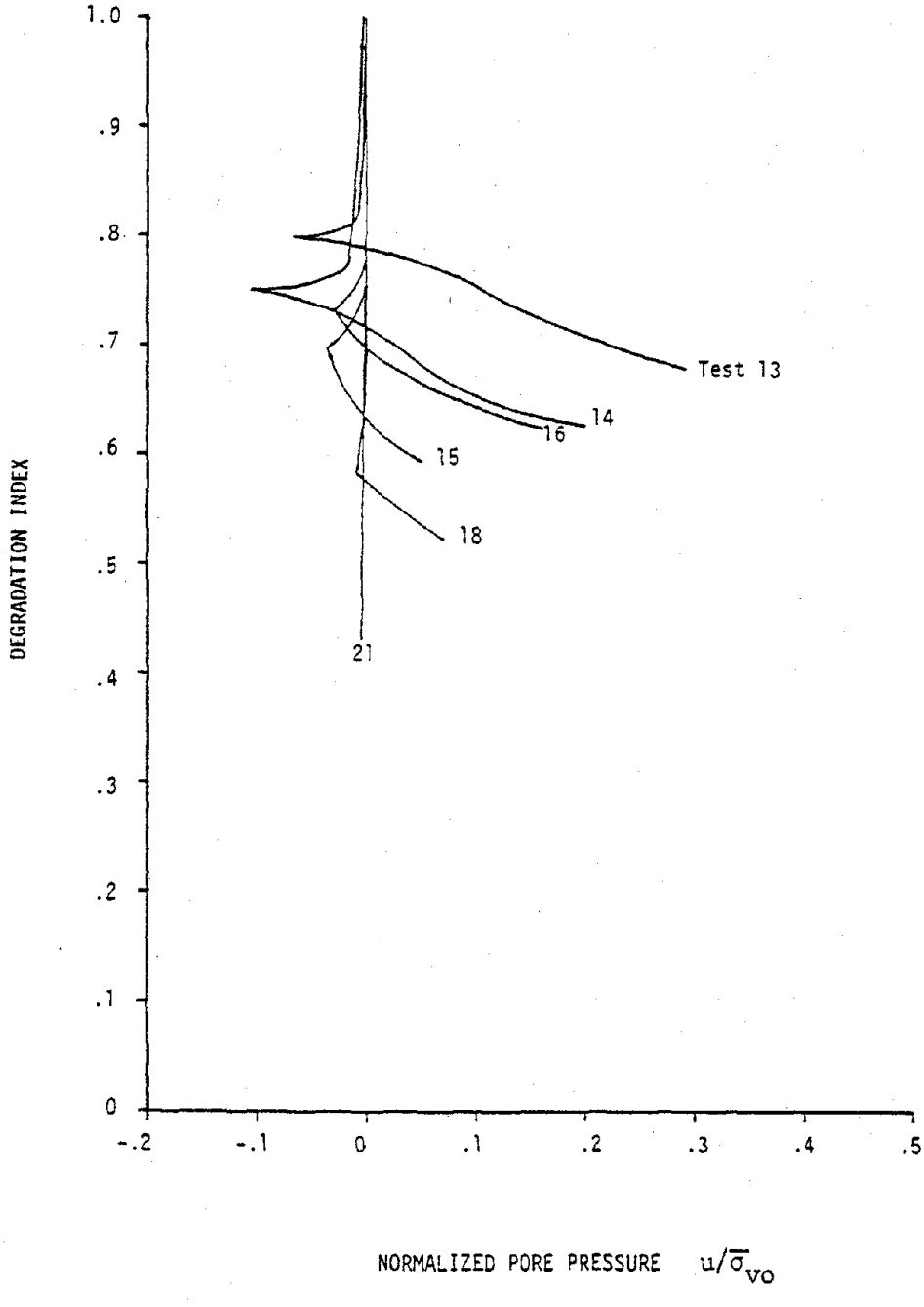

FIGURE 10a. SHEAR STRAIN VS. NORMALIZED PORE PRESSURE FOR NORMALLY CONSOLIDATED CLAYS

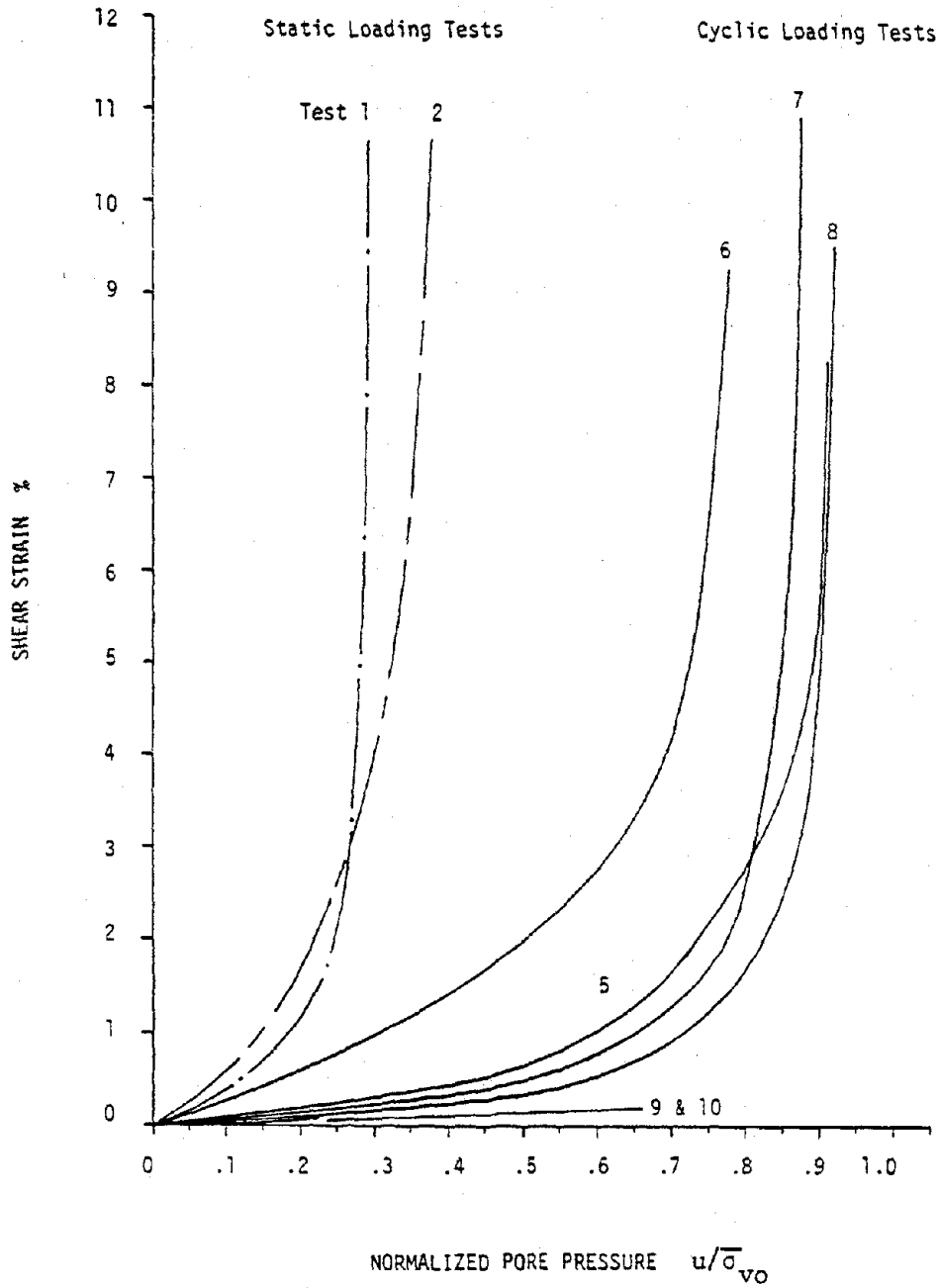

FIGURE 10b. SHEAR STRAIN VS. NORMALIZED PORE PRESSURE FOR OVERCONSOLIDATED CLAYS

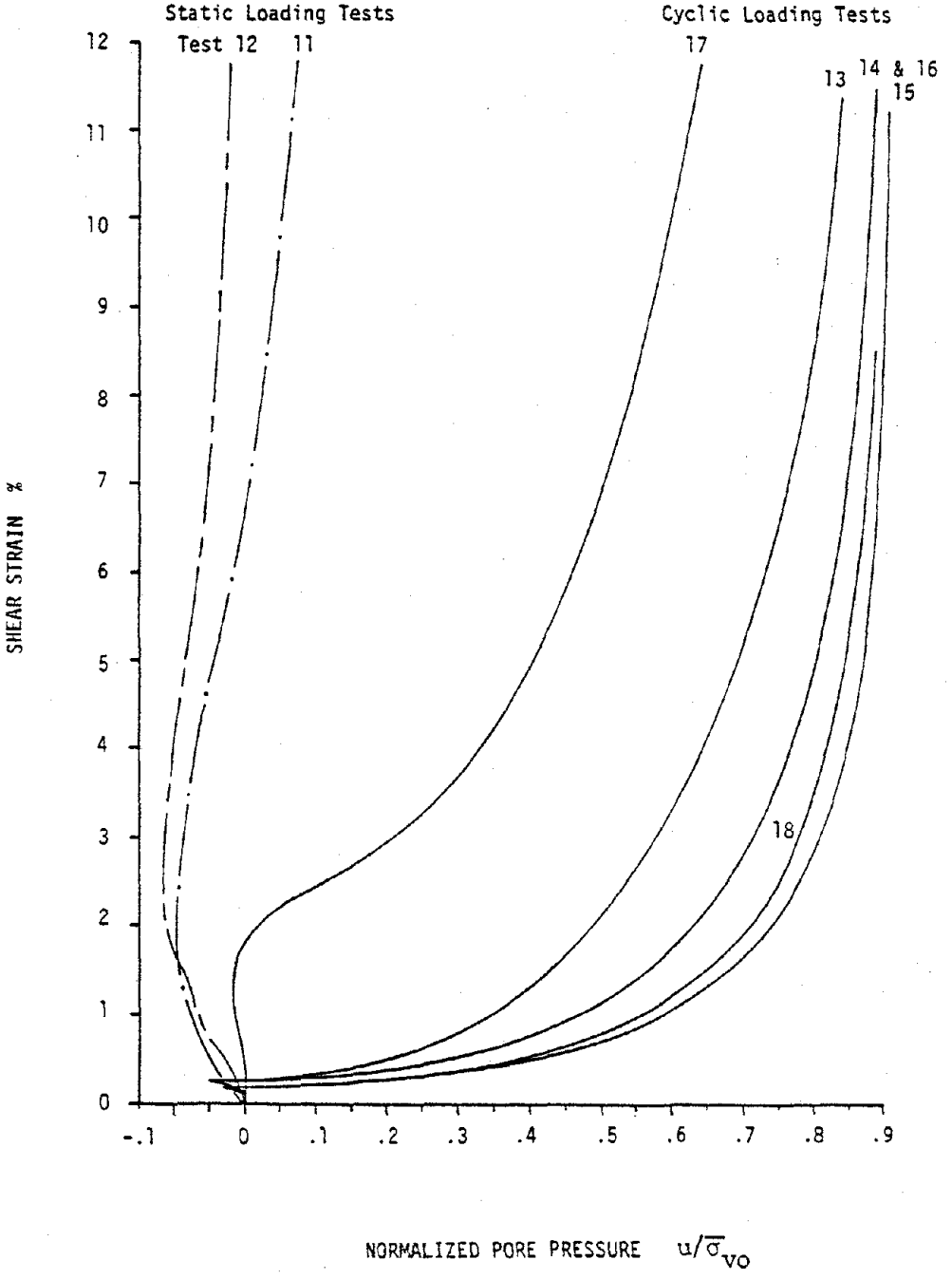

FIGURE 11. SHEAR STRAINS AND PORE PRESSURES VS. N CYCLES FOR TEST 5

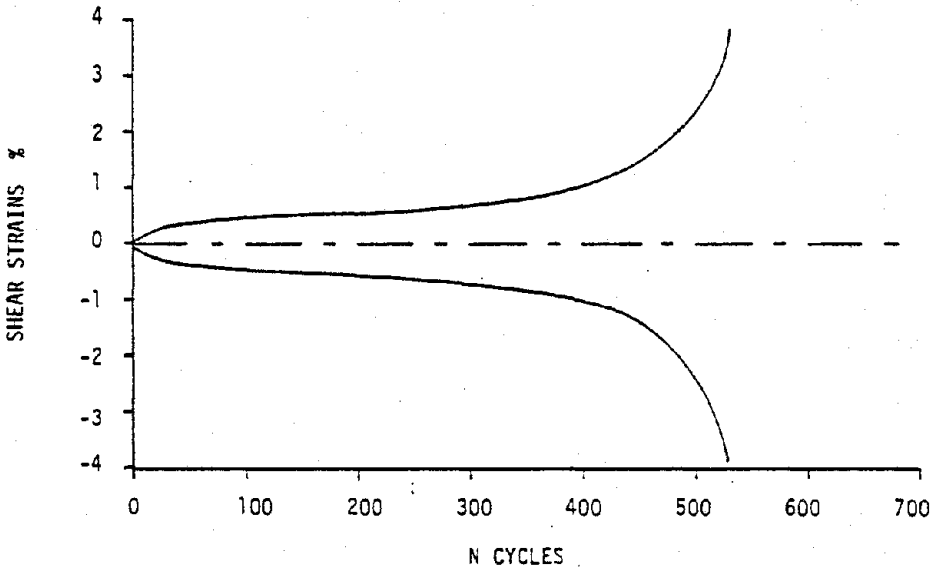

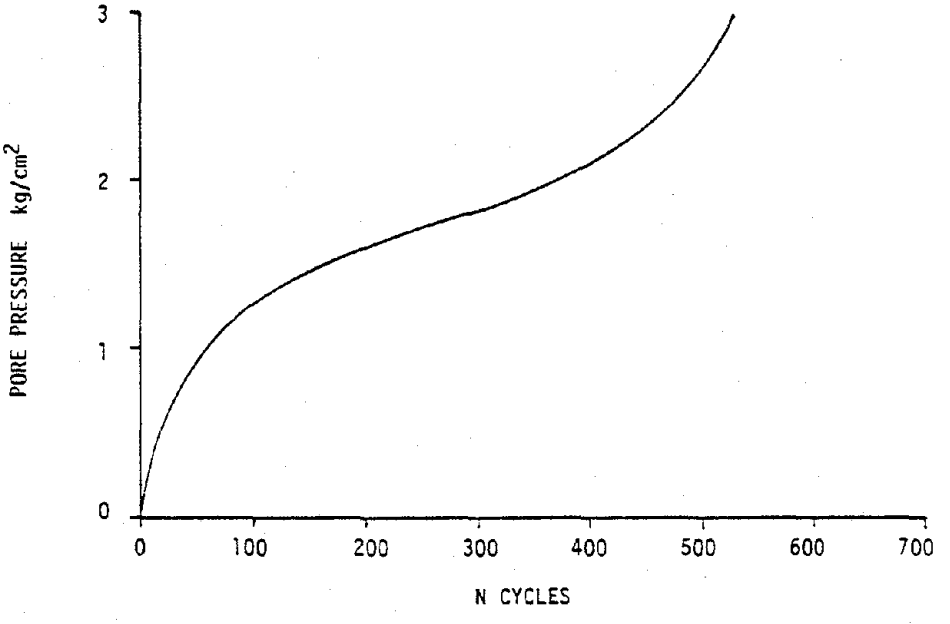

FIGURE 12a. NORMALIZED PORE PRESSURE VS. N CYCLES FOR NORMALLY CONSOLIDATED CLAYS

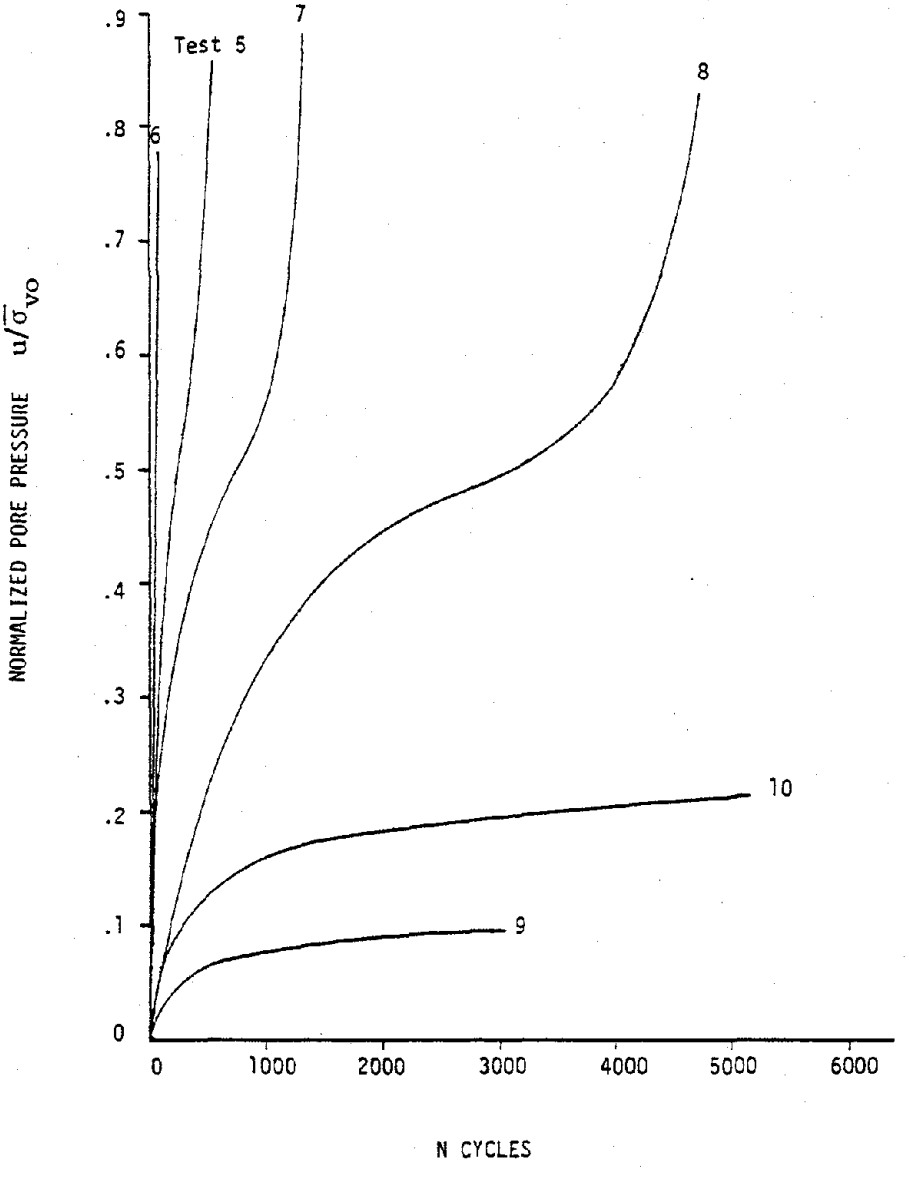

FIGURE 12b. SHEAR STRAIN VS. N CYCLES FOR NORMALLY CONSOLIDATED CLAYS

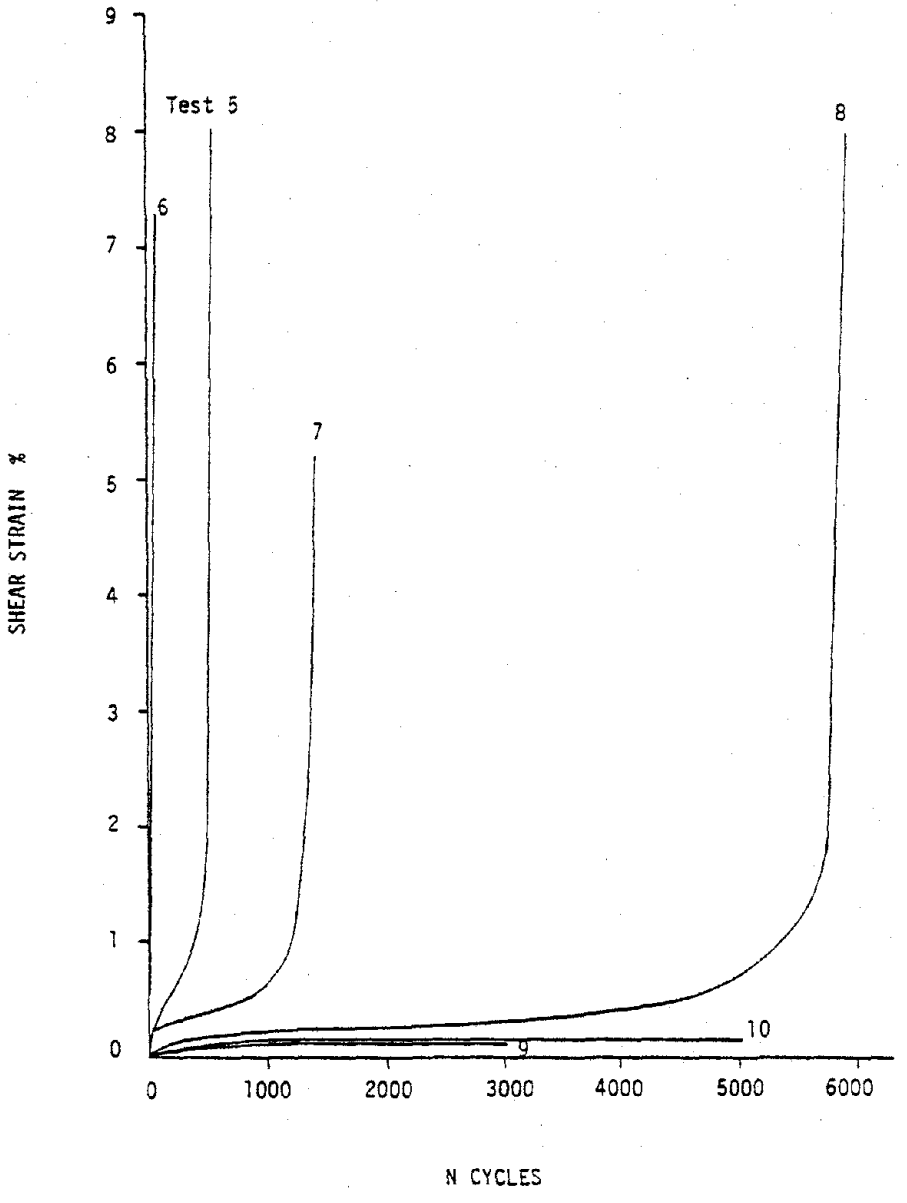

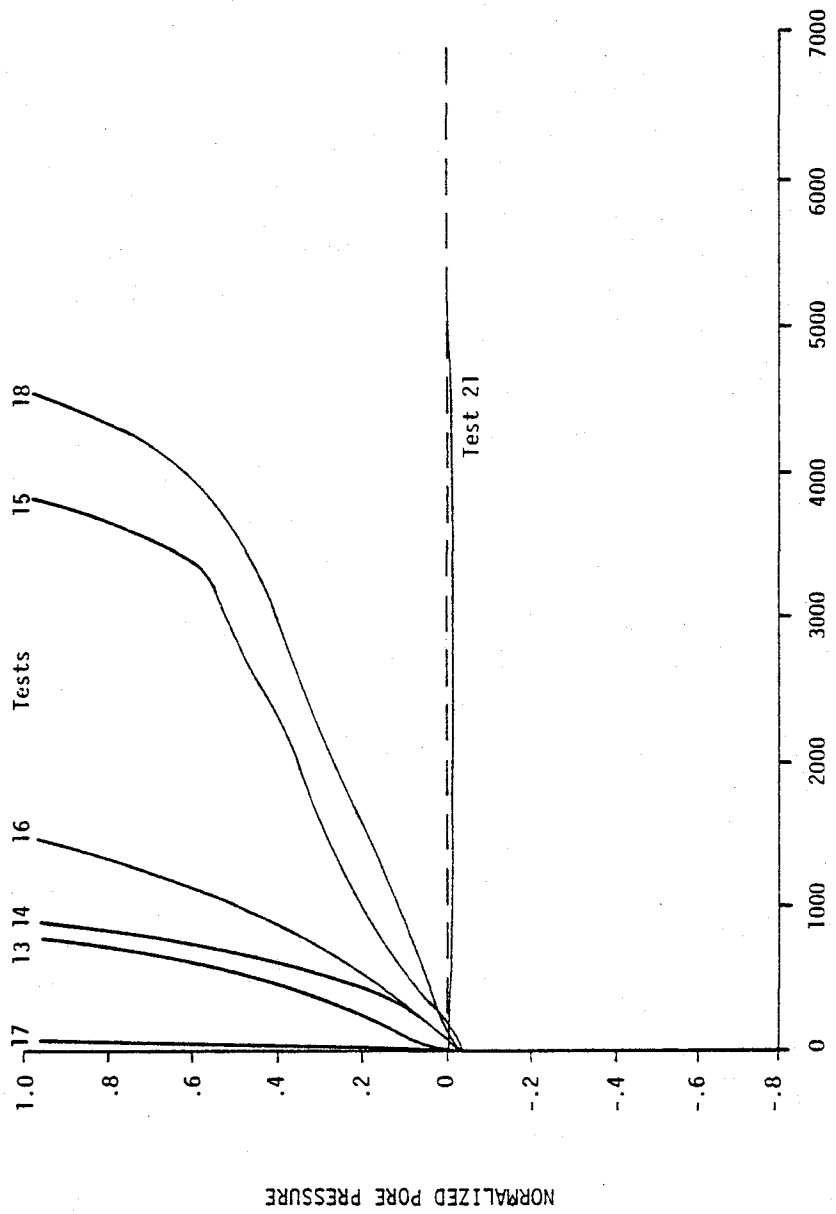

FIGURE 12c. NORMALIZED PORE PRESSURE VS. N CYCLES FOR OVERCONSOLIDATED CLAYS

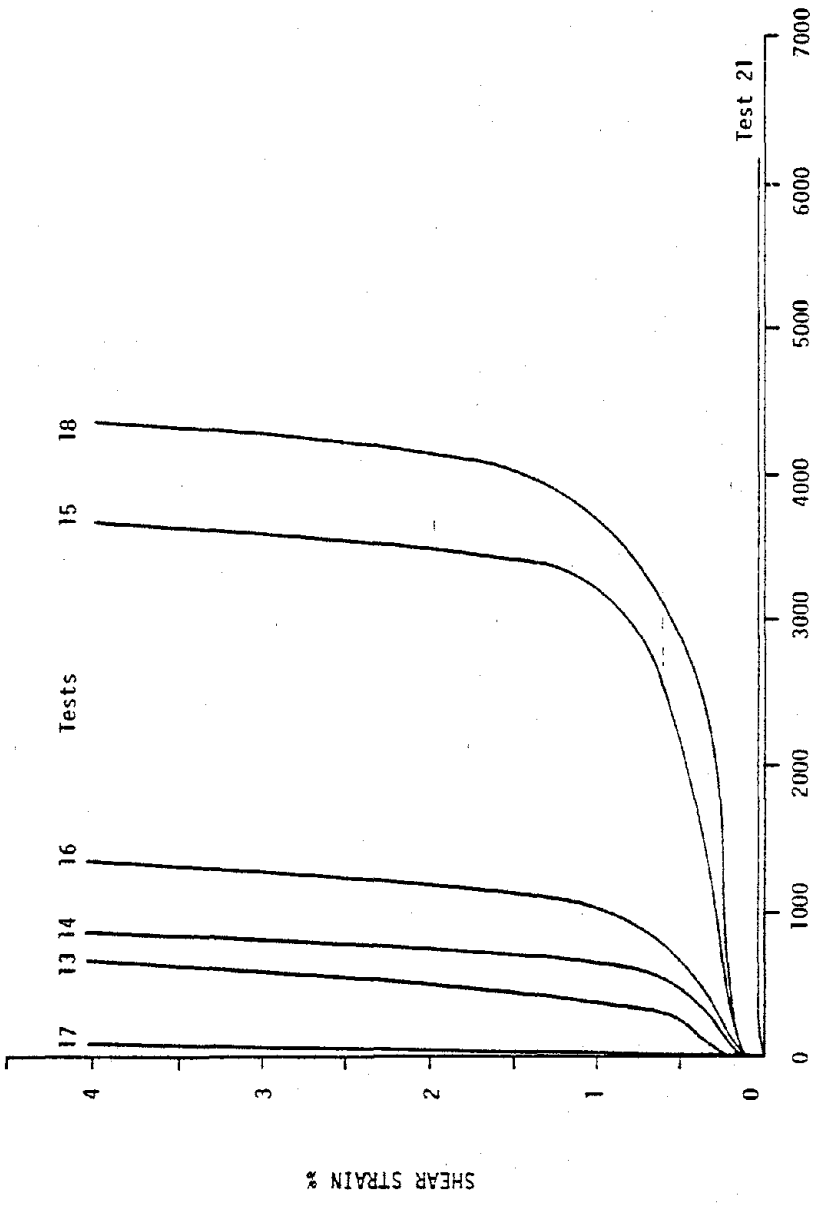

FIGURE 12d. SHEAR STRAIN VS. N CYCLES FOR OVERCONSOLIDATED CLAYS

FIGURE 13a. TOTAL SHEAR STRESS LEVEL VS. N CYCLES
FOR NORMALLY CONSOLIDATED CLAYS

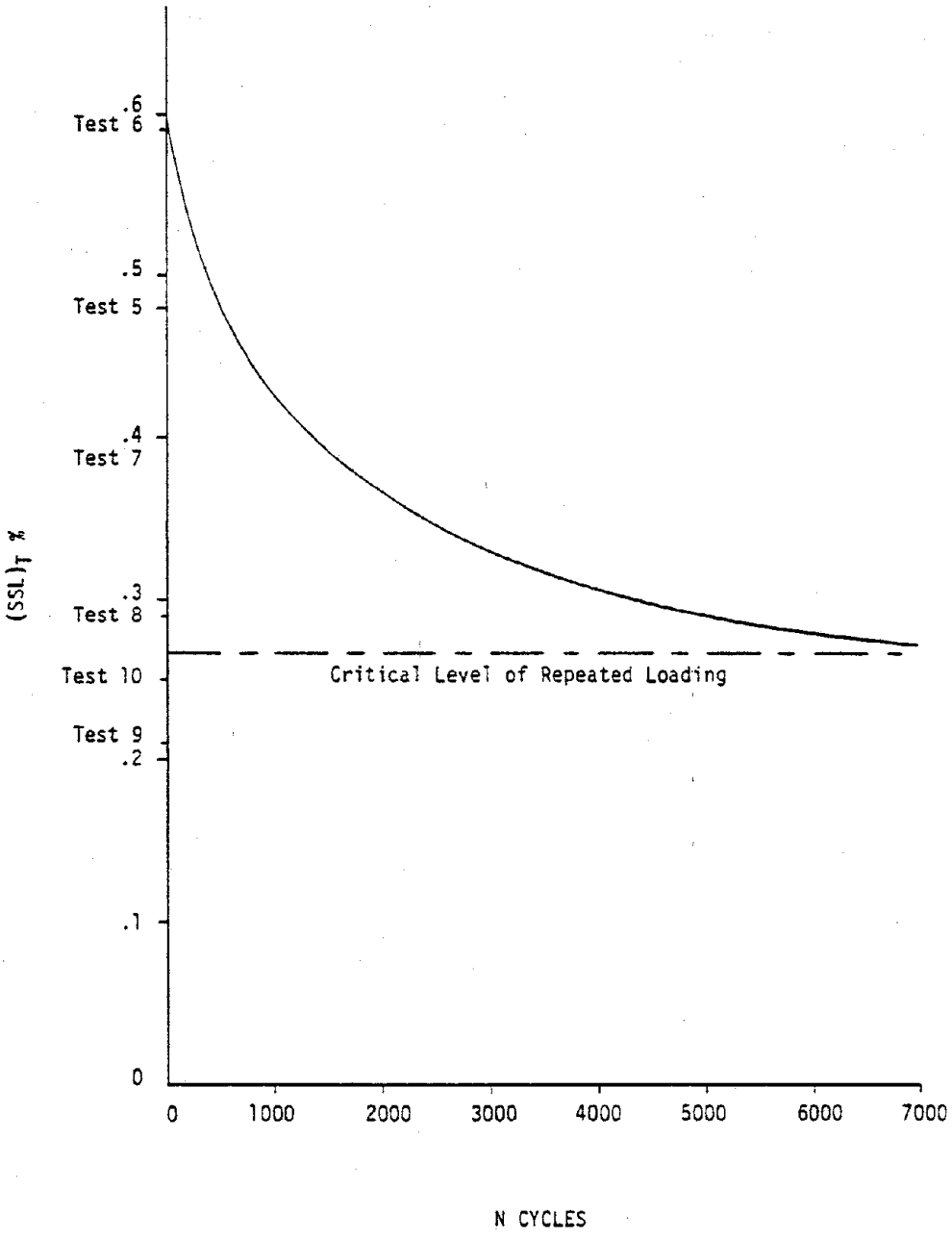

FIGURE 13b. TOTAL SHEAR STRESS LEVEL VS. N CYCLES
FOR OVERCONSOLIDATED CLAYS

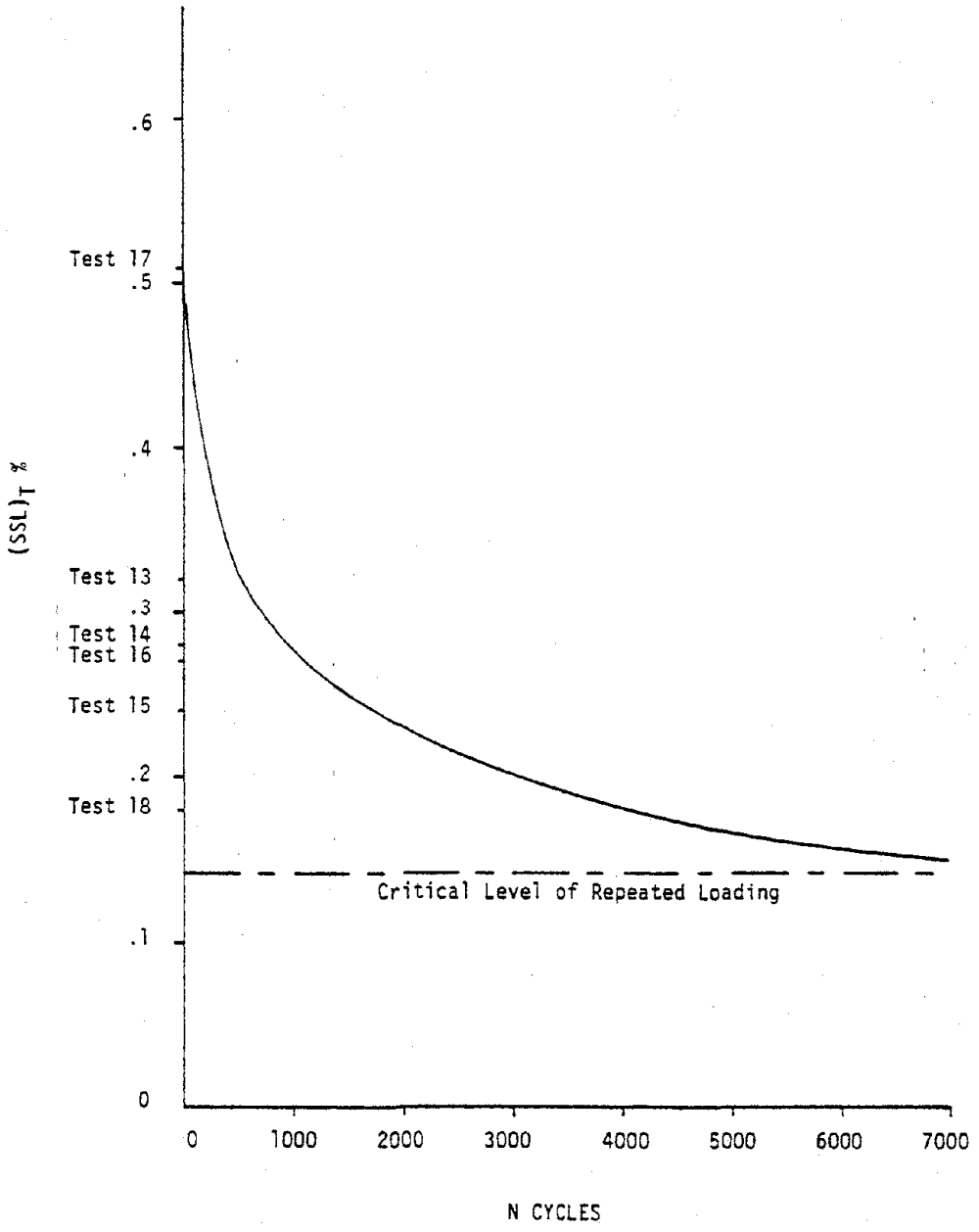

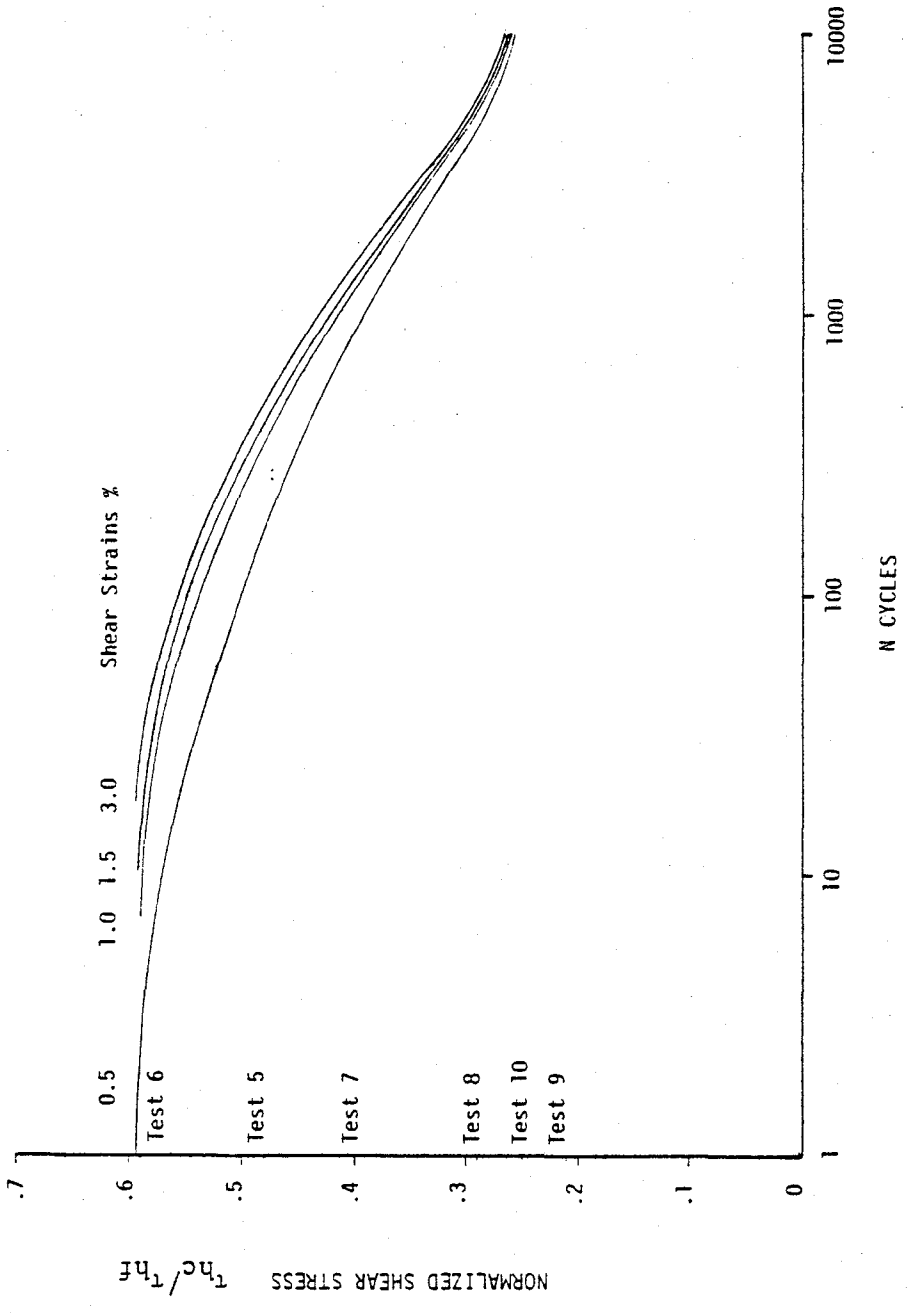

FIGURE 14a. NORMALIZED SHEAR STRESS VS. N CYCLES EVALUATED AT VARYING SHEAR STRAINS FOR NORMALLY CONSOLIDATED CLAYS

FIGURE 14b. NORMALIZED SHEAR STRESS VS. N CYCLES EVALUATED AT VARYING SHEAR STRAINS FOR OVERCONSOLIDATED CLAYS

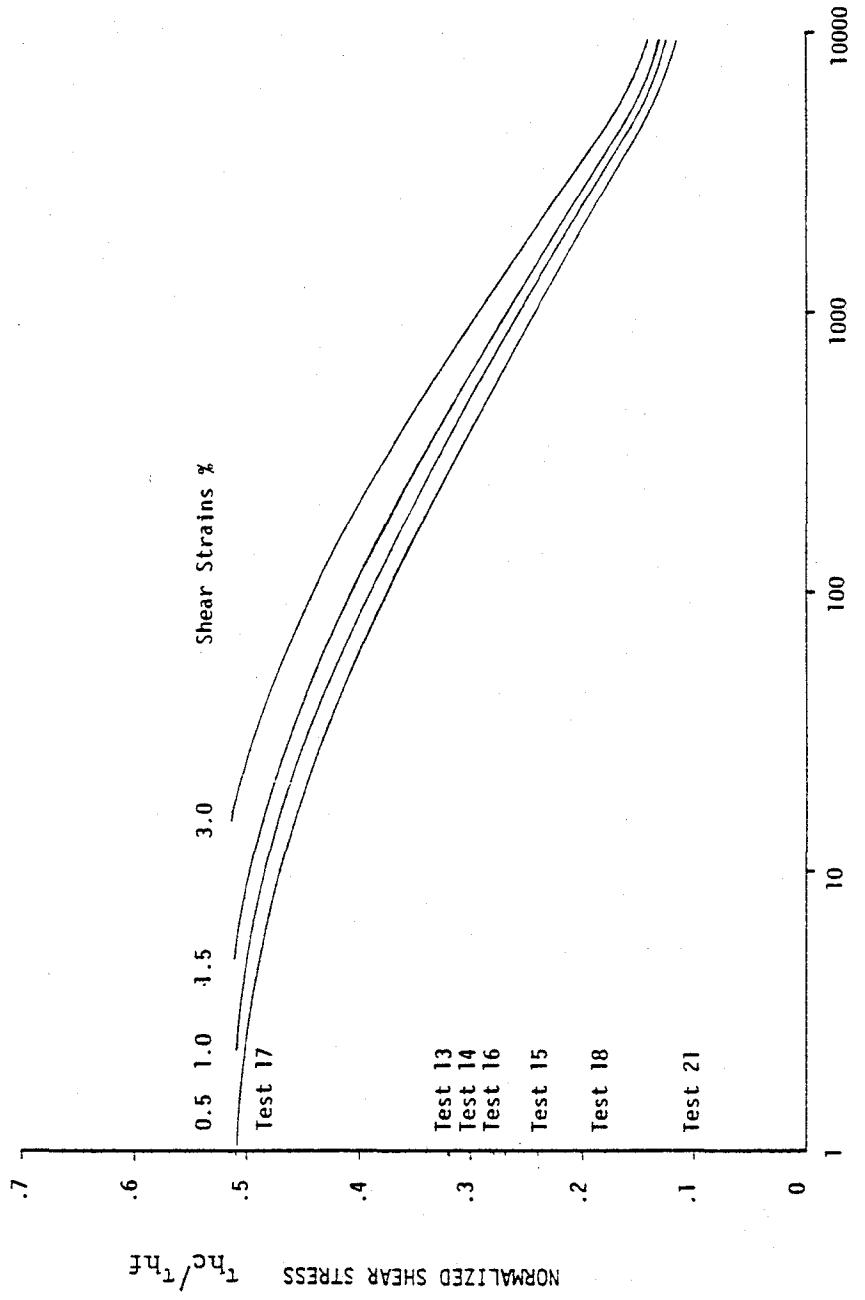

FIGURE 15. EFFECTIVE SHEAR STRESS LEVELS VS. SHEAR STRAIN FOR VARIOUS CYCLIC LOADING TESTS AND CLAYS

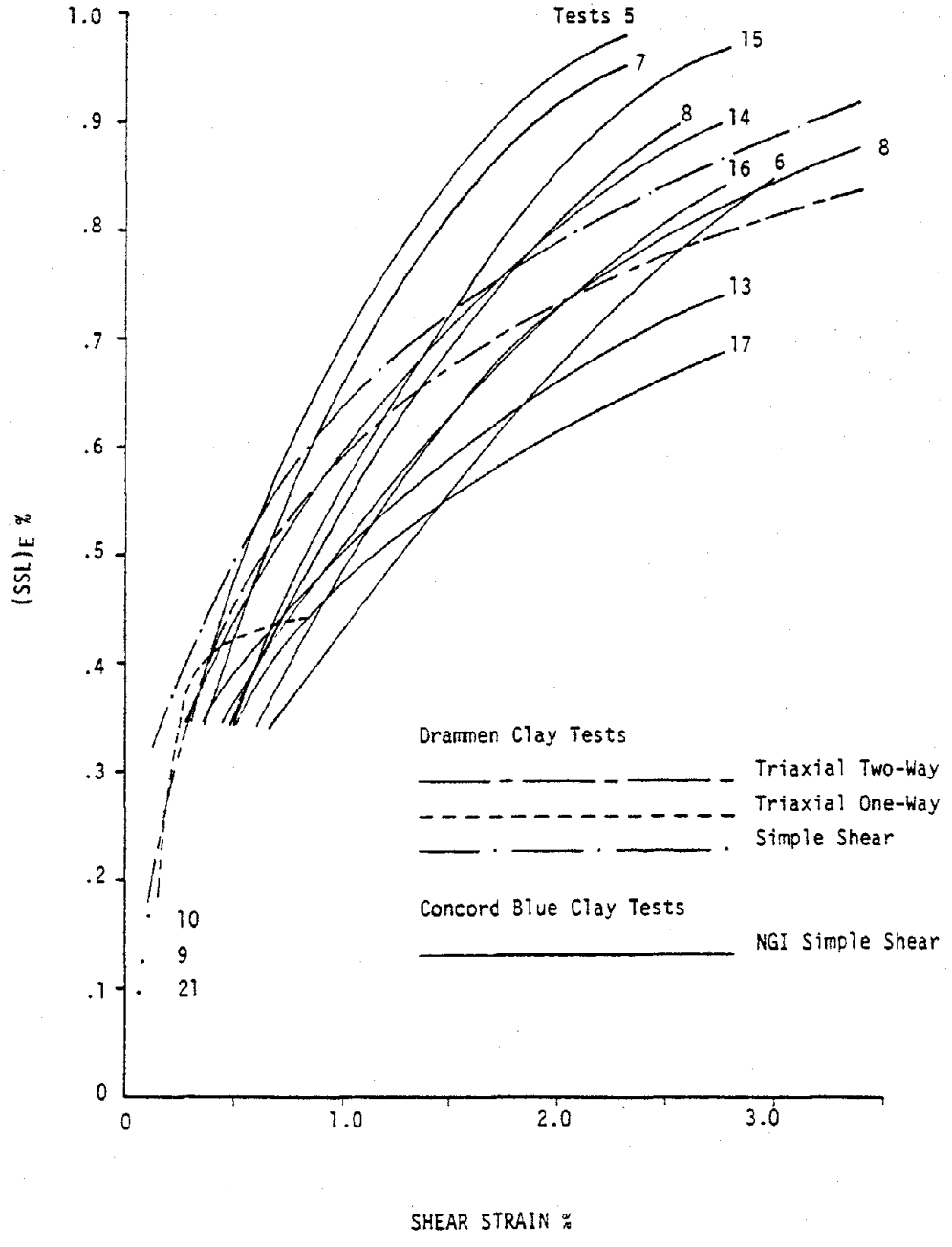

FIGURE 16. DETERMINATION OF γ_y FROM INITIAL BACKBONE CURVES FOR BOTH CLAY TYPES

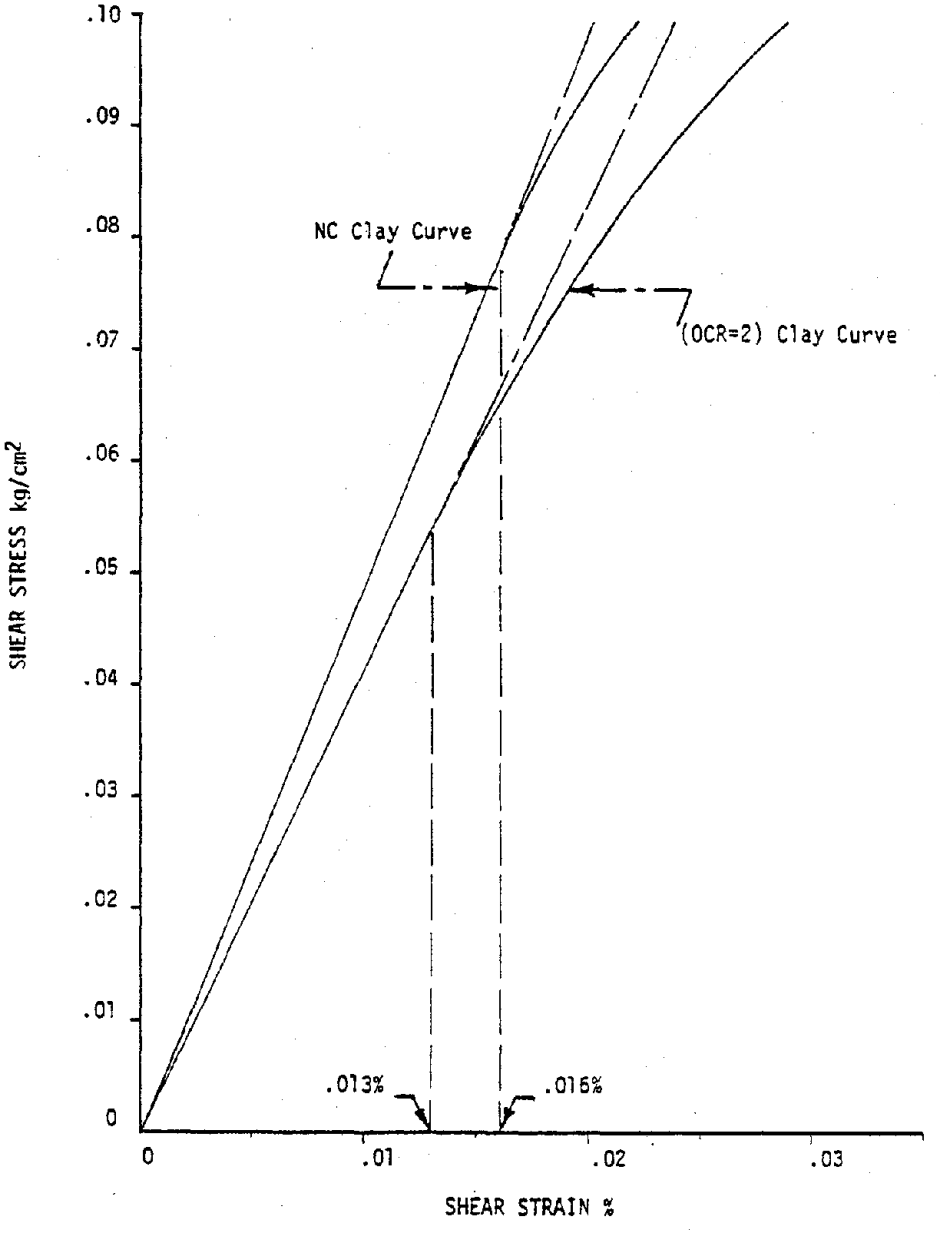

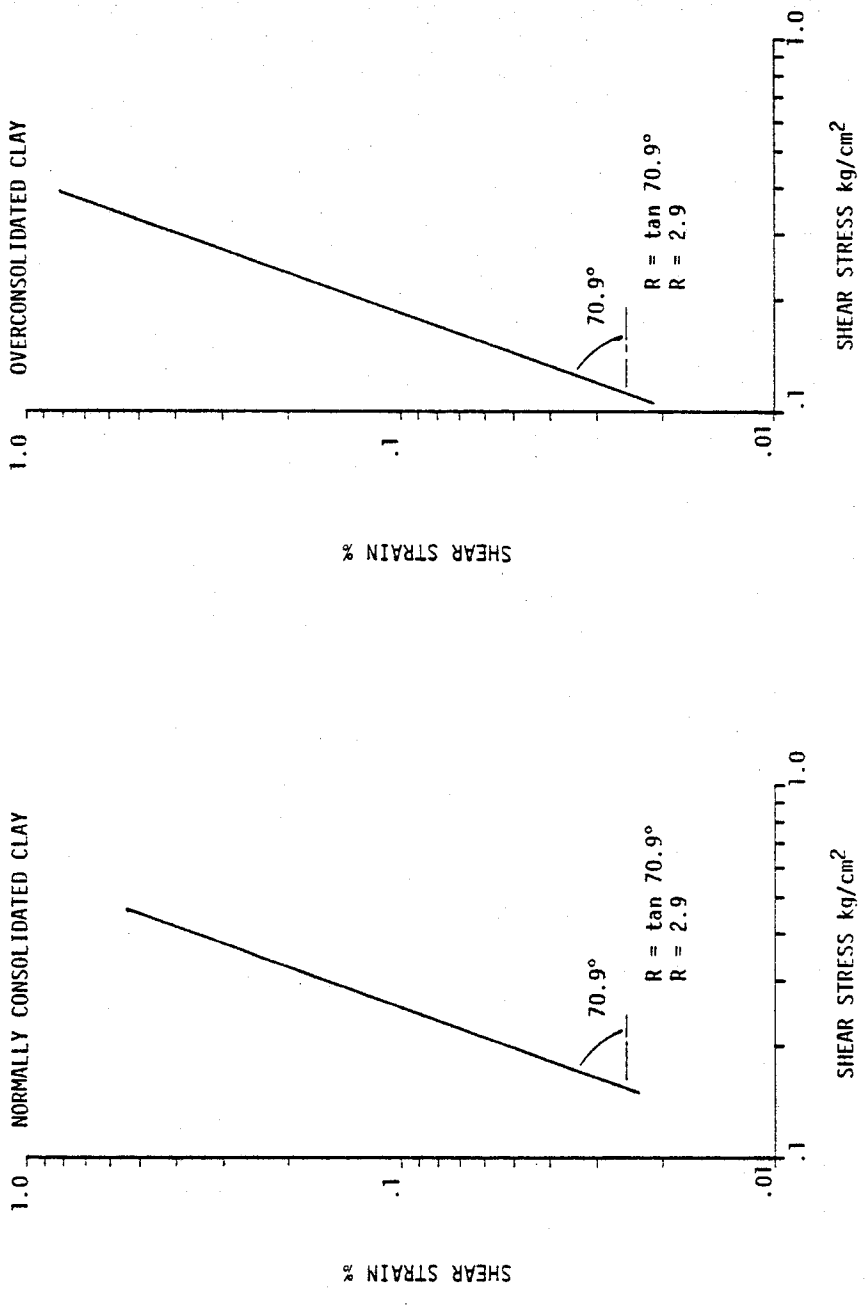

FIGURE 17. DETERMINATION OF R FOR BOTH CLAY TYPES

FIGURE 18a. RAMBERG-OSGOOD MODEL BACKBONE CURVES FOR NORMALLY CONSOLIDATED CLAYS

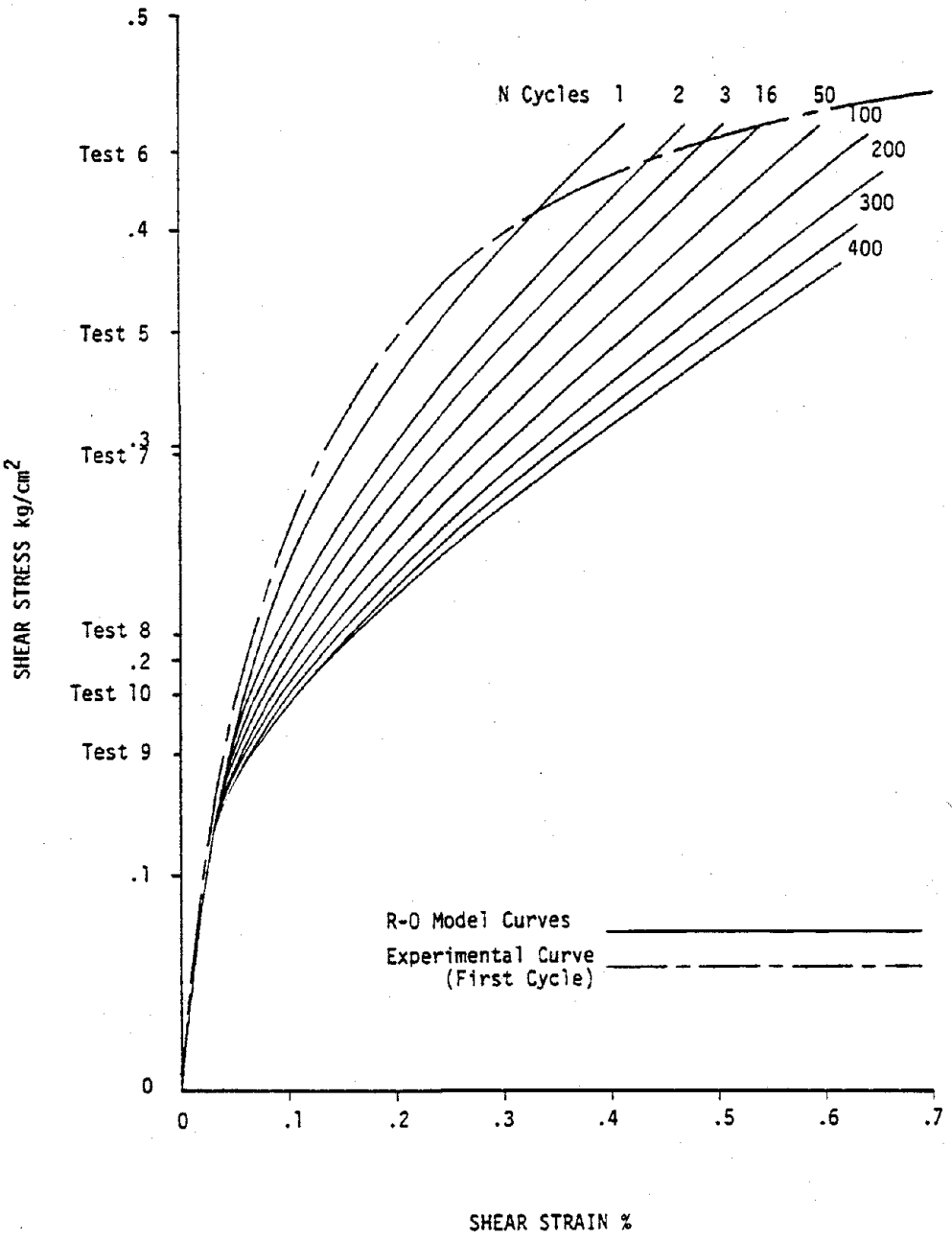

FIGURE 18b. RAMBERG-OSGOOD MODEL BACKBONE CURVES
FOR OVERCONSOLIDATED CLAYS

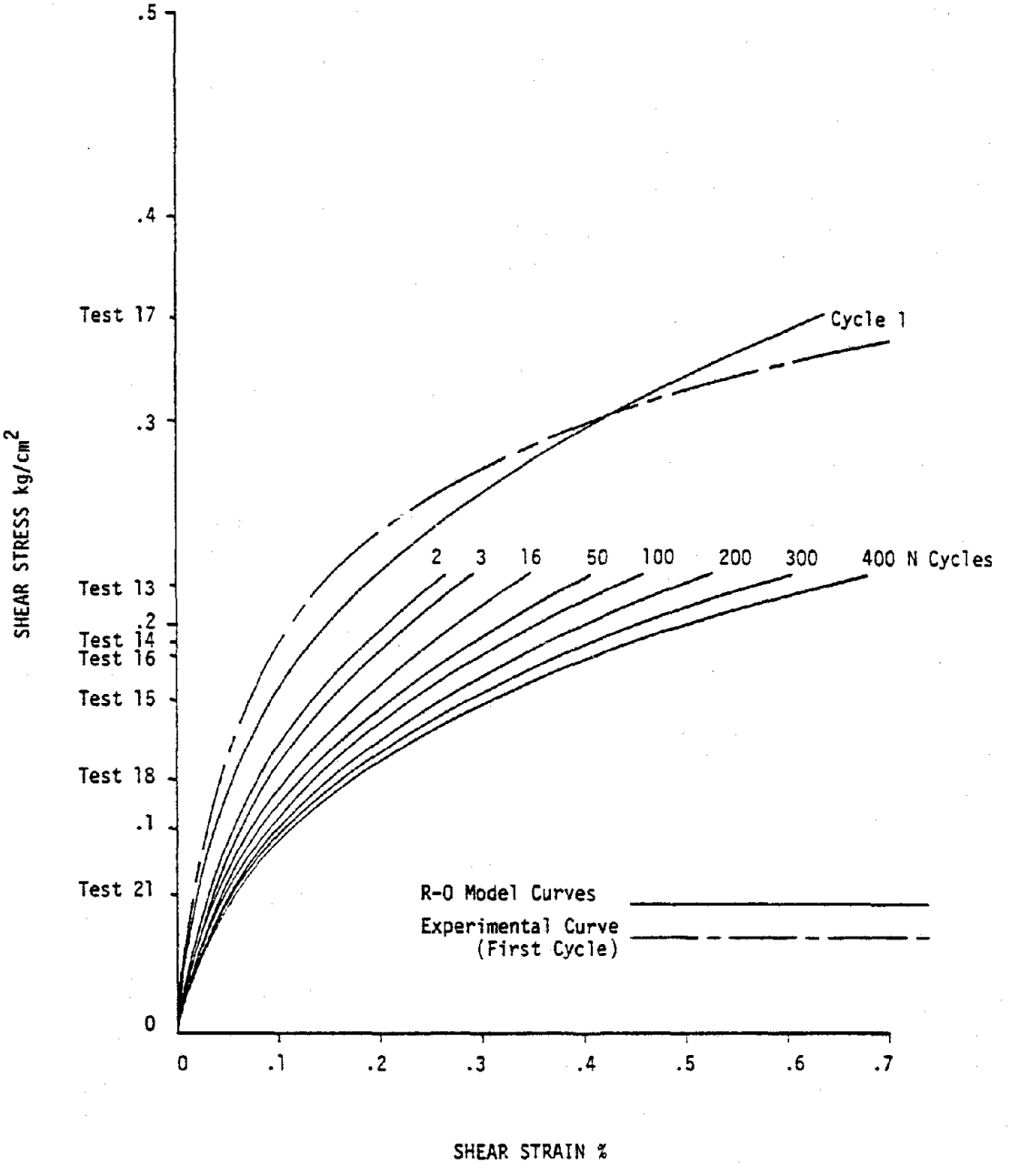

FIGURE 19a. SHEAR MODULUS VS. SHEAR STRAIN FOR NORMALLY CONSOLIDATED CLAYS

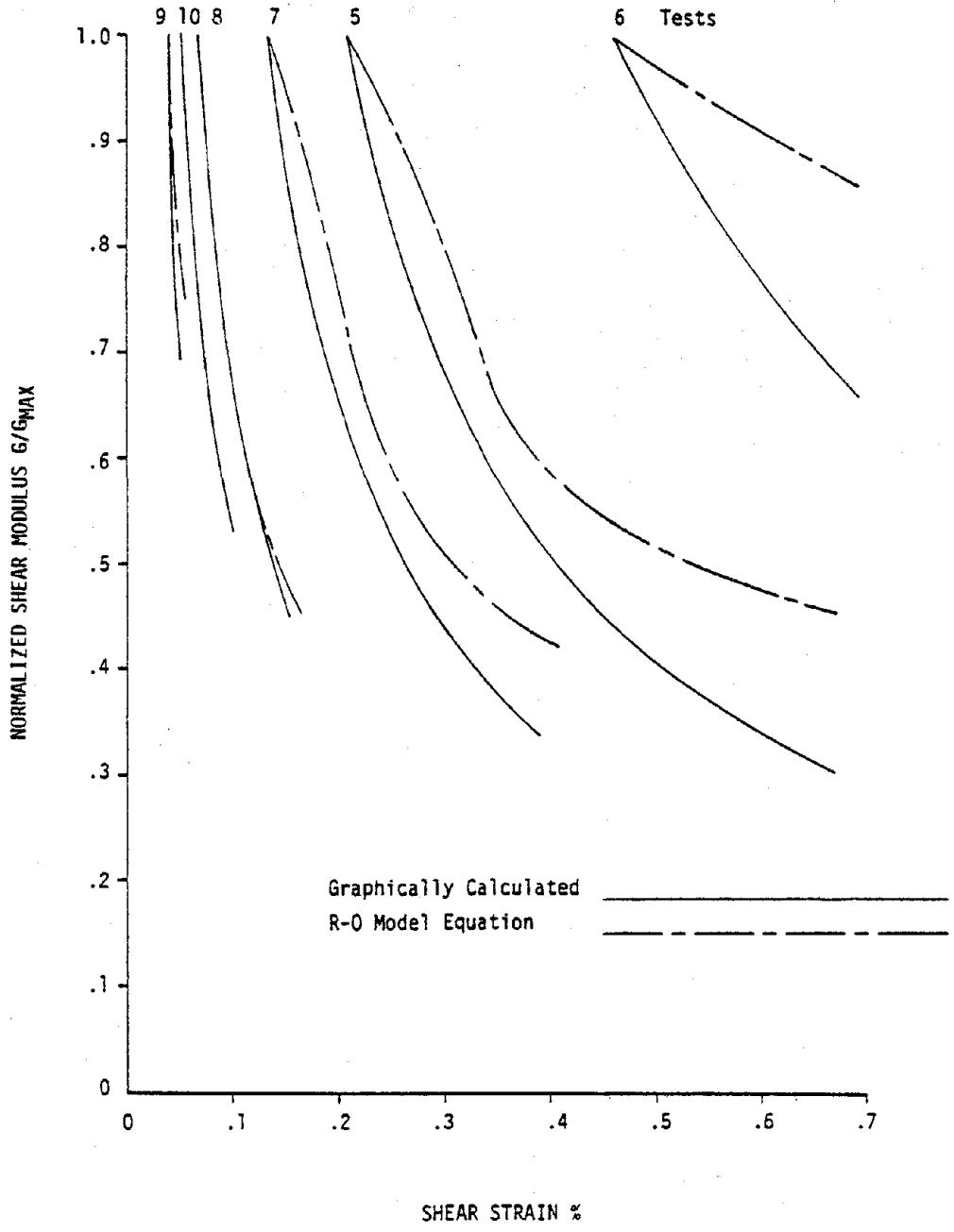

FIGURE 19b. SHEAR MODULUS VS. SHEAR STRAIN FOR OVERCONSOLIDATED CLAYS